CHARACTERIZATION OF PLASTIC HYPODERMIC NEEDLES

A Thesis
Presented to
The Academic Faculty

By

Eric Busillo

In Partial Fulfillment
Of the Requirements for the Degree
Master of Science in Mechanical Engineering

Georgia Institute of Technology

December, 2008

CHARACTERIZATION OF PLASTIC HYPODERMIC NEEDLES

Approved by:

Dr. Jonathan S. Colton
George W. Woodruff School of Mechanical Engineering
Georgia Institute of Technology

Dr. David N. Ku
George W. Woodruff School of Mechanical Engineering
Georgia Institute of Technology

Dr. Mark R. Prausnitz
School of Chemical and Biomolecular Engineering
Georgia Institute of Technology

July 9, 2008

All good things come round to him who will but wait

Tales of a Wayside Inn, The Student's Tale (1863)

Henry Wadsworth Longfellow

ACKNOWLEDGMENTS

I would like to thank everyone that has helped me complete this thesis and stood by me for the past two years. First and foremost, my advisor, Dr. Colton has been continually pushing me forward with my work and opening my eyes to new ideas and opportunities within the realm of this project. I am grateful for his assistance and guidance through the research. He has helped to make me a better engineer and a better writer.

I would also like to thank my parents and my sister, Alison, who have given me their full support throughout my time here at Georgia Tech. Even though they have been over 700 miles away, I have often felt like they were right here with me. My fellow graduate students, Chris Blandin, Taylor Stellman, Jordan Hamilton, and Tom Forbes, have been instrumental in helping me with my research, and I am thankful for the assistance they have given me. Also, my friends from back home, who are too numerous to individually mention, have been incredibly supportive throughout my work as well, even though I moved away from them for the opportunity to complete this thesis.

The machine shop has been very helpful by completing parts that I have needed to complete this research, and I could not have conducted my experiments without them. Also, I would like to thank Dr. Ku and Dr. Prausnitz for serving on my thesis committee. Finally, this research could not have been completed without the funding and needles from SS&B Technology Ltd, and I appreciate all that they have done.

TABLE OF CONTENTS

LIST OF TABLES

LIST OF FIGURES

LIST OF SYMBOLS

A	Cross sectional area
a	Crack length / 2
E	Elastic modulus
F	Applied force
I	Moment of inertia
ID	Inner diameter
J_{IC}	Fracture toughness
K	Effective length factor
L	Column length
L_{cr}	Critical length
M	Internal moment
OD	Outer diameter
P	Applied load
P_{cr}	Critical buckling load
P_S	Punch load
p_S	Average penetration pressure on punch
R	Needle radius at tip
r	Radius of gyration
r_p	Punch radius
t	Sheet thickness
v	Deflection, volume fraction
x	Axial distance along column
α	Strain hardening exponent
δl	Incremental depth
δS_E	Work required to open crack
δW_C	Work required to create crack
ε_t	Tensile strain
λ	Stretch ratio
μ	Shear modulus
ν	Poisson's ratio
σ	Stress
σ_y	Compressive yield strength
θ	Bending angle

SUMMARY

Significant potential for plastic hypodermic needles exists as an alternative to current steel needles, especially in developing regions where proper needle disposal is problematic. Needle reuse causes tens of millions of hepatitis and HIV infections each year. Plastic needles may reduce reusability and increase the opportunities for safe disposal. Plastic needles also will help with medical waste disposal, by removing metal from the waste stream, hence making it easier to reprocess needles and syringes into useful products such as car battery cases and pails.

This thesis presents the design and testing of one type of plastic hypodermic needle. The buckling and penetration characteristics of the needles were modeled and analyzed analytically and by finite element analyses. Experimental penetration tests using steel and plastic hypodermic needles and skin mimics, specifically polyurethane film and pig skin, were performed to determine penetration and friction forces. Penetration tests also were conducted to determine whether the needles could penetrate butyl rubber stoppers that cover drug vials. Various lubricants, including silicone oil and a medical grade silicone dispersion, were also used. In addition, the needles underwent perpendicular bending tests and cannula stiffness tests. Finally, fluid flow tests were conducted to determine fluid flow rates through the needles. Experimental results were compared to each other and finite element analyses and discussed.

Testing indicated that the plastic needles began buckling under a load of about 4 N for 38.1 mm length needles and about 10 N for 25.4 mm length needles. This is significant because these are approximately the forces required to penetrate polyurethane rubber when lubricated with a silicone dispersion. Needles without the silicone lubricant were unable to penetrate the polyurethane film, while lubricated needles have a 37% penetration rate for a cannula length of 38.1 mm and a 75% penetration rate for a cannula length of 25.4 mm. Similar results are achieved for tests into pig skin, for which lubricated plastic needles of 38.1 mm length did not penetrate, and needles of 25.4 mm length penetrated for 75% of the tests. Tests utilizing butyl rubber as the penetration medium also had a high penetration success rate for 25.4 mm length needles, but the needles were unable to penetrate the polyurethane film following penetration into butyl rubber, a result that will need to be improved upon before the needles are mass produced. Further tests confirm that the plastic needles have the potential to replace steel needles, as evidenced by the success of the perpendicular force test and the relatively similar forces required to expel fluid from a syringe using both the plastic needles and steel needles. The research presented in this thesis demonstrates that with further design modifications, plastic needles may become suitable for mass replacement of steel needles, thus helping to eradicate the many health and environmental risks brought upon by steel needles.

CHAPTER 1

INTRODUCTION

This thesis studies the performance of plastic hypodermic needles as replacements for steel hypodermic needles. The needles are studied from theoretical, simulative, and experimental standpoints.

1.1 Background of hypodermic needles

Each year, billions of people receive injections from steel hypodermic needles. Steel is presently the only material used in the mass production of hypodermic needles. It is beneficial because it is a strong material that is well suited for penetrating human skin. However, syringe-needle combinations must be sterile for use. As a result, they are designed to be used safely only once. In developing countries, proper needle and syringe disposal is problematic. Needle reuse causes tens of millions of hepatitis and HIV infections each year [1]. Thus, significant potential for plastic hypodermic needles exists as an alternative to current steel needles. Plastic needles may reduce reusability and increase the opportunities for safe disposal. Plastic needles also will facilitate medical waste disposal by removing metal from the waste stream, hence making it easier to recycle needles and syringes into useful products such as car battery cases and pails.

The issues surrounding proper medical waste disposal and unsafe injections have been documented [1-15]. Often, cost is a major issue, especially for developing countries

that lack the resources and materials for proper waste disposal. Due to improper disposal, unsafe injections are frequently given, resulting in the spread of blood-borne diseases. As a result, many attempts have been made to provide for safer disposal and to prevent needle reuse. Some technologies focus on better destruction of existing needles [2, 3, 5], while others focus on preventing reuse, but do nothing for proper disposal [11-15]. Another approach is to refine the needles themselves so that neither disposal nor reuse is a problem. For certain medications, microneedles can be an effective means of delivery, and metal, silicone, and biodegradable polymer microneedles have been extensively studied [16-19]. However, these require that the molecules comprising the medicine are small enough to be delivered by the microneedles and absorbed via the skin. For many medications and vaccines, this is not a viable option.

Therefore, hypodermic needles will continue to be the primary means of conveyance of most drugs, and the needles must be refined to solve the problems of disposal and reuse. Previously, prototype plastic hypodermic needles were produced and tested [20, 21]. These were fabricated by injection molding using a metal wire core. Their hole was located at the end of their cannula, and they were approximately 25 mm long. Another research group created polymer needles specifically for patients receiving insulin [22]. Their focus was primarily on the manufacture of the needles, as the needles were neither rigorously tested nor refined. For this thesis, the research involved extensive testing, both physical and simulated, to determine the effectiveness of a certain design of plastic hypodermic needles.

1.2 Needle used for testing

The plastic needles studied for this paper are manufactured by SS&B Technology Ltd., Australia. They have a 38.1 mm long cannula, a 0.72 mm outside diameter at the tip, and a 70% ID/OD ratio. This diameter corresponds to a traditional 22 gage needle. The needles taper over the length of the cannula to an outside diameter of 1.2 mm at the hub. The hub is 8.25 mm long, has an OD of 4.6 mm and an ID of 4.1 mm (Figure 1) to fit a Luer slip connection, and has a mass of 0.15 g. Unique features of the needle are its taper, which is not easy to form with a steel needle and leads to a more efficient mechanical design, and that its hole is on the side rather than at its tip, which allows for a solid, stronger tip and reduces coring of the rubber vial stoppers, which can contaminate vaccines or other medicines.

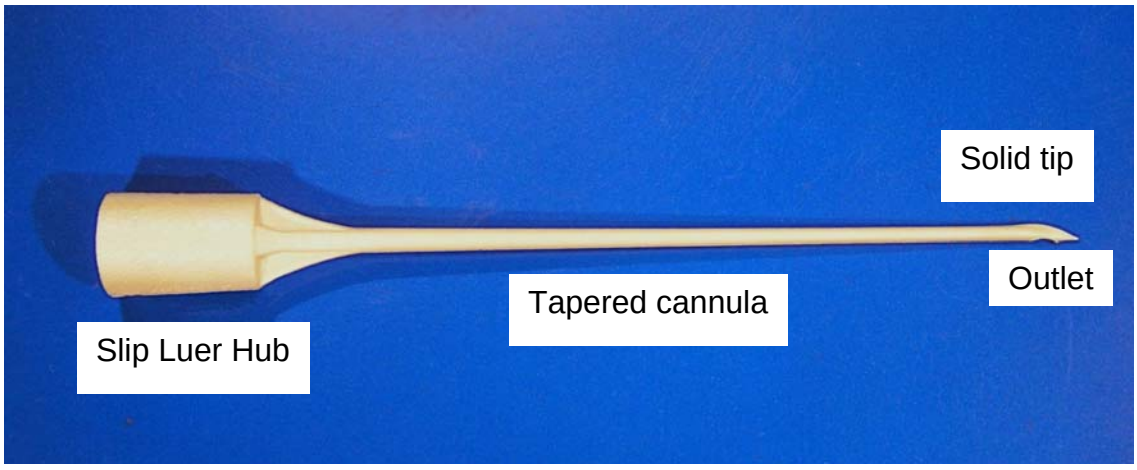

Figure 1 - 38.1 mm LCP needle

The plastic material utilized is Ticona Vectra 1300MT, an unfilled medical grade (USP class VI) liquid crystal polymer (LCP). LCPs feature a higher modulus and strength than traditional plastics, and have the unique feature of an increase in strength as

wall thickness decreases [23]. They also have good properties when subjected to creep and fatigue. LCPs can be easily molded because of their low shear viscosity and low thermal expansion coefficient [24], which allows them to be used in high temperature processes with minimal changes in dimensions. This is advantageous for creating large numbers of parts at relatively low cost. While the retail cost of Ticona Vectra 1300MT is $0.0836/g, the actual material cost per needle is $0.0125. A comparison between Ticona Vectra 1300MT and other engineering materials is shown in Table 1 [25]. The needles are manufactured using a gas-assisted injection molding (GAIM) process [26].

Table 1 - Mechanical properties of engineering materials compared to LCP

Material	Elastic Modulus (GPa)	Tensile Strength (MPa)
Ticona LCP 1300 MT	10.6	182
Polyethylene	1.67-4.18	27
Polyethylene-terephathalate	12.2	50
Polyamide 66	5.0	80
Polyamide 66 / 30% glass fiber	8.0	160
Steel	217	460
Aluminum	71	80
Glass	77.6	3500
Carbon	240-400	2100-2800

1.3 Objective

The goal of this thesis is to examine these plastic needles from theoretical, simulative, and experimental standpoints and to compare them to steel hypodermic needles. This involves analyzing needle buckling and penetration equations to ensure that the needles will penetrate skin before buckling. Finite element analyses (FEA) are performed to simulate needle buckling and penetration, and experimental buckling and

penetration tests are conducted to gage the needles' responses under more functional conditions. The insertion and friction forces during needle penetration are studied, and lubrication techniques are developed to limit these forces as much as possible. The needles are tested in polyurethane, pig skin, and butyl rubber to most accurately simulate actual operating conditions. Other tests to determine the strength of the needles and their ability to transmit fluid are included in this research. The results of these tests are analyzed to determine whether the plastic needles are capable replacements for steel hypodermic needles, and recommendations are made for modifications that will improve the plastic needles' performance.

1.4 Thesis outline

Chapter 2 focuses on the needles' buckling behavior. This includes applying the Euler buckling formulas to the needles to determine an approximate buckling load. FEA simulations are performed using solid models of the needles, and buckling tests are conducted to determine the actual buckling loads for the needles.

Chapter 3 examines the theoretical and simulative behavior of the needles during penetration. Equations are developed to calculate the strain in the skin and the loads on the needle before and during penetration. FEA simulations are conducted that simulate needle penetration into a skin mimic.

Chapter 4 presents the experimental tests performed on the plastic needles as well as steel needles and compares the results between them. Penetration media for these tests include polyurethane rubber as a skin mimic, pig skin, and butyl rubber vial stoppers. It

also focuses on lubrication techniques to reduce the friction between the needle and the penetration medium.

Chapter 5 describes other tests performed on the plastic needles, including perpendicular force tests, cannula stiffness tests, and fluid flow tests. These are necessary to comply with ISO standards.

Chapter 6 presents the conclusions of this research as well as recommendations for future work.

CHAPTER 2

NEEDLE BUCKLING

During a needle insertion, an axial load is applied by the syringe to the needle's hub. This force is resisted by the skin into which the needle is inserted. Under this loading scenario, the needle acts as a thin-walled column, for which buckling should be the most common and most likely failure mode. As a result, it is necessary to perform simulated and experimental buckling analyses on the needles. This provides a benchmark for the maximum loads that the needle can sustain before failure occurs.

2.1 Determination of theoretical buckling load

Buckling theory [27] is governed by Equation 1, the differential equation relating the internal moment of a column to its deflected shape.

$$EI\frac{d^2v}{dx^2} = M \tag{1}$$

In Equation 1, E is the material's elastic modulus, I is the moment of inertia, v is the deflection, x is the axial distance along the column, and M is the internal moment. Substituting $M = -Pv$, where P is the applied load and solving the resulting differential equation for the critical load, P_{cr}, yields Equation 2:

$$P_{cr} = \frac{\pi^2 EI}{(KL)^2}, \tag{2}$$

where L is the length of the column and K is an effective-length factor that takes into account the end conditions of the column and scales the equation accordingly. This is the Euler load, which is valid for long columns.

To determine whether this equation is accurate for this problem, it is necessary to verify that the needles used in this analysis can be represented as long columns. This requires the use of the needle's slenderness ratio, defined as KL/r, where r, the radius of gyration, is equal to $\sqrt{I/A}$, where A is the cross sectional area of the needle. The critical length, L_{cr}, determines the validity of the Euler buckling load, and is defined in Equation 3 [28] as:

$$L_{cr} = r\pi\sqrt{\frac{8E}{\sigma_y}}, \tag{3}$$

where σ_y is the compressive yield strength of the material. The properties of the needle, including all values for these equations, can be found in Appendix D. Assuming that the compressive yield strength is identical to the tensile yield strength, the critical length, taken for an average diameter of 0.96 mm, is 28.3 mm. As this is shorter than the needle length of 38.1 mm, the Euler buckling formula can be used to evaluate the buckling characteristics of the needles. For the 25.4 mm length needles, the average diameter is 0.88 mm, and the critical length becomes 26.0 mm. As this figure is close to the actual length of the needles, both the Euler formula and the Johnson formula for intermediate length columns are utilized to determine the theoretical buckling load. Equations 4 and 5 describe the Johnson buckling formula [28].

$$\frac{P_{cr}}{A} = \sigma_y - b\left(\frac{L}{r}\right)^2 \tag{4}$$

$$b = \frac{1}{4E}\left(\frac{\sigma_y}{2\pi}\right)^2 \tag{5}$$

Using the Euler buckling formula, the critical load is approximately 6.1 N for the 38.1 mm length needles and 9.7 N for the 25.4 mm length needles. When the Johnson formula is applied to the 25.4 mm needles, the resulting buckling load becomes 19.0 N. These results are estimates because of the irregular shape of the needles, the inexact direction and location of loading at the needle tip, and the estimate of the end conditions on the cannula. However, they do provide estimates of the needles' buckling loads, and these results can be verified by both finite element analysis and experimental testing.

2.2 Buckling finite element analysis

2.2.1 Model and meshing

A finite element analysis (FEA) was performed to determine the loads that caused the cannula to buckle. This test utilized the ANSYS Workbench versions 10.0 and 11.0 software. The first step was to create solid models of the needle from the surface models generated at SSB. These were generated using Solidworks 3D CAD software. From the original design, which contained the same shape and dimensions as the actual needle, multiple models were subsequently created, reflecting possible changes in the design. These models each featured different configurations with changes in the cannula taper (either tapered or straight), length (38.1 mm, 25.4 mm, or 19.0 mm), and cross sectional shape (round or elliptical). For the straight needle models, the OD of 0.72 mm was constant over the length of the cannula. The cross sectional shape reflects the geometry of the actual needles, which feature an elliptical cross section, as opposed to one that is perfectly round, which would typically be present in a hypodermic needle. By generating

multiple needle configurations for FEA testing, it would be possible to determine which would be more effective in practice from a buckling standpoint. The 38.1 mm length, tapered needle is shown in Figure 2, and its mesh is shown in Figure 3.

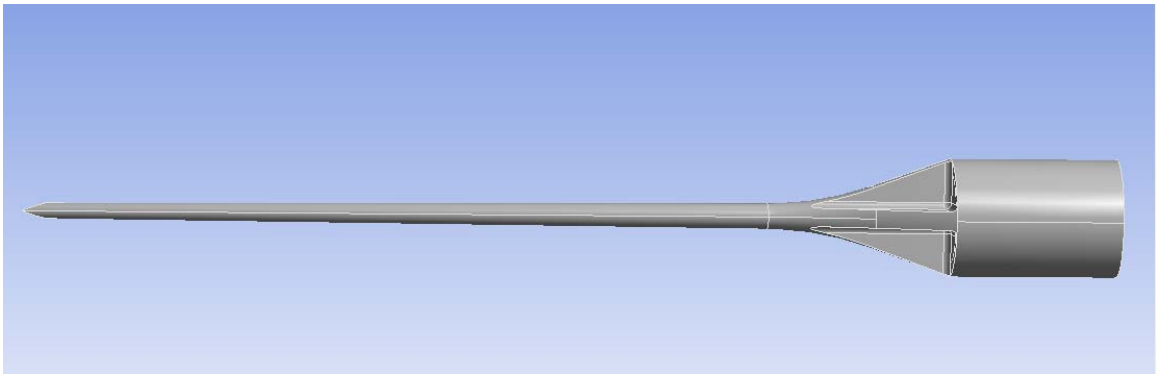

Figure 2 - Needle solid model geometry

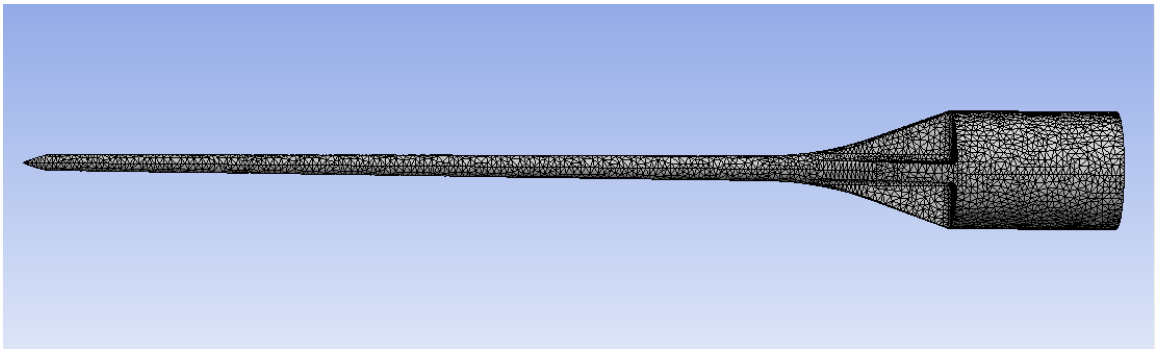

Figure 3 - Needle solid model mesh

The mesh was generated through the "automatic" option within the software, creating tetrahedral elements. Trial tests showed convergence of the solution for an element size of 0.2 mm. The end conditions were chosen to reflect those present when a needle penetrates the skin. In the model, the hub was given a fixed end condition, which

allows for no displacement or rotation. This simulates the condition during loading, in which the hub is held in place by the syringe to which it is attached. The tip was given a fixed displacement during the simulation. With the orientation of the needle aligned so that the length is along the x axis, the displacement was fixed so the y and z axes were restricted from displacement. This allowed free movement in the x direction, as well as free rotation about any of the three axes, simulating a pinned joint end condition. These constraints on the movement of the needle replicated its motion during initial contact with the skin. The load acting along the needle was simulated in the FEA by applying a point load to the tip, acting along the x axis. A load of 1 N was applied, which was used to "scale" the analysis. The needle models have the material properties (elastic modulus, Poisson's ratio, yield strength) found in Appendix D.

2.2.2 FEA results

The results from the FEA include a load factor, which is a multiplier that, when multiplied by the applied force, provides the actual buckling load. By inputting 1 N as the applied load, the output will be the actual buckling load for the first buckling mode. The FEA conditions and results are summarized in Table 2. For comparison, two tip conditions were simulated – sharp and blunt. This enabled the effect of the presence of the tip on the results to be determined. A representative result of the deformation, showing a tapered 38.1 mm length needle, is shown in Figure 4 and the von Mises stress is shown in Figures 5 and 6. More results are included in Appendix F.

Table 2 - Buckling FEA results

Length (mm)	Cross-Section	Taper	Sharp tip load (N)	Blunt tip load (N)
38.1	Circular	Tapered	7.88	4.86
38.1	Elliptical	Tapered	6.68	3.19
38.1	Circular	Straight	2.88	1.73
38.1	Elliptical	Straight	2.94	1.31
25.4	Circular	Tapered	15.64	11.08
19.0	Circular	Tapered	26.17	20.12
25.4	Circular	Straight	6.36	4.11
19.0	Circular	Straight	11.14	7.76
25.4	Elliptical	Tapered	13.44	7.33
19.0	Elliptical	Tapered	24.63	13.42
25.4	Elliptical	Straight	6.44	3.13
19.0	Elliptical	Straight	12.92	5.97
38.1	Circular	(1/3) Tapered / (2/3) Straight	4.01	-
38.1	Elliptical	(1/3) Tapered / (2/3) Straight	3.11	-
38.1	Circular	(1/2) Tapered / (1/2) Straight	4.46	-
38.1	Elliptical	(1/2) Tapered / (1/2) Straight	3.53	-

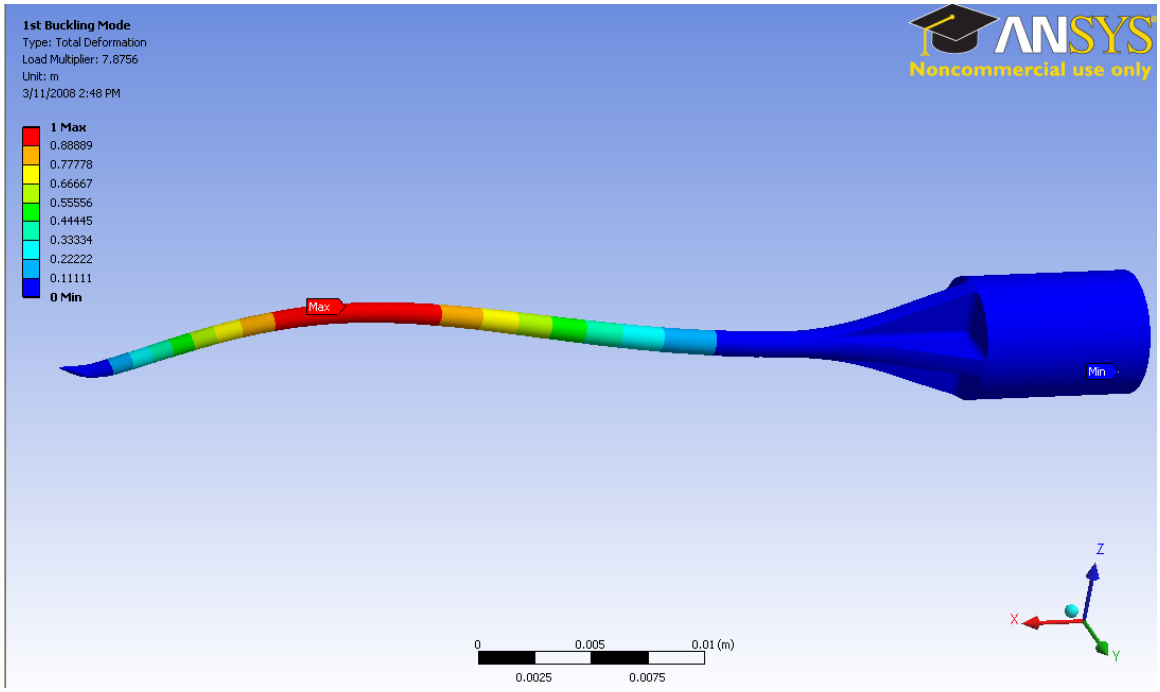

Figure 4 - Needle deformation in ANSYS buckling simulation (38.1 mm length, tapered cannula, circular cross section)

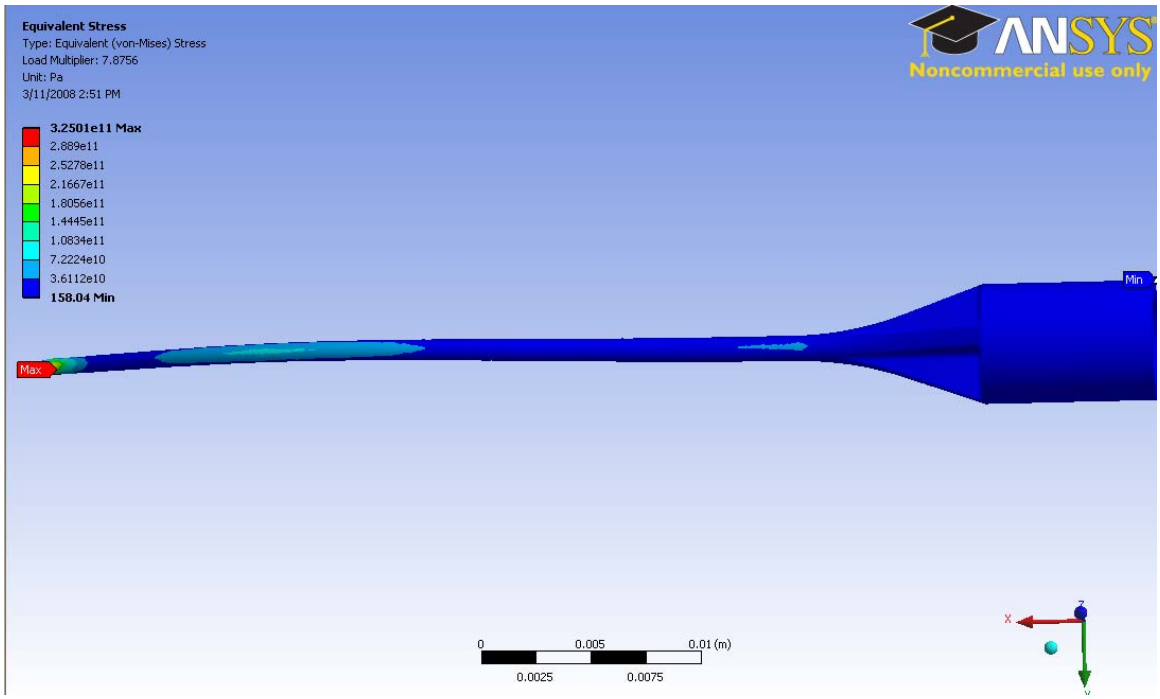

Figure 5 - von Mises stress distribution in ANSYS buckling simulation (38.1 mm length, tapered cannula, circular cross section)

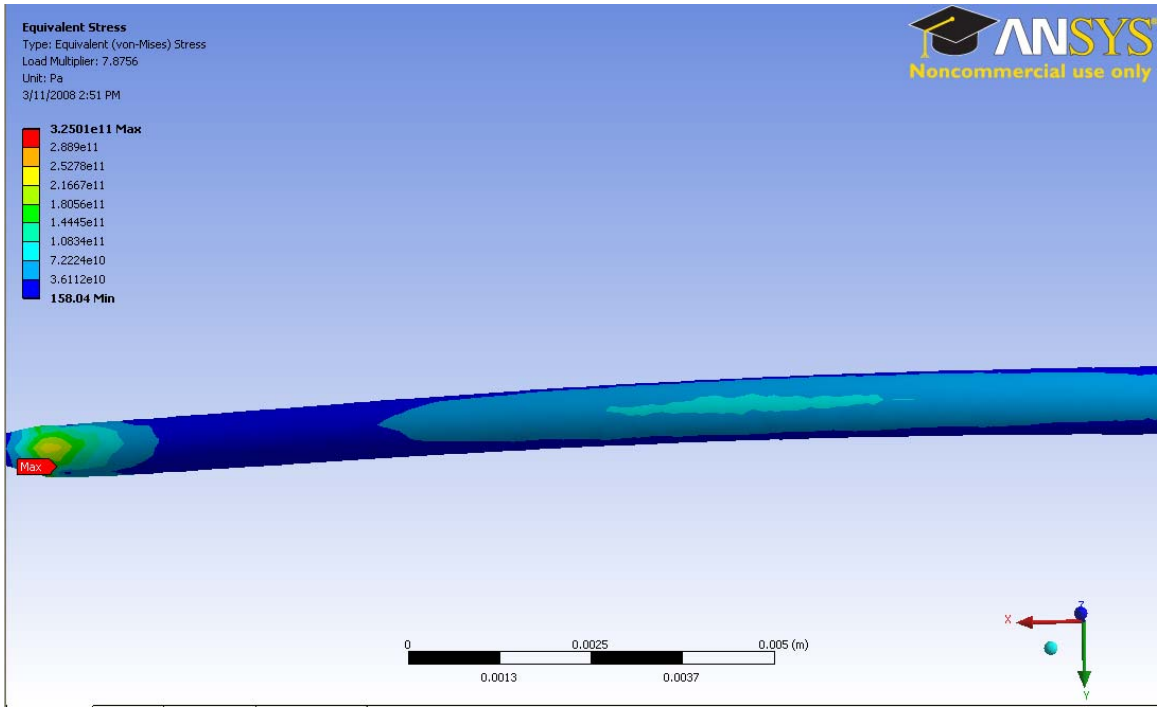

Figure 6 - von Mises stress at needle tip (38.1 mm length, tapered cannula, circular cross section)

The buckling simulations showed many trends concerning the effects of the variables. For both tips, the tapered needles had a buckling strength 125-175% greater than the straight needles of the same length and cross section at the tip due to the increased diameter at the hub. In addition, needles that had a combined straight/tapered cannula (straight at the tip, tapered near the hub) had strengths between those of the straight needles and those of the tapered needles, with the strength increasing as the length of the tapered section increases. For tapered needles, an elliptical cross section has a buckling strength 6-17% lower than the round cross section (here the major axis of the elliptical cannula is the same size as the diameter of the cylindrical cannula). However, for elliptical, straight needles, the opposite trend exists; the buckling strength is 1-17% higher than the elliptical, tapered needle's strength. Changing the length also had a large effect on the buckling strengths. Reducing the length from 38.1 mm to 25.4 mm increased the strength 98-120%. Further decreasing the length from 25.4 mm to 19.0 mm increased the strength another 68-100%. Removing the tip yields a decrease in the buckling force for all needle designs with the given end condition. These results provide a range for the results of actual buckling tests.

The results also indicate a difference in the buckling loads between the sharp tipped model and the blunt tipped model. For each needle configuration, the models with sharp tips consistently show a 30-109% higher buckling load than the blunt tipped models. This is beneficial in that it shows that under the conditions under which the needles are subjected, they are stronger than traditional columns. This result may be due to the area on which the load is placed, namely, the entire tip. The range of these results provides a reasonable estimate of the actual buckling strength of the needles.

Thus, from a pure buckling perspective, the 19.0 mm long tapered needles would be most favorable for implementation. This is expected, as column buckling theory would lead to the conclusion that shorter columns have higher buckling loads because the critical load increases as the column's length decreases. Also, the tapered columns feature more material than straight columns and can therefore resist higher axial loads. However, from a more practical view, these needles may be too short to be effective for many uses of hypodermic needles. Thus, although the simulated buckling loads are a factor in the determination of the most appropriate needle, other forms of testing are required to make the best choice for a suitable plastic hypodermic needle.

2.3 Experimental buckling tests

To confirm the results of the FEA simulations, buckling tests were conducted on plastic hypodermic needles as per the "Single Needle Testing Protocol" in Appendix A.

2.3.1 Mechanical testing machine

The tests were conducted using an Instron model 33R4466 testing machine (Instron Corp., Canton, MA) utilizing the Series IX software. The machine was upgraded to a 3300 model using the Bluehill version 2.0 software during the thesis research. The machine, shown in Figure 7, consists of a crosshead that moves vertically, a load cell attached to the crosshead, and either an aluminum plate at the base for buckling tests, or a fixture at the base to support the rubber/skin samples for penetration tests. The needles were attached via the hub to a 25 N capacity load cell (Interface SMT1-25N, Scottsdale, AZ), which transmits the measured force to the computer. The connection simulates the

manner in which the needles are attached to a syringe, which is from the inside of the hub.

2.3.2 Test conditions

The buckling tests were performed by driving a needle vertically into an aluminum plate at 60 mm/min, similar to the speed of the penetration tests described in Chapter 4. The needles were tested with their tips intact, as that is the condition in which they will be used in practice. Side motion of the needle was prevented by a small dimple in the aluminum plate. This more accurately replicates the test from the FEA, in which the buckling is modeled as a fixed-pinned condition. The lack of a dimple would create a fixed-free buckling condition due to the low levels of friction between the plate and the needles. This is not representative of a needle insertion loading scenario.

2.3.3 Buckling test results

The tests showed that buckling occurs at axial force levels of between 4 and 6 N. Similar results were achieved for the 25.4 mm long needles (needle 9 from Table 2) – 10 to 12 N – and the 19.0 mm long needles (needle 10 from Table 2) – 21 to 22 N. The results are summarized in Table 3. These tests validated the results from the FEA simulations for the expected buckling force at each length of the needle. Pictures of the needles after buckling are included in Figures 8-10, and a comparison of the needle tip prior to and following buckling is seen in Figure 11.

Table 3 - Plastic needle buckling results

Length (mm)	Buckling load (N)
38.1	4.4
38.1	4.8
38.1	5.3
38.1	5.3
25.4	10.4
25.4	11.6
19.0	21.7
19.0	21.4

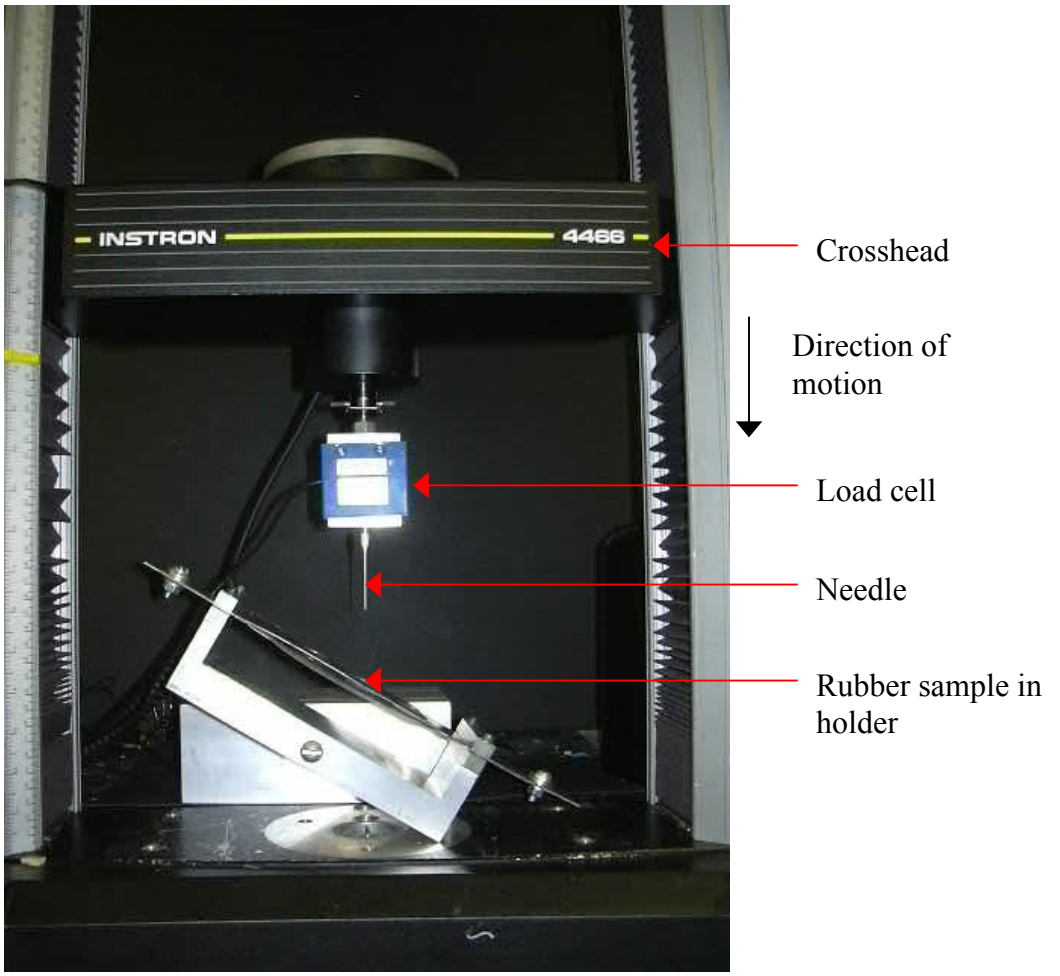

Figure 7 - Instron mechanical testing machine (shown in a steerability test setup)

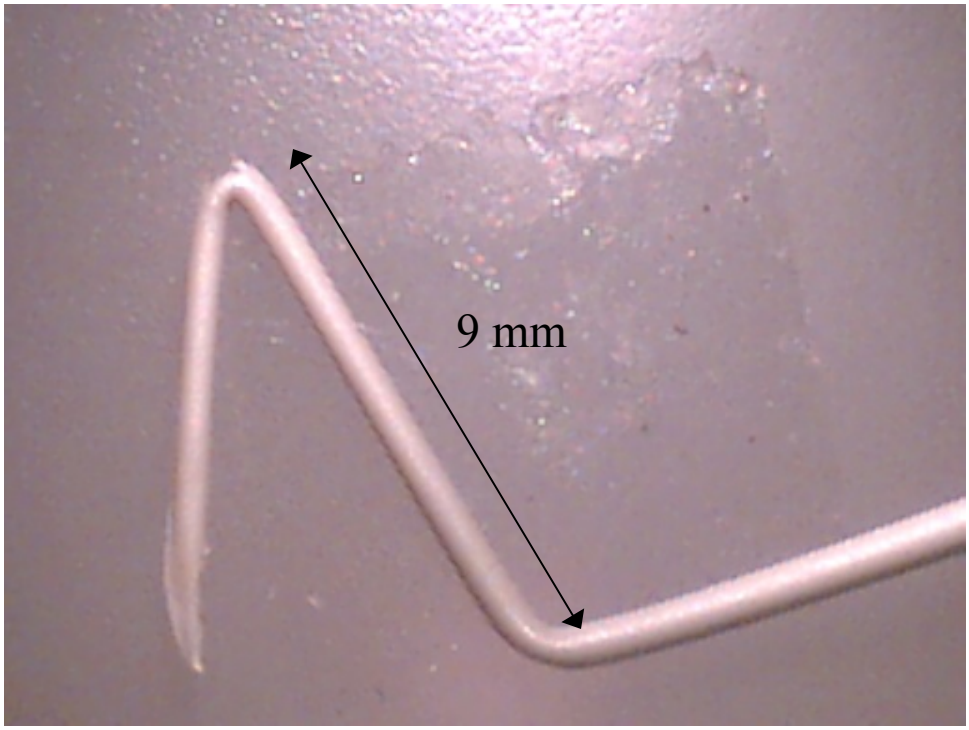

Figure 8 - Needle following buckling (38.1 mm length)

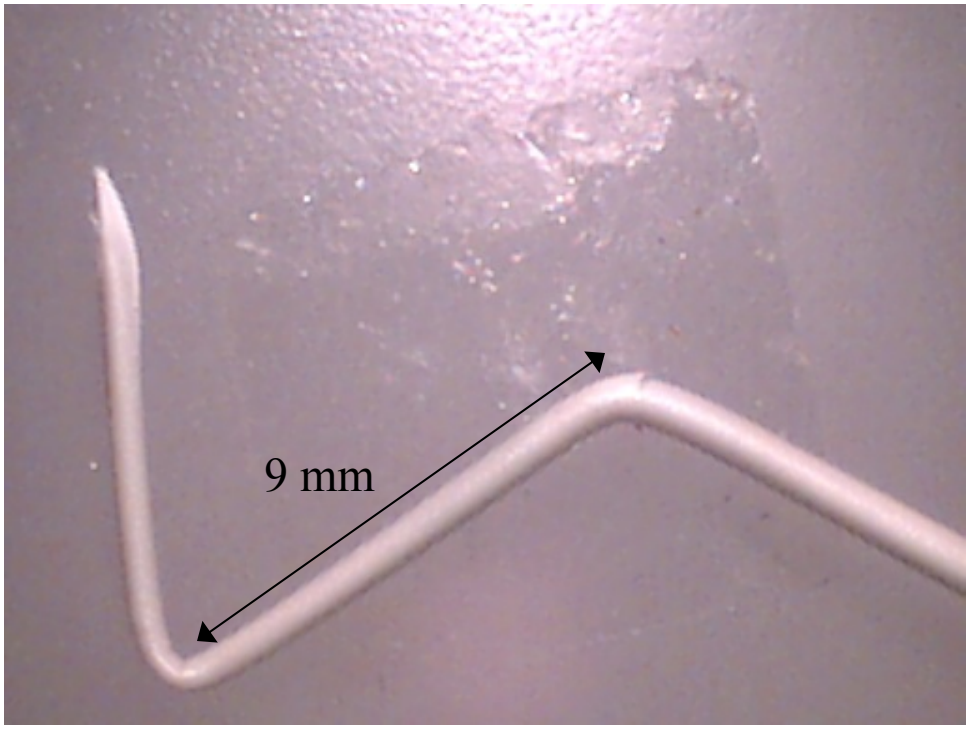

Figure 9 - Needle following buckling (38.1 mm length)

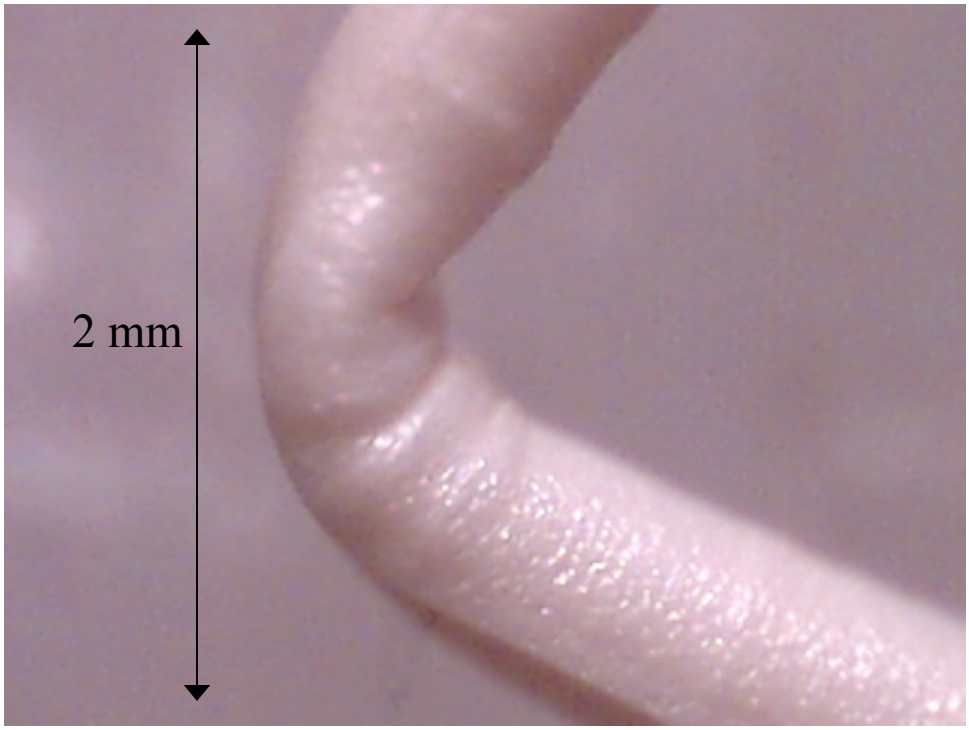

Figure 10 - Closer view of needle bending (38.1 mm length)

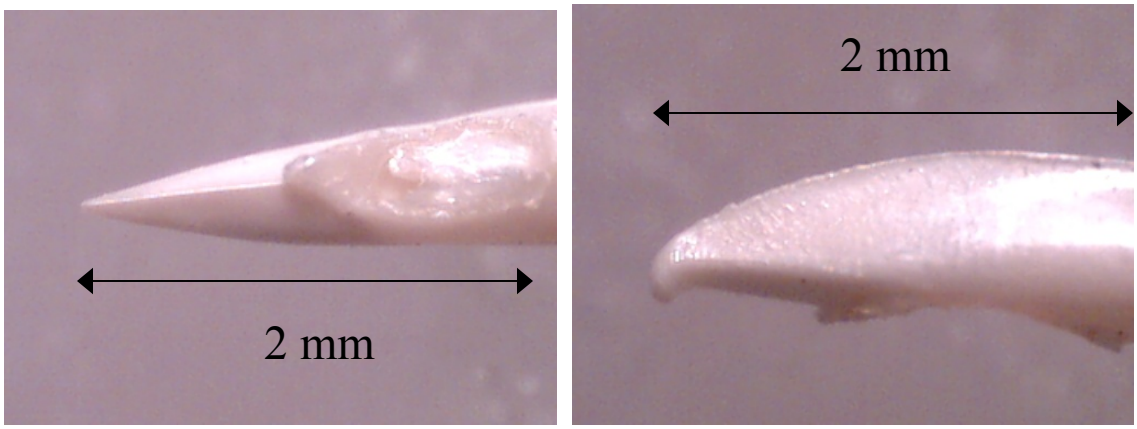

Figure 11 - Shape of needle tip before (left) and after (right) buckling (38.1 mm length)

2.4 Discussion

The needle buckling tests indicate that the buckling forces increase as the needle length decreases, with all other factors held constant. They also show consistent results among the three tests performed. For the 38.1 mm length tapered plastic needles, the Euler buckling equations predict buckling at 6.1 N, the FEA predicts buckling at 3.2-7.9 N, and the experimental tests show buckling at 4-6 N. Similarly, for 25.4 mm length tapered plastic needles, the equations predict buckling at 9.7 N, the FEA simulation predicts buckling at 7.3-15.6 N, and the experiments show buckling at 10-12 N. These results are summarized in Table 4. This demonstrates the accuracy of both the analytical equations and the FEA, which indicates that these are suitable predictors for needle behavior.

Table 4 - Needle buckling results summary

Needle Length (mm)	Buckling Load - Equations (N)	Buckling Load - FEA (N)	Buckling Load - Testing (N)
38.1	6.1	6.7	4-6
25.4	9.7	13.4	10-12

2.5 Summary

In this chapter, needle buckling simulations were performed on the ANSYS Workbench software package. These were compared to actual buckling tests conducted on the needles. The buckling tests provide benchmarks for the penetration tests in Chapters 3 and 4, as penetration must occur at lower forces than the buckling loads from these tests for plastic needles to be successful. Given the accuracy of the equations and

FEA at predicting the results of the experimental tests, these two methods will be used in Chapter 3 to analyze the loads that occur during needle penetration.

CHAPTER 3

NEEDLE PENETRATION – THEORY AND SIMULATIONS

A needle insertion is performed by forcing the needle against an object until it penetrates. This is one of the two primary goals of a hypodermic needle injection, with the other being the safe delivery of the fluid transmitted through the needle either to or from the object receiving the insertion. As a result, it is crucial to demonstrate that the plastic needles are capable of penetrating skin. This involves both computer modeling and experiments. In this chapter, FEA simulations will model the needle's ability to penetrate a skin mimic, and the FEA results will be verified by penetration experiments in chapter 4. The theory behind needle penetration also will be discussed.

3.1 Penetration theory

Needle penetration into human skin (or a skin substitute) can be broken down into three components. The first component, a trampoline effect that occurs as the load transmitted from the needle increases, takes place prior to penetration. This consists of the skin sagging in the vicinity of the needle while the needle continues downward against the skin. The second component, the penetration itself, is characterized as a tearing of the skin as the needle punctures it. These two components of needle penetration are different mechanical functions and are described by two independent sets of equations in this thesis. The third component is the sliding that occurs following the

penetration. This component is highly variable depending on the needle's lubrication and the penetrated medium. Equations were not developed for this latter frictional force. However, it was measured during the penetration experiments, and these results can be found in Chapter 4.

3.1.1 Bending prior to penetration

The first component of penetration is a combined action of skin bending and stretching. During a needle penetration, skin within a localized region of the penetration is deformed by bending and stretching, while skin outside this region is unaffected. To simulate this behavior using a rubber skin mimic, the rubber is clamped in place, leaving an exposed area in the center where the penetration and localized deformation occur. With this physical constraint applied, the bending represents the change in the angle of the sheet from flat over time from where it is in contact with the needle to where it is clamped in the supporting fixture, and the stretching represents the change in distance between those two locations. The bending, illustrated in Figure 12, is similar to sheet metal bending, in which a punch is lowered onto a flat sheet of metal and bends it into the shape of the die below. The stretching is equivalent to a tensile load applied to the edges of a plate.

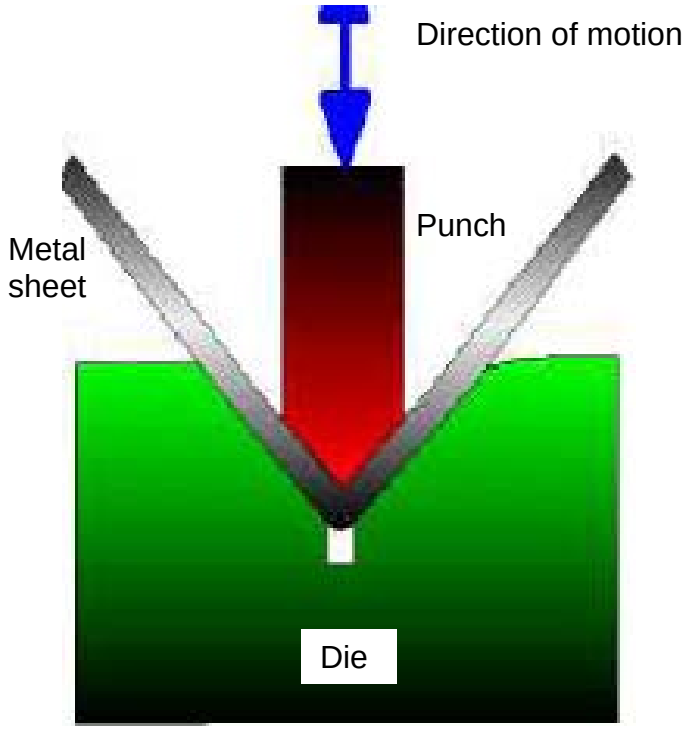

Figure 12 - Schematic of sheet metal bending

When analyzing sheet metal bending, it is important to note the plastic (as opposed to elastic) deformation in the part, which is a controlled failure of the part. This is also relevant to the bending of the polyurethane prior to penetration, as deformation occurs as the needle penetrates the polyurethane. Until penetration, the deformation is purely elastic. Failure is assured when the tensile strain in the sheet is greater than the elastic strain. The tensile strain in the sheet created by bending, ε_t, is given by Equation 6, and is illustrated in Figure 13.

$$\varepsilon_t = \frac{\Delta \ell}{\ell} = \frac{\overline{OA'} - \overline{OA}}{\overline{OA}} \tag{6}$$

By applying the substitution $l = r \cdot \theta$, the tensile strain becomes Equation 7.

$$\varepsilon_t = \frac{\left(r_p + t\right) \cdot \theta - \left(r_p + t/2\right) \cdot \theta}{\left(r_p + t/2\right) \cdot \theta}, \tag{7}$$

where r_p is the punch radius, θ is the angle created by the bending, and t is the thickness of the sheet. This equation simplifies to Equation 8.

$$\varepsilon_t = \frac{t/2}{r_p + t/2} \tag{8}$$

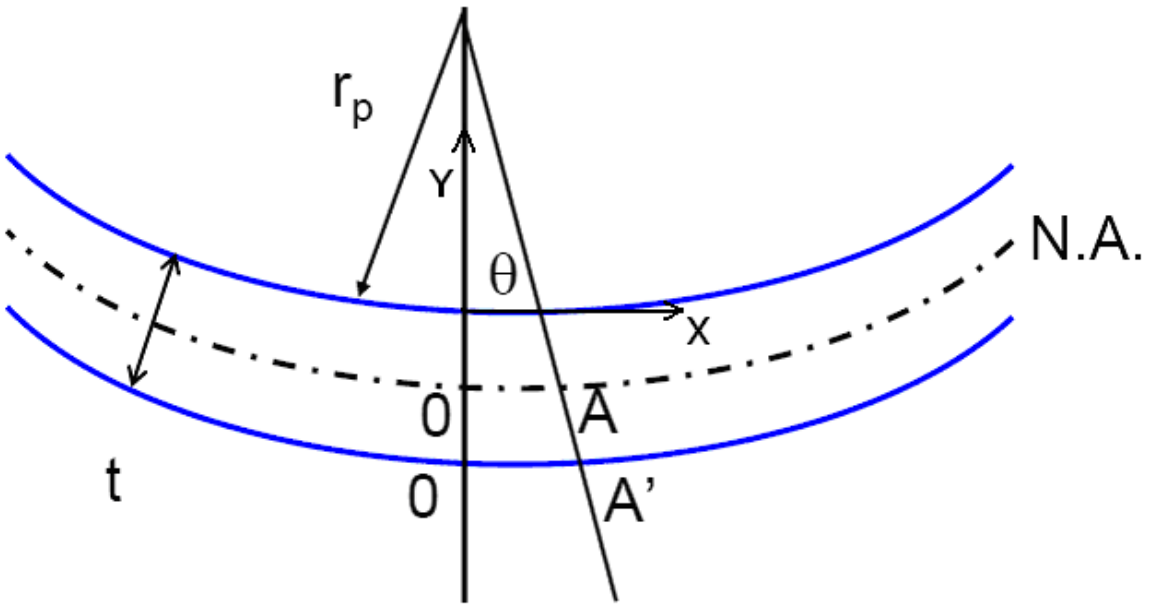

Figure 13 - Strain in sheet during bending

This is valid, given the assumption that the neutral axis (N.A.) is located at t/2, as shown in Figure 13. The neutral axis is an axis along which no stresses or strains are present.

3.1.2 Stretching before penetration

The polyurethane and skin also experience stretching before needle penetration. This is a straightforward tensile stretch, with a stress of $\sigma = F/A$, where F is the applied

force and A is the cross-sectional area, and, from Hooke's Law, a strain, ε, is shown in Equation 9.

$$\varepsilon = \frac{F/A}{E} \tag{9}$$

Combining these two parts of the strain yields Equation 10, the overall strain acting on the polyurethane prior to actual penetration occurring.

$$\varepsilon = \frac{t/2}{r_p + t/2} + \frac{F/A}{E} \tag{10}$$

To measure the deformation prior to penetration, this strain must equal the elastic strain in the polyurethane, which is represented as Equation 11.

$$\varepsilon_{elastic} = \frac{\sigma_{yield}}{E} \tag{11}$$

Thus, the strain equation that describes the lowering of the needle into the polyurethane before penetration is described by Equation 12.

$$\frac{\sigma_{yield}}{E} = \frac{t/2}{r_p + t/2} + \frac{F/A}{E} \tag{12}$$

The outer skin layer is the only one included in these calculations. It is tougher than the other layers (see Table 5), and the polyurethane skin mimic, into which the needles are being penetrated during the experiments, only simulates the epidermis layer. The subsurface layers are thus ignored for these calculations.

Table 5 - Properties of skin [29], [30]

Layer	Thickness (mm)	Elastic Modulus (MPa)
Stratum Corneum	0.01-0.02	12000
Living Epidermis	0.03-0.13	16
Dermis	1.1	12
Subcutaneous Fat	1.2	20

Inserting the known values of the polyurethane material properties, found in Appendix D, into Equation 12 yields the maximum load attained prior to plastic strain in the polyurethane. With a measured needle tip radius of 0.043-0.065 mm (see section 4.1 and Appendix G, Table 40), the calculated penetration load ranges from 3.98-7.33 N.

3.1.3 Penetration

The second component of the penetration is the actual puncture of the rubber or skin. The governing equations for this action, Equations 13-15, were derived by Shergold and Fleck [31] as the penetration of a soft solid by a sharp-tipped punch. These are applicable to hypodermic needle punctures into skin.

$$P_S \cdot \delta\ell = \delta W_C + \delta S_E \tag{13}$$

$$\delta W_C = 2J_{IC} \cdot a \cdot \delta\ell \tag{14}$$

$$\delta S_E = R^2 \cdot \mu \cdot \delta\ell \cdot h\left(\frac{a}{R}\right) \tag{15}$$

where P_S is the load required to advance the punch, δl is an incremental depth into the solid, δW_C is the work required to create a crack in the solid, δS_E is the work required to open the crack, J_{IC} is the fracture toughness of the solid, a is half the crack length, R is the radius of the needle at the tip, μ is the shear modulus of the polyurethane/skin, and $h(a/R)$ is a nondimensional function that represents the stretching of the crack as a function of the crack length and punch radius. The shear modulus can be determined from the elastic modulus, E, and Poisson's ratio, v, of the polyurethane via Equation 16.

$$\mu = \frac{E}{2(1+\nu)} \tag{16}$$

The dimensionless function *h(a/R)* is evaluated from the average penetration pressure on the punch, p_S, determined by Equation 17.

$$\frac{p_S}{\mu} = \frac{2}{\pi}\left(\frac{J_{IC}}{\mu R}\right)\left(\frac{a}{R}\right) + \frac{1}{\pi}h\left(\frac{a}{R}\right) \tag{17}$$

Shergold and Fleck generated graphs of p_S/μ vs. $J_{IC}/\mu R$ and a/R vs. $J_{IC}/\mu R$ for different values of α, a strain hardening exponent for the material. The constant α can be found using the Ogden strain energy density function [32] in Equation 18.

$$\sigma = \frac{2\mu}{\alpha}\left(\lambda^{\alpha-1} - \lambda^{-1-\alpha/2}\right) \tag{18}$$

Substituting the yield stress of the polyurethane for σ and assuming a stretch ratio (λ) of 2.9 due to the strain at puncture of 1.9 from $\varepsilon = \sigma/E$ and $\lambda = 1 + \varepsilon$ yields a value of 2.02 for α. With a known α and the necessary mechanical properties of the polyurethane, *h(a/R)* can be determined from the equation for the penetration pressure on the punch. These equations are valid for skin because it can be modeled as a soft solid in the same manner as the polyurethane.

3.1.4 Determination of theoretical penetration force

Substituting the necessary values into Equations 13-15 yields the required force for penetration to occur. As the fracture toughness for polyurethane was unobtainable, values similar to those of silicone rubber (9100 N/m) and human skin (2500 N/m) [31] were chosen, and the penetration force was determined. Also, the shear modulus was varied to obtain a more accurate range of data for the penetration force. With polyurethane as the skin mimic, this force varies from 1.6-3.5 N. The experimental tests in Chapter 4 will verify the validity of these values for the penetration force. The

penetration force in polyurethane is shown as a function of the possible fracture toughness values in Table 6. Also shown are the forces required to create the crack and to open the crack in the rubber. For human skin, using known properties [31], the penetration force is approximately 1.9 N. These numbers can vary based upon the strength of the puncturing device, tip design, and friction, but they provide a basis to estimate the penetration force.

Table 6 - Theoretical penetration load in polyurethane

J_{IC} (N/m)	Penetration Force (N)	Force to Create Crack (N)	Force to Open Crack (N)
2000	1.63	0.72	0.91
4000	2.17	0.86	1.31
6000	2.65	0.86	1.78
8000	3.05	0.57	2.48
10000	3.53	0.72	2.81

These results indicate that as the fracture toughness increases, the required penetration force increases. In addition, the overall force required to create a crack in the rubber under these penetration conditions remains relatively constant. This is primarily due to the combination of increased work in creating the crack in a tougher material and a decreased crack size as toughness increases. However, the required force to open the crack increases steadily as the fracture toughness increases. This occurs because of the decreased crack size found in the tougher material. As the initial crack created is smaller, more force is then required to expand the crack to obtain the hole size necessary for needle insertion.

3.2 Finite element simulations

Finite element simulations are conducted to model the needle's behavior during penetration into a rubber skin mimic. This enables the results of the penetration tests and the stress distribution during penetration to be determined.

3.2.1 Penetration simulation setup

The FEA penetration simulations are performed using ABAQUS version 6.6-1. The model consists of the needle model from the buckling experiments and a thin rectangular piece used to represent the rubber. A dynamic, explicit test is run to characterize the needle's motion into the rubber. The needle model used for this analysis is the same model used for the buckling simulations that represented the needles that were manufactured for this research, with a length of 38.1 mm and a tapered cannula. The rubber model was created as a thin, circular sheet approximately the size of the exposed rubber area in the penetration tests. The parts then were meshed within the program. Meshes are generated by creating seeds on the part, which specify the mesh density, and then creating elements throughout the part that correspond to the seed size in each region of the part. Both the needle and the rubber were meshed with a variable seed size. This allowed smaller elements to be generated near the tighter radii along the needle and larger elements around areas of fewer critical features. For the rubber, smaller elements were generated in its center near the needle insertion point and larger elements towards the edges, where such accuracy is less important. As both parts were three-dimensional, they were assigned three-dimensional element types for the mesh. The

rubber was free meshed with hexahedral elements, and the needle was structure meshed with tetrahedral elements.

The parts also were assigned a material definition that corresponded to the properties of the materials from which they are comprised. Standard SI units were chosen; as all dimensions in ABAQUS have no units, they must be held consistent relative to each other. Both materials were modeled with elastic-plastic behavior, as modeling the rubber as hyperelastic yielded inaccurate results. The needle was given a density of 1400 kg/m^3, an elastic modulus of 1.06×10^{10} Pa, a Poisson's ratio of 0.3, and a yield stress of 6×10^7 Pa. The rubber had a density of 1185 kg/m^3, a Young's modulus of 1.59×10^7 Pa, a Poisson ratio of 0.5, a yield stress of 4.7×10^6 Pa, and a fracture strain of 100% (see Appendix D). Both materials were approximated as isotropic, even though the needle has some anisotropy [33]. These parameters were provided in the literature [23, 34] for each product with the exception of the elastic modulus of the rubber, which was determined experimentally from tensile tests conducted on polyurethane samples in accordance with ASTM D882-02 [35]. The tests were conducted on rubber samples measuring 100 mm × 12 mm × 0.37 mm, and stress-strain curves were generated from the five load extension curves included in Appendix D to determine the rubber's material properties.

To create the assembly, the needle is oriented perpendicular to the rubber with the tip touching the rubber's top surface. Although penetration tests, as well as most actual needle insertions, are run with the needle not initially contacting the skin (or rubber), the FEA can have initial contact because the test is run with the needle moving at a constant velocity. The needle will not change as it is passing through air in the simulation, so

computing power and time can be saved by the given initial location of the needle. One time step is used for the simulation, as the boundary conditions do not change over time. The boundary conditions are chosen to include a fixed condition (no displacement or rotation) over the edges of the rubber, and a constant velocity of 1.667 mm/s, the speed at which the penetration tests are run, is applied to the top surface of the needle hub. Other conditions, with the exception of the interactions between the two objects, are set to the ABAQUS defaults. The model assembly is shown in Figure 14.

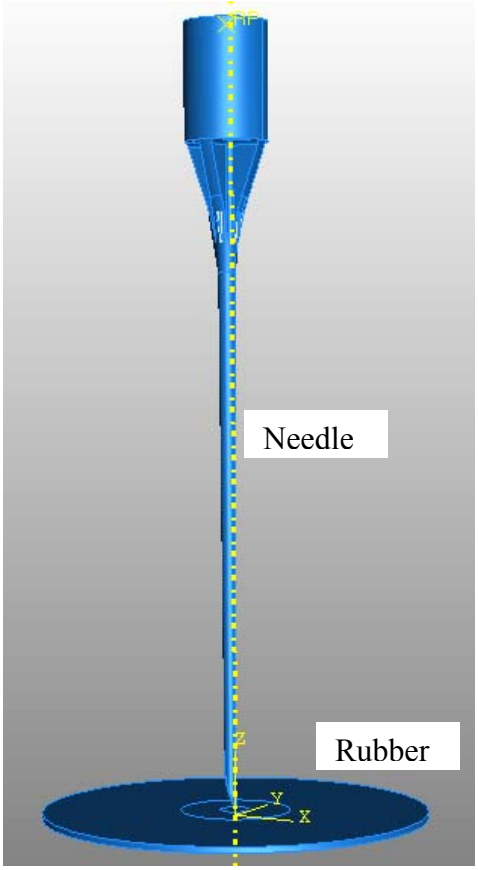

Figure 14 - FEA penetration setup

An interaction must be created between the contacting surfaces of the two objects. The interaction properties should include the ABAQUS defaults with the exception of adding a friction component to the model. However, these simulations were run approximating the contact as frictionless. Given that the friction coefficient is unknown, much iteration would be required to obtain the correct value. As this work was performed to generate a reasonable penetration model, future work should focus on optimization. For the interaction itself, either general contact or surface-to-surface contact, both of which work in an explicit framework, can be chosen, as the differences between the two are minimal. General contact between two surface pairs is used for this analysis, with the surface pairs being the contacting surfaces of the parts. After the setup is complete, the simulation is performed.

3.2.2 Penetration simulation results

Two different models were run for the penetration simulations. The first, described above, modeled the needle as a deformable body. The second modeled the needle as a rigid body.

3.2.2.1 Deformable needle results

The penetration simulation indicated that the needle should not be able to penetrate the polyurethane, even under frictionless conditions. Despite changes in the code (see Appendix C) that would allow for greater deformation than the ABAQUS defaults, thus creating an unrealistic deformation condition, the simulation still aborted due to excessive deformation in the needle, specifically around the area of the tip. This

indicates that either changes in the tip design or a reduction in the length of the needle is necessary for successful penetration. Although the failure occurred near the tip, as seen in Figure 15, it could be due to instability caused by the length of the needle. It is also apparent in Figures 16-18, which show the needle with the rubber removed at different time steps in the penetration, that the von Mises stress distribution throughout the needle is significantly lower than the stresses found at the tip where the needle deformed.

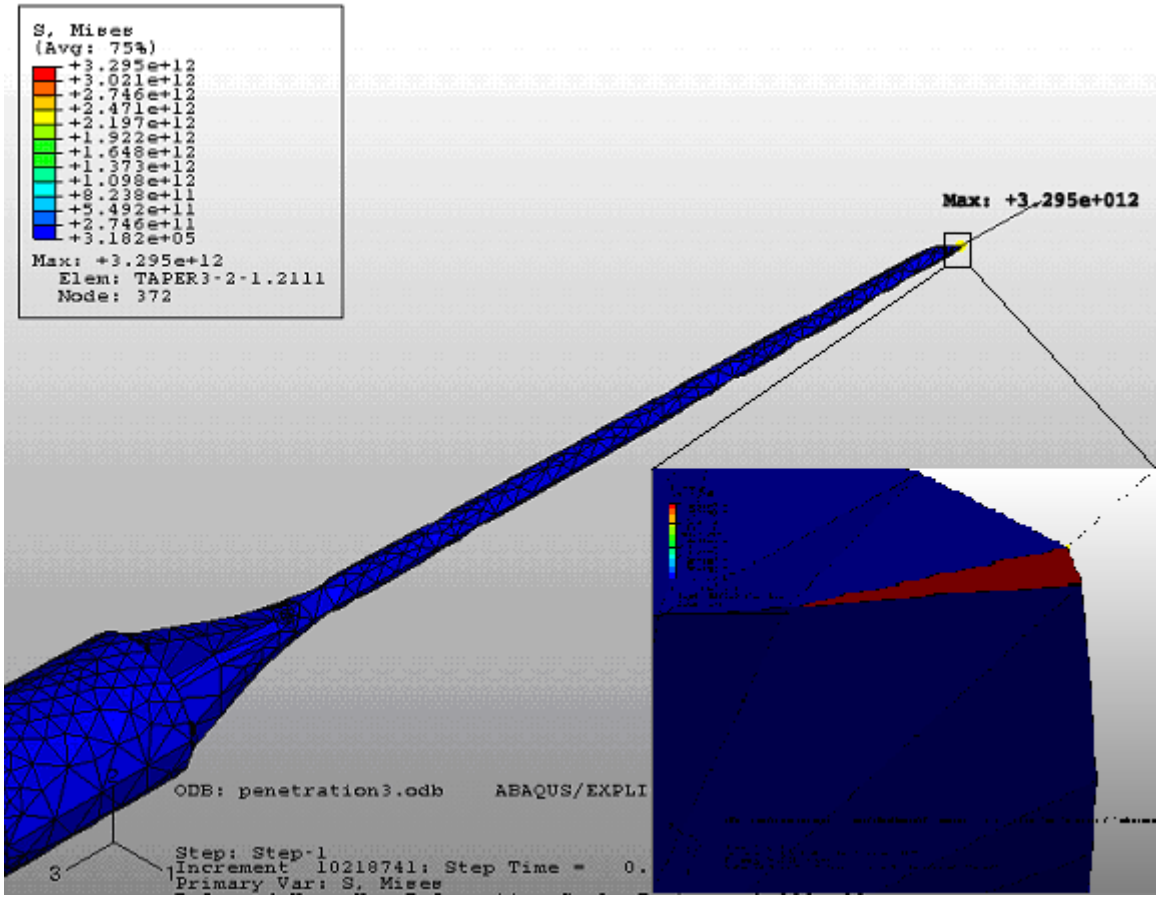

Figure 15 - Location of failure during penetration simulation at 0.298 seconds (note the excessively stressed element on the tip)

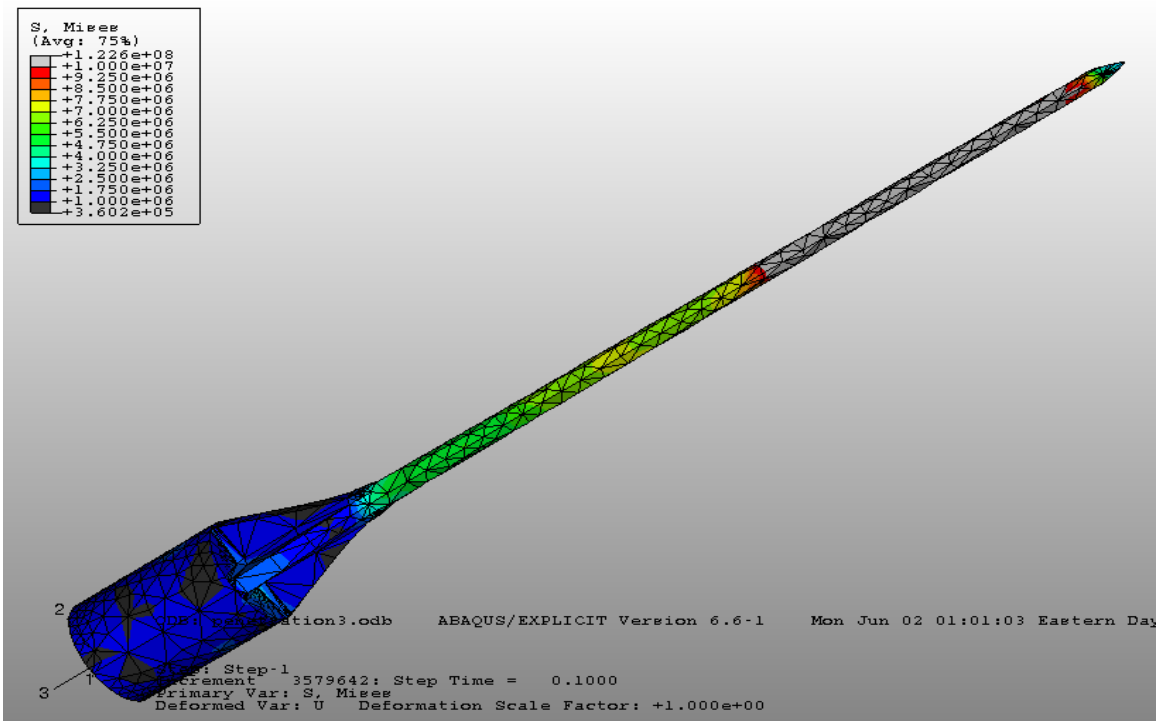

Figure 16 - Stress distribution in needle at 0.1 seconds during penetration

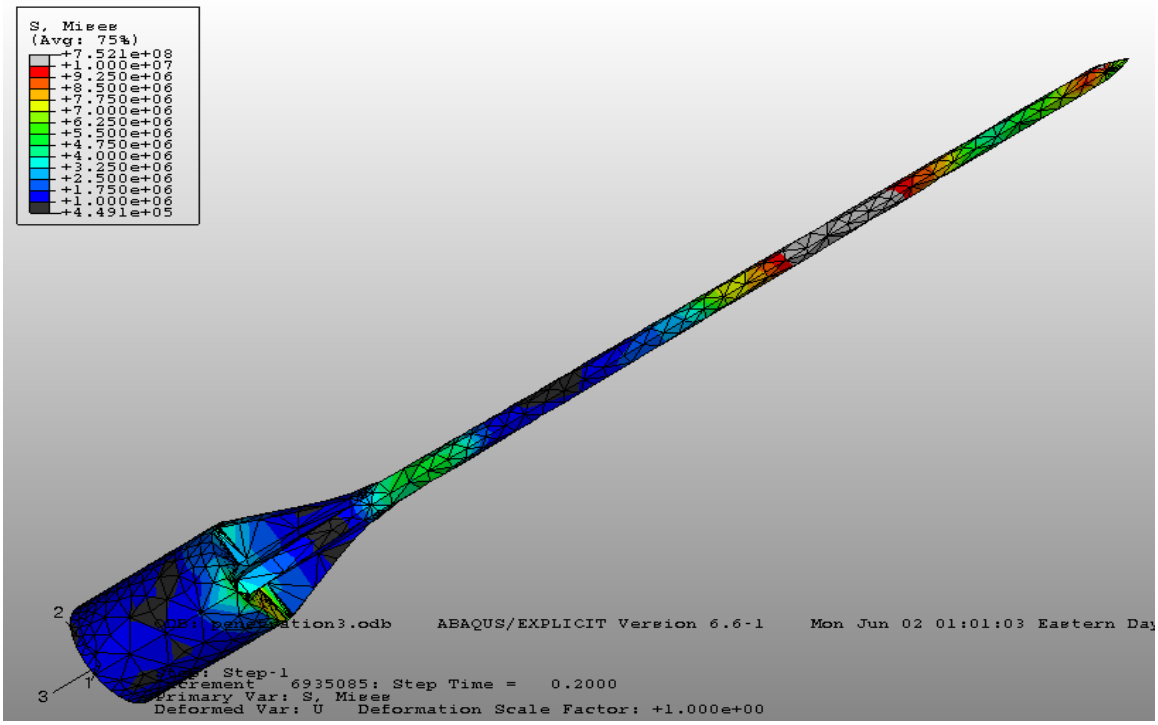

Figure 17 - Stress distribution in needle at 0.2 seconds during penetration

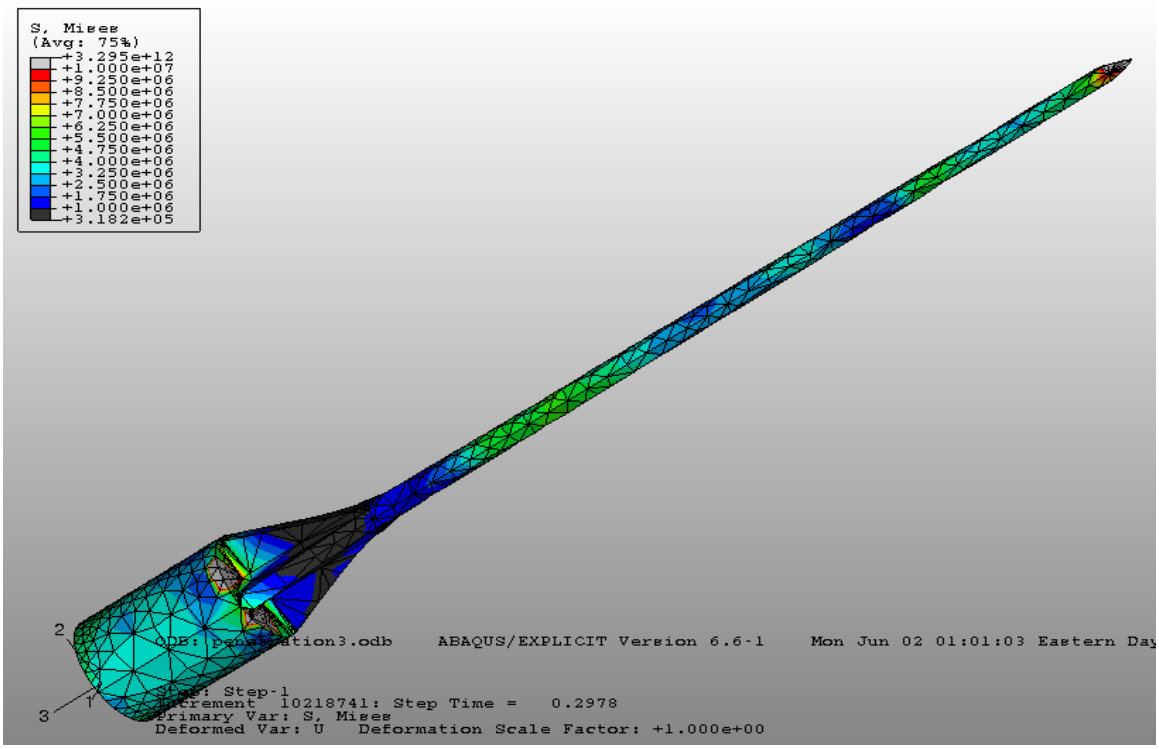

Figure 18 - Stress distribution in needle at 0.298 seconds during penetration

A stress of 3300 GPa was calculated near the tip at the moment of failure. The stresses throughout the remainder of the needle did not exceed 100 MPa, and were considerably lower in most areas. Stresses along the cannula varied for each time step, as shown in Figures 16-18, but never reached a level that would cause failure in the cannula. With tip failure occurring at approximately 0.3 seconds into the attempted penetration, these results do not demonstrate how the needle will react further along into the penetration. Should tip failure occur during the experiment in a similar manner as the simulation, data can continue to be collected until the needle ultimately buckles. However, the simulation is instructed to end once a measurable failure occurs, and the stress distribution in the cannula for the remainder of the penetration cannot be

determined. As penetration into a skin mimic had not occurred during this simulation, the needle was modeled as a rigid body to prevent deformation and possibly allow penetration to occur. Thus, it will be determined whether an accurate needle penetration model can be generated using the rigid body condition.

3.2.2.2 Rigid body needle results

To apply a load to a rigid body in ABAQUS, one point on the body must be selected as a rigid body reference node. This is in contrast to the area over which a load can be applied to a deformable body. Whereas the load was applied to the entire hub for the previous simulation, this simulation required a flat surface covering the hub to allow for the load to be placed at its center. As the needle is a rigid body, this will not affect the results at the location where the needle contacts the rubber. By approximating the needle as a rigid body, the simulation was able to model needle penetration into the rubber. The simulation indicated that penetration would begin to occur after approximately 2.7 seconds, when it demonstrated rapid element distortion in the center of the rubber close to the needle's insertion point. The results over time are shown in Figures 19-23, with the time step immediately prior to insertion, before element distortion, shown in Figure 22. Figure 23 shows the stress distribution in the rubber for this time step, with the needle removed.

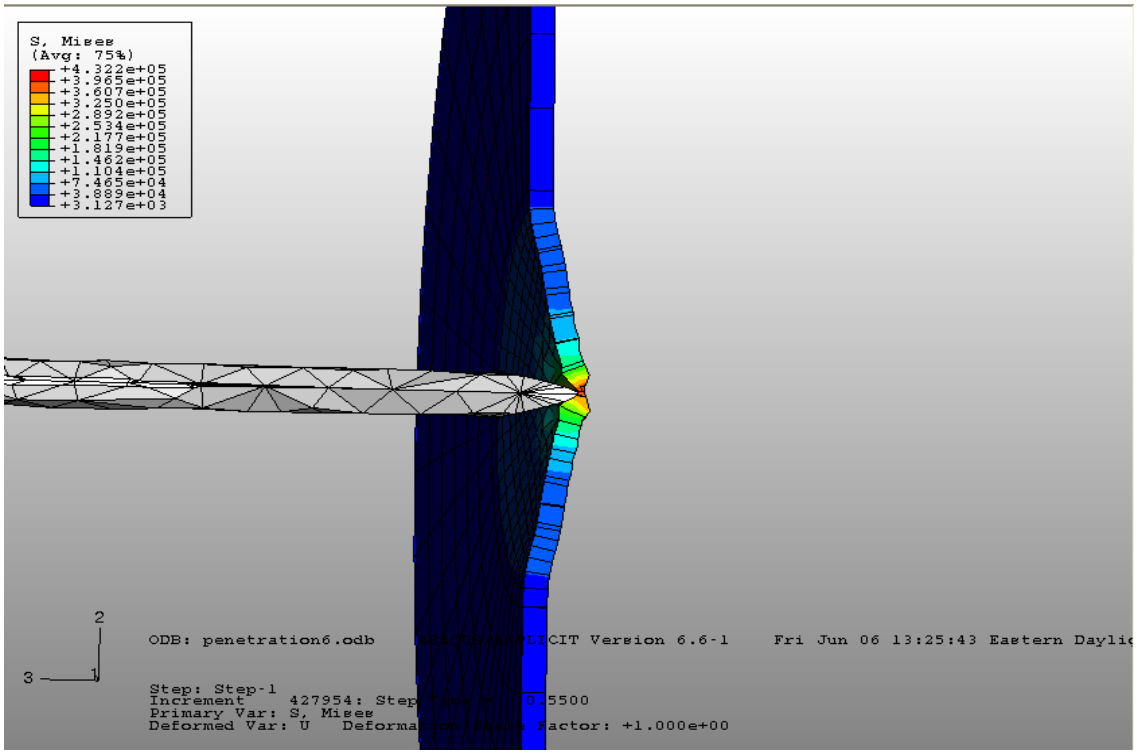

Figure 19 - Section view of rigid needle penetrating rubber skin mimic at 0.55 seconds

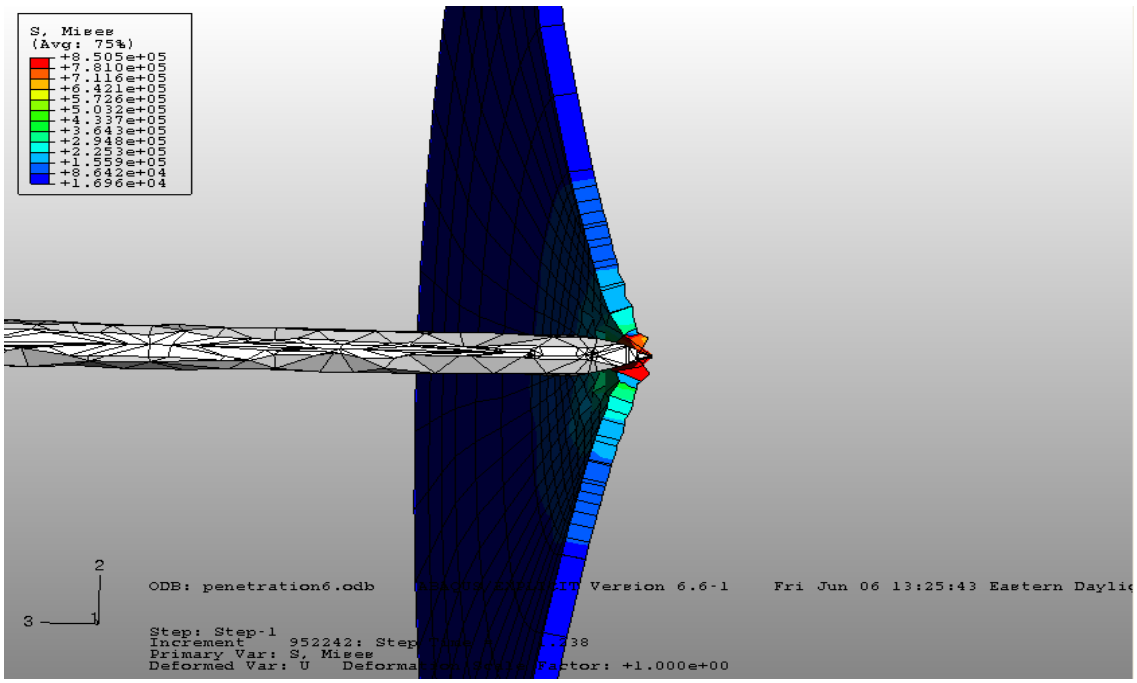

Figure 20 - Section view of rigid needle penetrating rubber skin mimic at 1.24 seconds

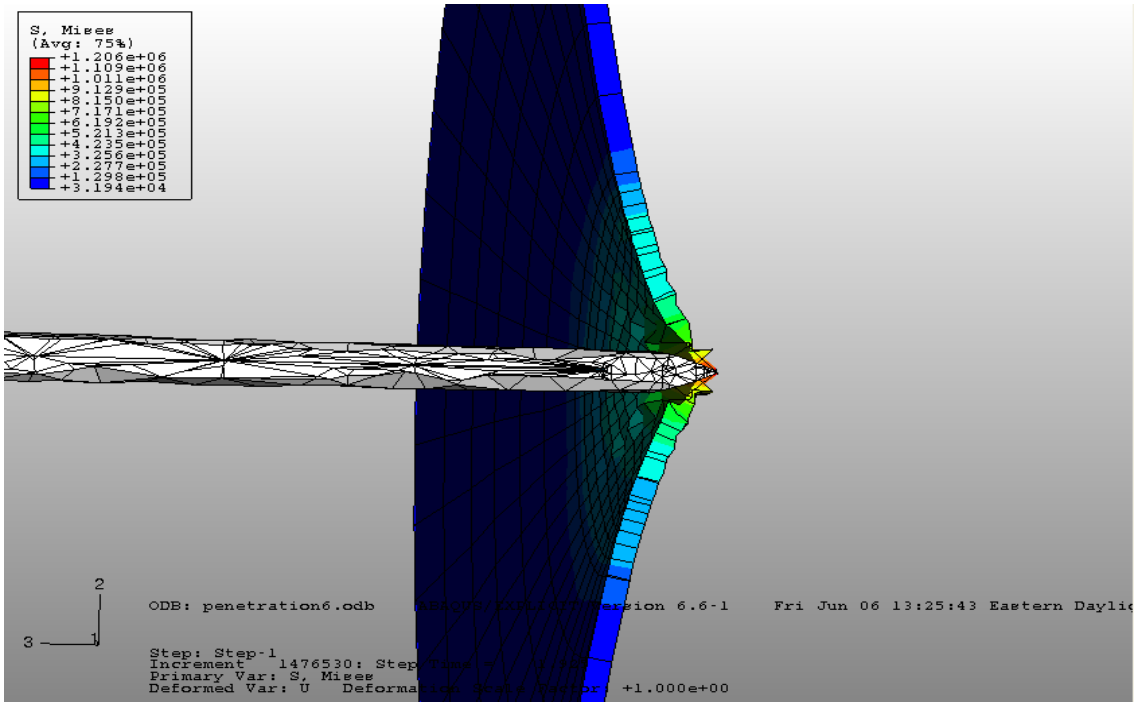

Figure 21 - Section view of rigid needle penetrating rubber skin mimic at 1.93 seconds

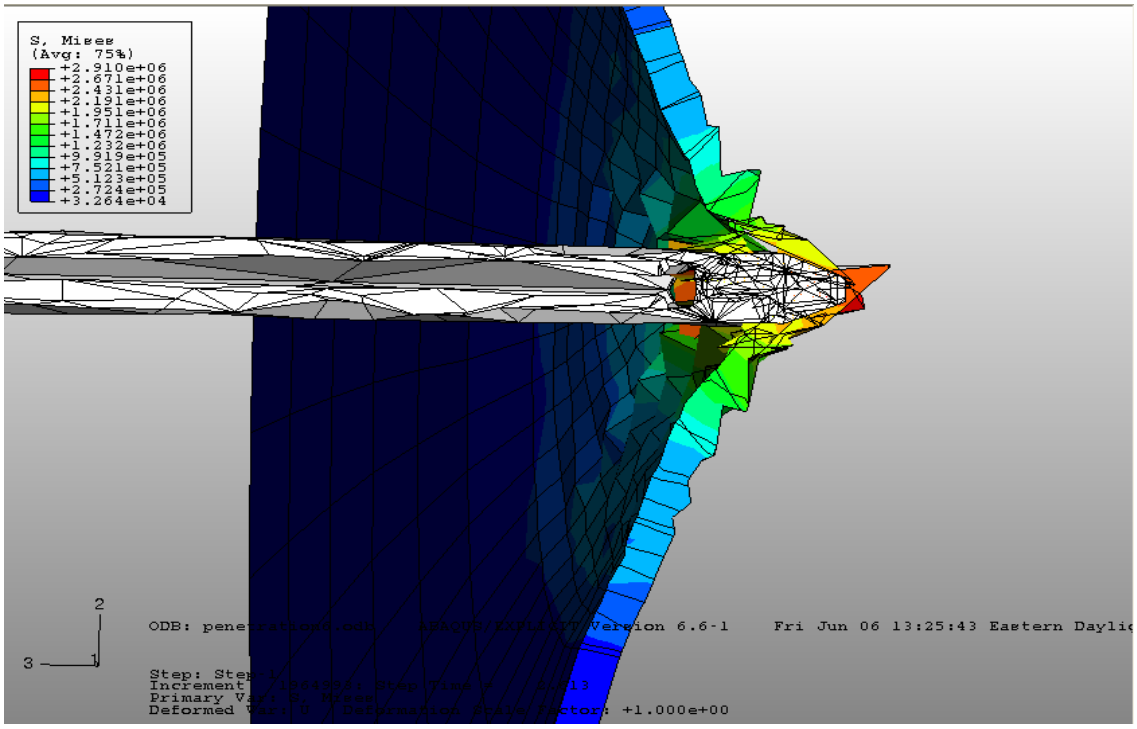

Figure 22 - Section view of rigid needle penetrating rubber skin mimic at 2.61 seconds

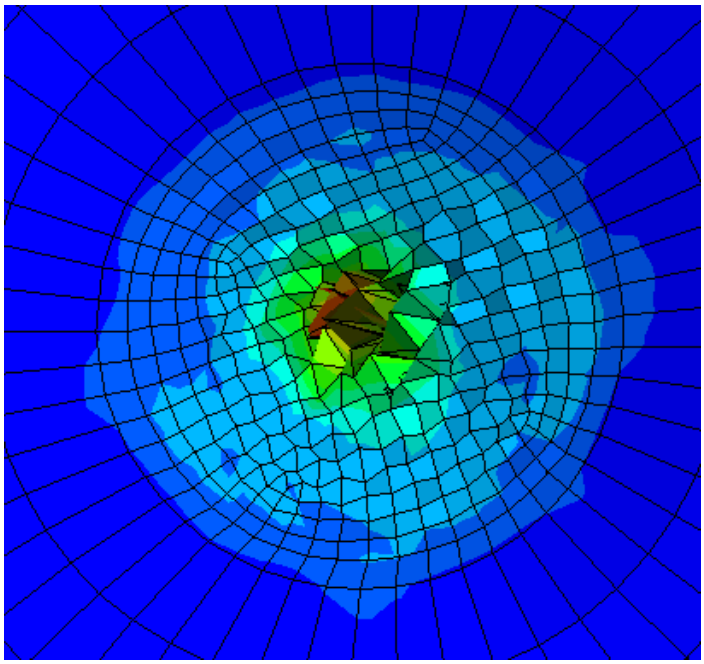

Figure 23 – Stress distribution of rubber skin mimic at 2.61 seconds after needle insertion

The results show the von Mises stress distribution throughout the rubber as the needle is inserted into the rubber. Figures 19-22 show a gradually increasing stress distribution throughout the rubber during penetration. As the needle is described as a rigid body, no stress calculations are performed for the needle, and no deformation occurs within the needle. As expected, the highest stress and deformation in the rubber occur closest to the needle insertion location. Penetration does not occur until the strain reaches the prescribed limit, as specified in the material description. With an assumed plastic strain at failure of 100%, the rubber's failure stress is thus 4.7 MPa, as determined from the stress-strain curve obtained from material tensile testing on the polyurethane. The simulation yields a material failure at that particular stress, indicating penetration through the rubber. This occurs at approximately 2.7 seconds. Thus, with an infinitely rigid

needle with the geometry of the needle in this model, penetration should occur approximately 2.7 seconds after initial contact with the rubber, given a constant speed of 100 mm/min.

Although the simulation also produced results for the forces acting on the rubber, these were inconsistent with both the predicted forces from section 3.1 and those measured in penetration tests in Chapter 4. The two types of force output from ABAQUS include contact forces and reaction forces. In this model, the reaction forces were only located along the edges where the boundary conditions were applied. The contact forces were measured between the defined contact areas on both the rubber and the needle. These were calculated to be as high as 10^8 N, and they were only present on alternating time steps (with a force of 0 N on the other time steps). This result may be due to an incorrect definition in determining how the forces are calculated. Overall, the forces calculated by the simulation are extremely high and erratic; therefore, these results are not used in predicting the needle penetration behavior.

3.3 Discussion

Both the needle penetration equations describing the motion before and during penetration and the finite element simulations are employed to characterize needle penetration and predict the performance of the needles during their actual penetration tests. Table 7 presents these results.

Table 7 - Theoretical and simulated penetration forces compared to buckling load for 38.1 mm plastic needles

Test	Resulting Load (N)
Pre-penetration equations (bending/stretching)	4.0-7.3
Penetration equations (Shergold & Fleck)	1.6-3.5
FEA (automatic)	10^8
FEA (calculated from stress)	1.9
Experimental buckling	4-6

The penetration equations developed by Shergold and Fleck predict penetration forces between 1.6 and 3.5 N; these equations assume a sharp needle tip. The pre-penetration equations developed in this thesis, which use the actual radii of the needles, predict a penetration load of between 4.0 and 7.3 N; experimental results in Chapter 4 will support these predictions. As the Shergold and Fleck equations demonstrate that the forces one would expect with optimal tip sharpness are smaller, sharper tips should be the targets for future needle designs.

This is in contrast to the results from the finite element simulation performed with a rigid needle, which predicts a contact force of up to 10^8 N. With a buckling force for the 38.1 mm length needles of 4-6 N, obtained in Chapter 2, it is clear that the simulation is calculating an invalid force, as the needles have no ability to approach that value. The remaining calculations and results from the simulations were more legitimate. Multiplying the stress at penetration, 4.7 MPa, by the approximate area of the needle at the tip yields a penetration force of 1.9 N. While this is lower than expected, it is much closer to the theoretical force values. As a result, the stress at penetration is reasonable.

The models with a rigid needle showed increasing stresses at the point of penetration until ultimate failure in the rubber occurred at the defined strain. When the model had a deformable needle, it showed an excessive deformation in the needle tip

prior to penetration. This would indicate that the needle is unable to penetrate the rubber with an intact tip. However, the deformed shape may still effect penetration, although this cannot be modeled in the simulation because it is ends with excessive needle deformation. Improvements that can be made to the needle to prevent this deformation from occurring include redesigning the tip to add more material, which is discussed in section 4.8, as well as using a stiffer material that will deform less under the same loading than the LCP.

3.4 Summary

In this chapter, needle penetration theory was developed, and finite element simulations were performed to predict penetration behavior. One model described the stretching that occurs in the rubber before penetration and the forces seen on the needle during penetration. The finite element simulation predicted needle failure at the tip prior to penetration. When the needle was modeled as a rigid body so that penetration would occur, the stress field shown in the simulation was an accurate representation of the expected stresses in a penetration, although the calculated contact forces were not as expected. These results will be supported by needle penetration tests in Chapter 4.

CHAPTER 4

NEEDLE PENETRATION EXPERIMENTS

The theory and computer simulations discussed in the previous chapter provide a basis to examine needle penetration with the plastic needles. This chapter focuses on experimental tests that verify the previously obtained results. The penetration tests primarily used synthetic rubber, with similar properties to skin, as a skin substitute.

4.1 Measurement of needle tip radius

The plastic needles were designed so that their tips are strong enough to penetrate skin without breaking. This required excess material behind the tip to allow for its added strength, described in section 1.2. However, the tips were not exceptionally sharp. To determine the approximate tip radius, ten tips were measured using a Starrett Sigma HB400 optical comparator (L.S. Starrett, Athol, MA). The test setup is shown in Figure 24, and an example of the needle's shape in the comparator is shown in Figure 25. The test indicated that the tip radius ranged from 0.043 mm to 0.065 mm (see Appendix G, Table 41).

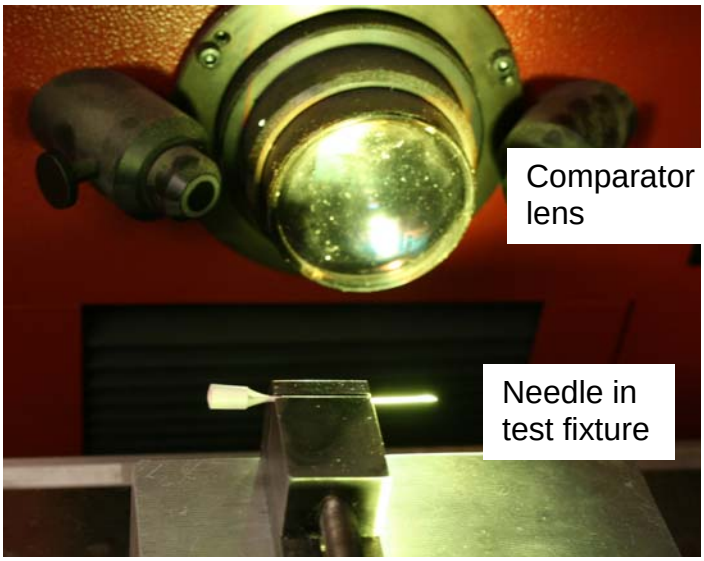

Figure 24 - Needle test setup in optical comparator

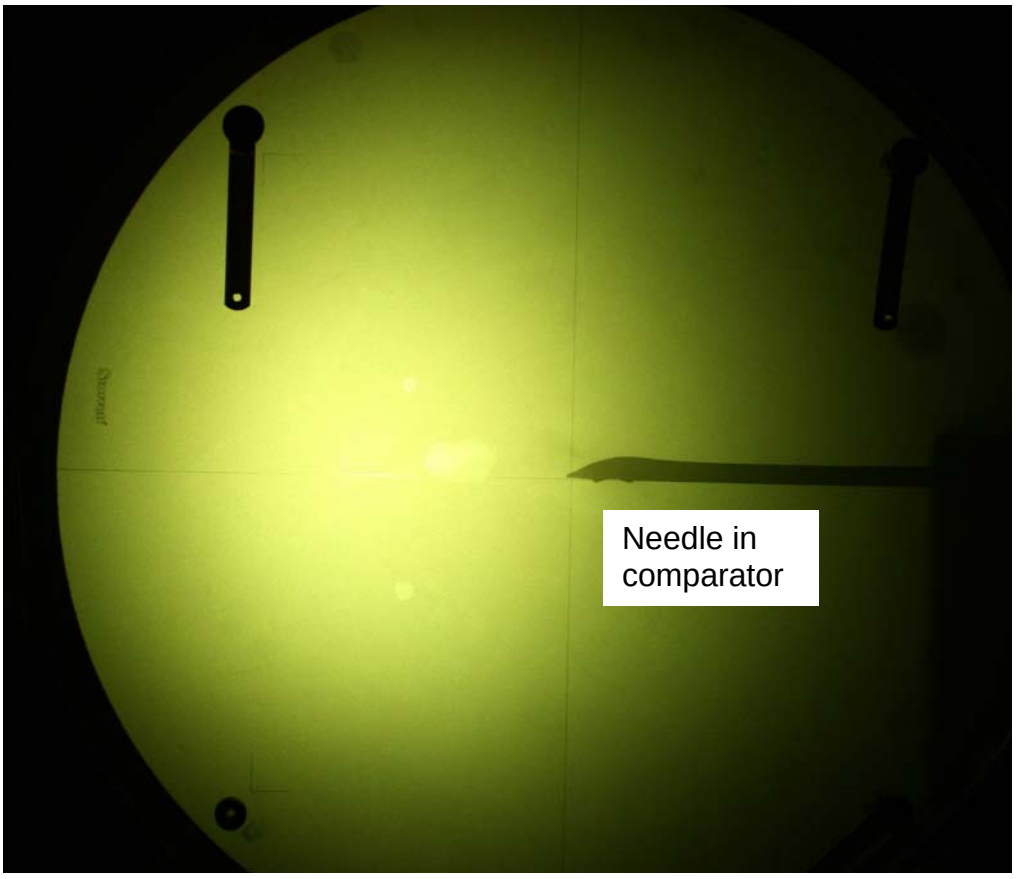

Figure 25 - Needle projection in optical comparator

4.2 Determination of skin mimic

The properties of human skin are listed in Table 4. The layers are listed in order from outer to inner layer. These must be taken into account when choosing an appropriate skin mimic; the rubber should have similar elastic properties because penetration is primarily an elastic process.

Originally, tests were performed using photoelastic sheets (Vishay Measurement Co., PS-4, 1.0 mm thickness) and class VI medical grade silicone rubber (McMaster-Carr, #87315K74 (1.02 mm thickness) and #87314K75 (1.52 mm thickness)) as skin mimics, but these materials proved ineffective. The photoelastic sheets, which had been previously used as a skin mimic for other experiments [18], were excessively sticky, and the needles could not penetrate them. The silicone, on the other hand, had some natural lubricity and was relatively easy to tear. As a result, all the needles penetrated it with very little resistance, which was not consistent with their expected behavior when penetrating actual skin. This led to the choice of polyurethane film (McMaster-Carr #1446T31, 0.37 mm thickness) as the skin mimic. This polyurethane was consistent with DIN 13097 [36]. It has an elastic modulus of 5.0 MPa, which is slightly lower than that of the lower layers of skin, and its thickness is near the typical range of the living epidermis. The rubber skin mimic was supported horizontally in a fixture at the base of the Instron and was elevated to allow the needle to penetrate.

4.3 Initial Penetration Testing

Penetration tests were performed using the plastic needles with cannula lengths of 38.1 mm and 25.4 mm. The tests were performed on an Instron model 33R4466 testing

machine. The test setup with a 25.4 mm length needle is shown in Figure 26. The penetration tests were performed at a speed of 100 mm/min, which is representative of the speed at which needles are routinely inserted into humans during insertions [37]. The exposed rubber area was 506.5 mm^2 (washer ID of 25.4 mm, illustrated in Figure 27) based upon a study of previous work [38], manufacturers' internal testing protocols [39], and international standards (DIN 13097 [36], ISO 7864 [40], ISO 9626 [41]). These are comparable to the insertion speed found in practice and the area of skin affected by a needle penetration.

Figure 26 - Penetration test setup

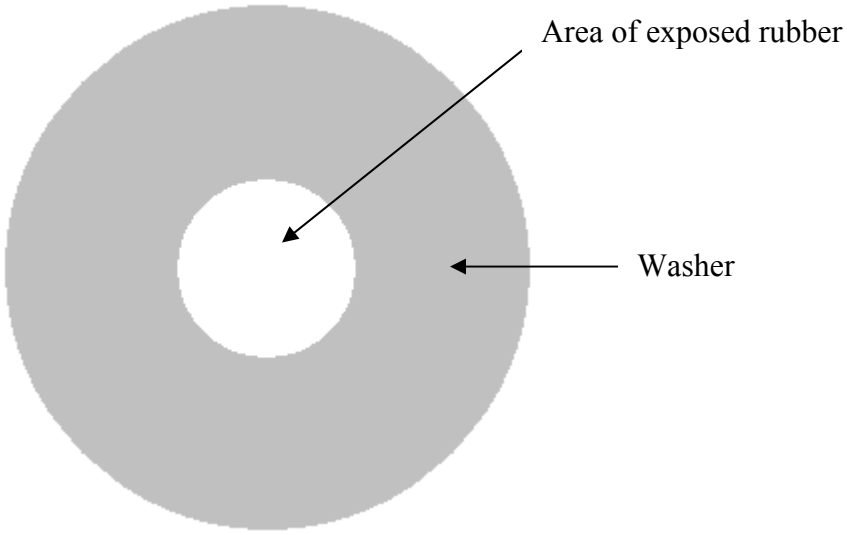

Figure 27 - Schematic of rubber skin mimic support

Initially, tests with the polyurethane were run without lubricating the plastic needles. To create the shorter needles, the full-length needles were cut short at their tips, leaving them attached to the hub and removing excess material at the tip end. A crude attempt was made to recreate a tip at what became the end of the needle (see Figure 28 for a comparison of the tips and Figure 29 for a view of the needle as a whole). As a result of the needles' taper, the diameters for the shorter needles were larger than the diameters of the full-length needles. The penetration tests then were performed using the standard specifications previously set forth. All of the early tests run with the polyurethane for full-length (38.1 mm) needles failed, as the needles buckled prior to penetration. The needles cut to 25.4 mm without the original tip also failed, and only two of the eight needles cut to 19.0 mm penetrated the polyurethane. However, the usefulness of the tests run on the shorter needles cannot be determined because of the

inaccuracies due to their larger overall diameters and the lack of appropriate tips. The tests demonstrated the need for a new method to create shorter needles, namely cutting the cannula perpendicular to the needle's longitudinal axis, leaving the tip end intact, and gluing the desired length into new polypropylene hubs (Small Parts, Inc., Part # NEHUB-0081-C (21 gage), Part # NEHUB-0091-C (20 gage)). This method is used on all remaining tests that involve shorter needles.

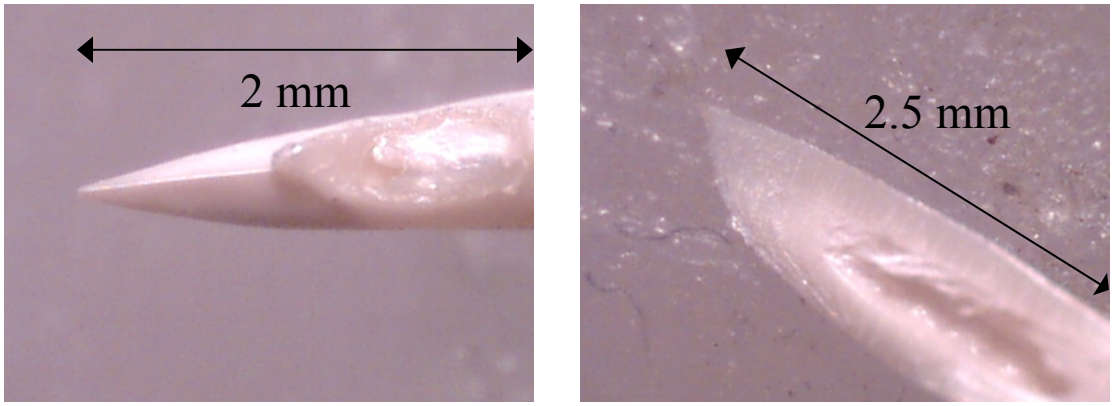

Figure 28 - Needle tip comparison (original tip on left, recreated tip on right)

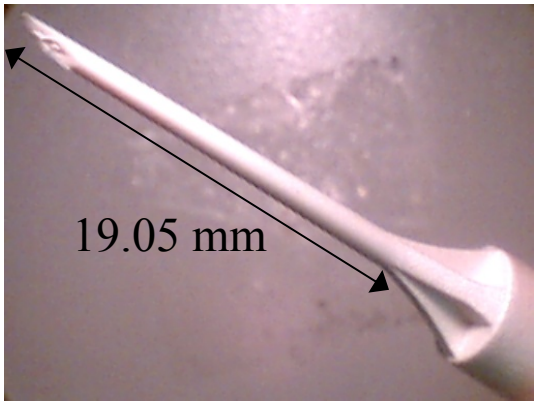

Figure 29 - 19.05 mm length needle

4.4 Lubrication Testing

Tests also were conducted to determine the influence of lubrication on the penetrative capabilities of the needle. It was originally hypothesized that lubrication would only create a reduction in the frictional forces between the needle and the rubber following penetration and would not affect the penetration. This is due to the belief that the tip's area was too small to be affected by the lubricant.

4.4.1 Silicone oil lubricant

The first lubricants used were silicone oils with viscosities of 100 cSt and of 500 cSt. The oil was applied by dipping the needles into a container of the oil for 5 seconds and then allowing the excess oil to drip off the needles. The needles were immediately loaded onto the load cell, and the penetration tests were performed (see Appendix A).

These tests demonstrated that these lubricants failed to influence the penetration of the needles into the polyurethane. All the needles tested were unable to penetrate the polyurethane, similar to the needles without lubrication. One of the issues with the silicone oil was that it did not bond to the needle's surface because the LCP is resistant to diphenyl-based products [23]; as a result, the oil was not an effective lubricant.

4.4.2 Silicone dispersion lubricant

Steel hypodermic needles are coated with a silicone lubricant; one commercial lubricant being Dow Corning MDX4-4159, 50% silicone medical grade. The MDX4-4159 is a silicone dispersion that chemically bonds to steel needles, keeping them lubricated until use. This contrasts with the behavior of the silicone oil, which would

coat the needle, but not bond with it. The original, as-received dispersion consists of 50% silicone oil-based material mixed [42], with the bulk of the material being a solution consisting of 70% mineral spirits and 30% isopropyl alcohol.

For the final lubricant, the necessary final silicone component content is <5% to ensure proper cure [43], so the original solution was diluted using a 70% mineral spirit, 30% isopropyl alcohol mixture to obtain the desired silicone component content. It should be noted that the lubricant was developed for steel, not for plastic, so adequate adhesion was not guaranteed to the plastic needles. In addition to lubricating the needles, a procedure also was developed to clean them. This was important because dirt and other particles could prevent the lubricant from fully contacting the needle, resulting in a poor coating. Also, in practice, needles will be cleaned prior to lubrication and sterilization. The procedure for both cleaning and lubricating the needles is detailed in Appendix B, "Lubrication Application Protocol."

4.4.2.1 Dispersion testing with plastic needles

To optimize the lubrication procedure, different coating procedures were tested on the plastic needles. The manufacturer stated that the final silicone content in the MDX4-4159 should be <5%, and it should cure at 70°C with 40-70% relative humidity for three to seven days following application [43]. Therefore, the silicone content and cure times needed to be tested to determine the appropriate level of each. The effect of humidity was not tested and was held approximately constant for each test. To test the silicone content, the lubricant was coated onto the plastic needles at 2.5% and 5% silicone contents with a cure time of three days. The needles also were tested either cleaned or

uncleaned (as-received) to determine if cleaning them affects their performance. To optimize the cure time, the needles were coated with the MDX4-4159 containing 5% silicone content and cured for either three or seven days. The results of these tests are described below.

4.4.2.1.1 Optimizing the silicone content

The two critical response variables from the penetration tests are the penetration force and the friction force, both of which can be determined from the load-displacement curve. The penetration force is defined as the load required to puncture the test sample; the friction force is the load required to continue to move the needle through the sample. The results detailing the penetration forces for the plastic needle penetration tests are summarized in Table 8 and detailed in Appendix G, Table 35. The test results show that a 5% silicone content coating enables a greater number of successful penetrations than 2.5% silicone content. The needles with 5% silicone content coating also have slightly lower average penetration forces and approximately equal friction forces as needles with 2.5% silicone content. On average, 30% of the lubricated needles at 38.1 mm length coated with 5% silicone content dispersion were able to penetrate the polyurethane. This increased to 67% successful penetration for 25.4 mm length needles due to a reduction in buckling. This trend was reversed with the 19.0 mm length needles, as they only obtained 33% penetration, including 0% with the 2.5% silicone content dispersion. These trends are apparent in the graphs for the tests, included in Figures 30-31 and Appendix E, with the friction force and penetration force noted in Figure 30. A possible cause for the lower penetration rate of the 19.0 mm length needles is that they benefit less

from the taper in the needle. This demonstrates that despite the findings from the buckling test, these needles are not as robust as 25.4 mm length needles under more functional conditions. The overall results demonstrate that the lubricated plastic needles are capable of penetrating the polyurethane skin mimic. Also, cleaning the needles has a minimal effect on their penetration capabilities. These results are encouraging, as neither the needle tip geometry nor the lubricant was optimized.

Table 8 - Penetrations with lubricated plastic needles in polyurethane

Solution	Cleaned before coating	Length (mm)	# of tests	Penetration rate	Avg. Penetration Force (N)	Avg. Buckling Load (N)
5%	N	38.1	15	40%	2.3	4.5
5%	Y	38.1	38	26%	3.4	4.6
2.5%	N	38.1	7	29%	3.2	4.4
2.5%	Y	38.1	7	14%	3.5	4.9
5%	N	25.4	8	63%	7.5	5.9
5%	Y	25.4	4	75%	8.3	8.6
2.5%	N	25.4	4	25%	6.0	8.3
2.5%	Y	25.4	4	25%	10.0	9.4
5%	N	19.0	8	25%	5.7	8.6
5%	Y	19.0	4	50%	8.1	9.7
2.5%	N	19.0	4	0%	-	12.1
2.5%	Y	19.0	4	0%	-	12.7

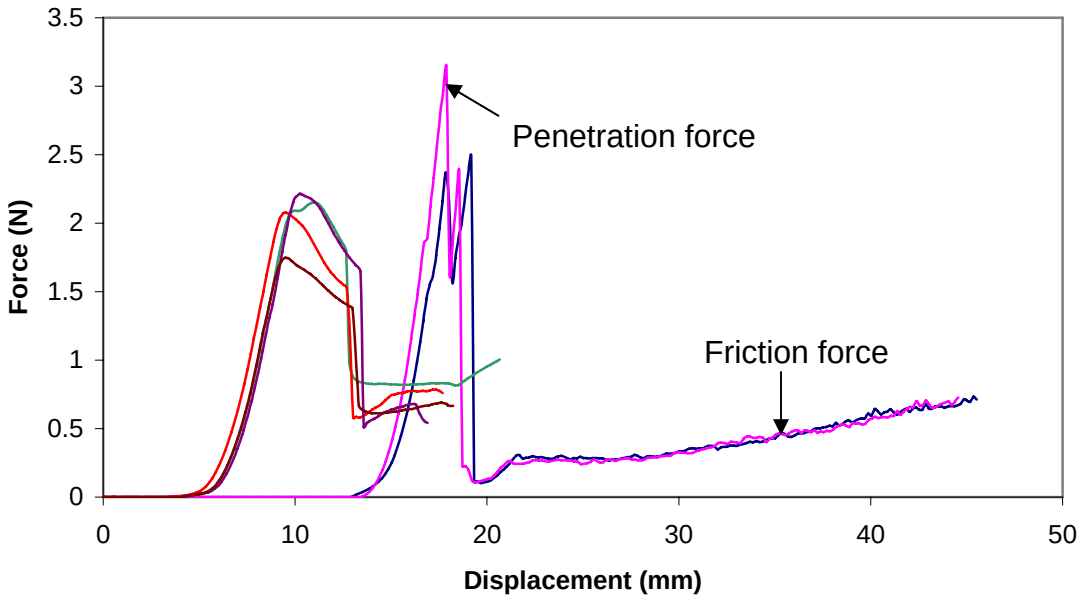

Figure 30 - Successful penetration tests for 38.1 mm, 5% silicone content, uncleaned plastic needles

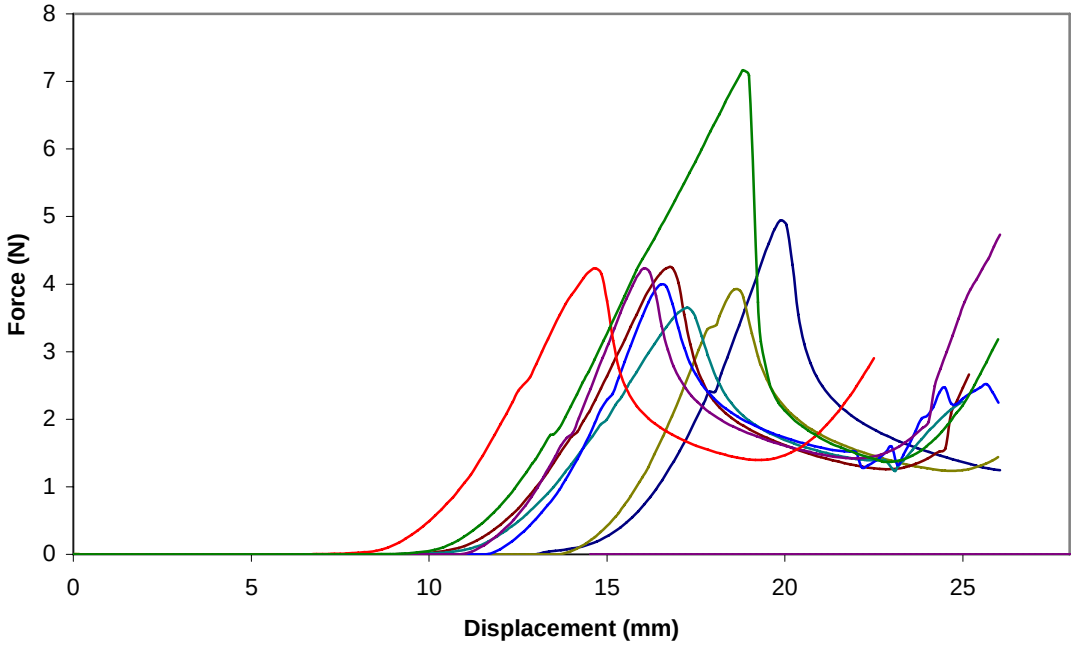

Figure 31 - Failed penetration tests for 38.1 mm, 5% silicone content, uncleaned plastic needles

4.4.2.1.2 Optimizing the cure time

One other variable considered when optimizing the application of the lubricant was the cure time. As shown in Table 9 and Appendix G, Table 36, penetration tests were performed on needles of both 38.1 mm length and 25.4 mm length following curing times of both three and seven days. The needles were coated with the dispersion containing 5% silicone content. The results indicated that a cure time of three days produces a higher percentage of successful penetrations than a cure time of seven days for both needle lengths. The differences between the penetration forces and frictional forces were minimal for each needle length. Thus, a cure time of three days at 70°C was chosen as the standard for the application of the MDX4-4159 to ensure a high penetration percentage while also maintaining the necessary lubricant properties.

Table 9 - Test of curing time

Cure Time (days)	Needle Length (mm)	# of tests	Penetration Rate	Avg. Penetration Force (N)	Avg. Buckling Force (N)
3	38.1	38	26%	3.4	4.6
3	25.4	4	75%	8.3	8.6
7	38.1	30	20%	3.7	4.8
7	25.4	29	37%	7.7	9.0

4.4.2.2 Dispersion testing with steel needles

To test the overall effectiveness of the MDX4-4159, prelubricated steel needles (InviroMedical InviroSNAP Exchangeable Needles, #110021, 22 gage, 38.1 mm length) were tested under three different scenarios. The first was with the original manufacturer's unknown silicone-based lubricant, with no alterations to the needles. The second set tested included needles that were stripped of their lubricant by immersing the

needles in a potassium hydroxide solution (0.5 N, <2% KOH, <95% ethanol, <5% methanol, <5% isopropanol) for at least two hours, as per the manufacturer's recommended removal procedure for MDX4-4159 [43], and then cleaning them with isopropyl alcohol. The third group of steel needles was removed of its lubricant by the above procedure, and then relubricated with a 5% silicone content of the MDX4-4159, utilizing the "Lubrication Application Protocol" in Appendix B, with a cure time of three days at 70°C.

The test results are summarized in Table 10 and detailed in Appendix G, Table 37, and the load-displacement curves for each needle set are shown in Figures 32-34. The first set, containing the as-received needles, produced an average penetration force of 0.5 N and an average friction force of <0.1 N. The second set of needles, with the lubricant stripped, penetrated the polyurethane with an average penetration force of 1.1 N and an average friction force of 0.7 N. This friction force is much higher and more inconsistent than the friction force from the as-received lubricated set, as evidenced in Figure 33, due to the lack of lubrication on the needles and possibly influenced by the KOH present. Finally, the third group, containing relubricated needles, had an average penetration force of 0.7 N and an average friction force of 0.2 N.

The results of the first and third set of steel needles, which directly compare the possibly different lubricants as applied to the same needles, are similar. These show lower penetration and friction forces than those of the second set. Although the MDX4-4159 needles have higher forces, the KOH solution may have altered the needles slightly. They also may have contained a different silicone content or cure time than the prelubricated needles, which demonstrates that more work is necessary to perfect the

lubrication content and procedure. These tests, along with those performed on the plastic needles, indicate the usefulness of lubrication to reduce the penetration and friction forces.

The load-displacement curves show a ragged pattern for the actual penetration, as multiple force spikes are present. This is likely caused by the polyurethane catching on either the hole in the steel needle or somewhere along the length of the needle near the tip, creating an excessive drag force. Previous work showed similar results with cleaned steel needles [44]. This occurrence is only occasionally present with the plastic needles, but it may be seen because of flash around the hole from the injection molding of the part.

Table 10 – Penetration test results for 38.1 mm steel needles

	Avg. Penetration Force (N)	Avg. Friction Force (N)
Lubricated by Manufacturer	0.52	0.06
Unlubricated	1.12	0.71
Relubricated	0.74	0.20

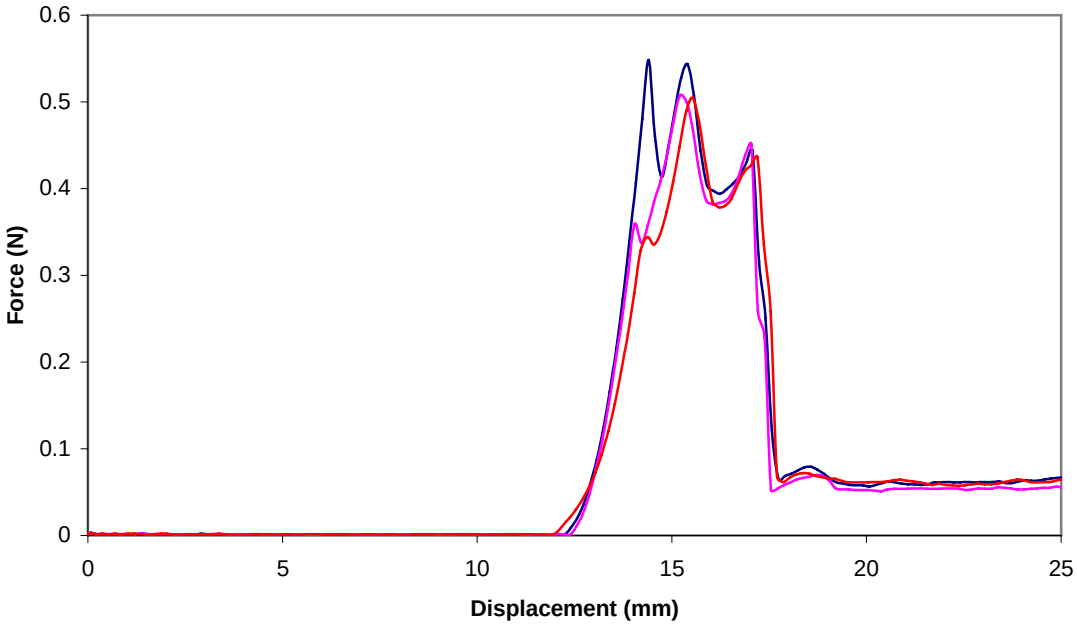

Figure 32 - Force vs. displacement curves for as-received steel needles

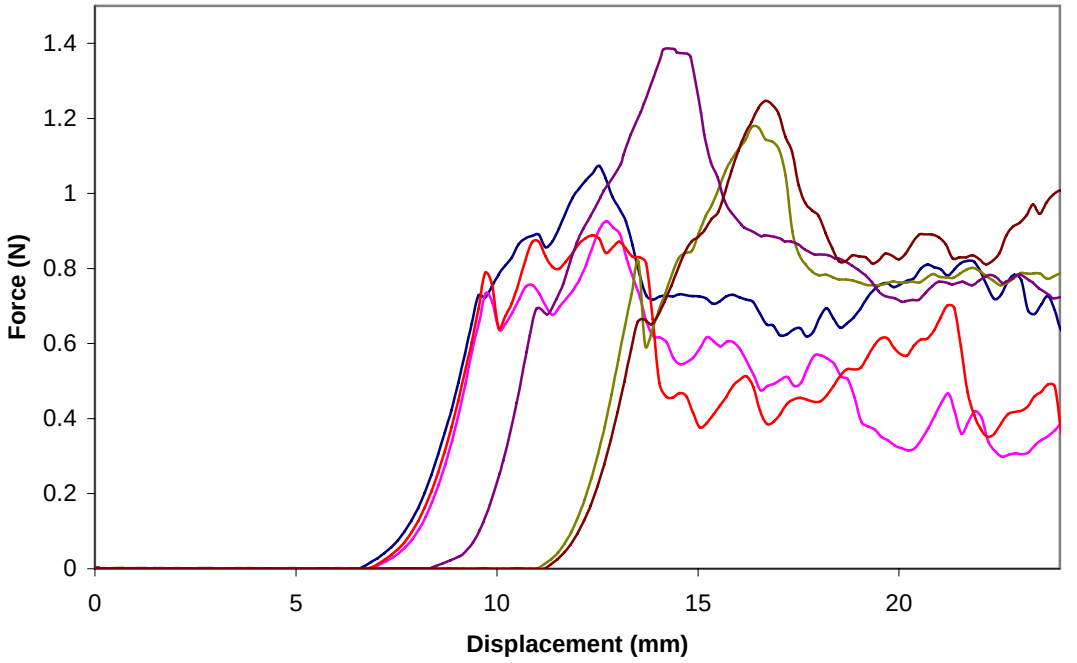

Figure 33 - Force vs. displacement curves for steel needles with lubricant removed

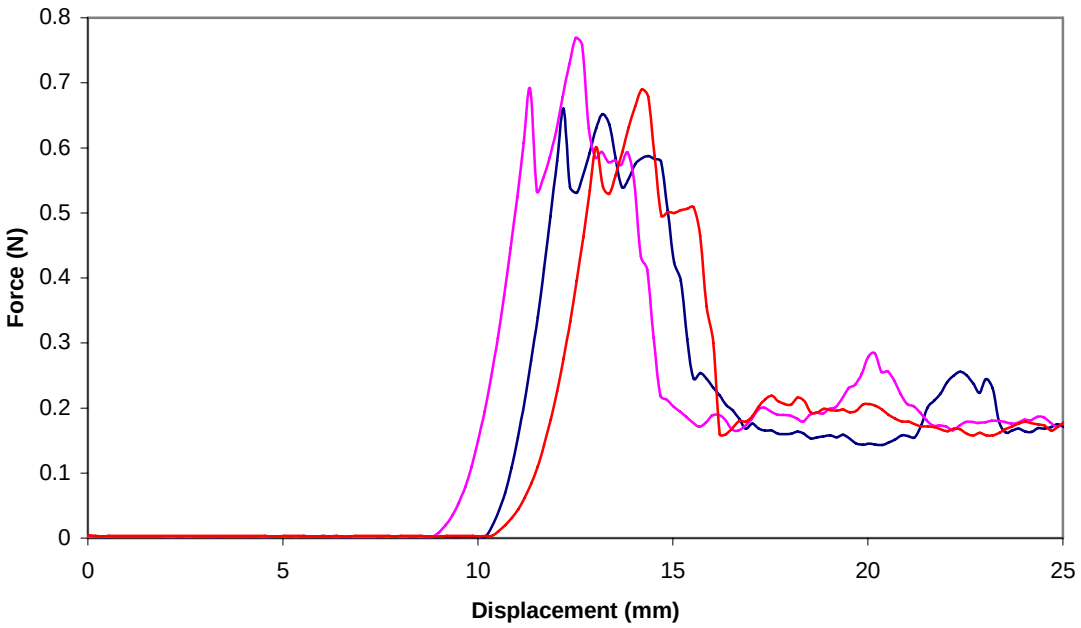

Figure 34 - Force vs. displacement curves for steel needles recoated with MDX4-4159

4.5 Pig skin testing

To gain a better understanding of the relationship between the polyurethane and human skin, penetration tests were performed using pig skin as the penetration medium. Only one set of tests using the pig skin was performed due to the small quantity available. The pig skin was stored frozen and was defrosted on the morning of the test by submersion in a cold water bath until it approached room temperature. The skin sample consisted of the skin layers as well as a layer of fat immediately beneath the surface of the skin. The skin was mounted in the test apparatus in a similar manner to the polyurethane film (see Figure 26).

The pig skin tests were conducted under the same protocol as the previous penetration tests, with lubricated needles, a vertical speed of 100 mm/min, and an

exposed skin area of 506.5 mm^2 (washer ID of 25.4 mm). The skin thickness, including the subcutaneous fat, was approximately 2 mm. The penetration forces, shown in Table 11 and Appendix G, Table 38, were slightly higher with pig skin than with polyurethane. This was most evident with the steel needles because of the consistency of their results. The penetration forces averaged 1 N for steel needles, compared to 0.5 N when penetrating polyurethane.

Table 11 - Needle penetrations in pig skin

Needle	Lubricated	Length (mm)	Penetration Rate	Avg. Penetration Force (N)	Avg. Buckling Force (N)
Plastic	Y	25.4	75%	8.4	6.0
Plastic	Y	38.1	0%	-	4.5
Steel	Y	25.4	100%	1.0	-

The 25.4 mm length plastic needles experienced similar penetration forces with pig skin as with polyurethane, along with a similar buckling load. For both tests, the ranges of the values for the penetration load were greater than seen in the steel needles, as there is more variability with the plastic needle penetration tests. This variability can be seen in Figures 35 and 36, load-displacement graphs for the 25.4 mm plastic needles and the steel needles respectively. In Figure 36, note the high penetration loads (the maximum load for each data set) for the three successful penetrations, compared to the test that experienced failure, at 6 N.

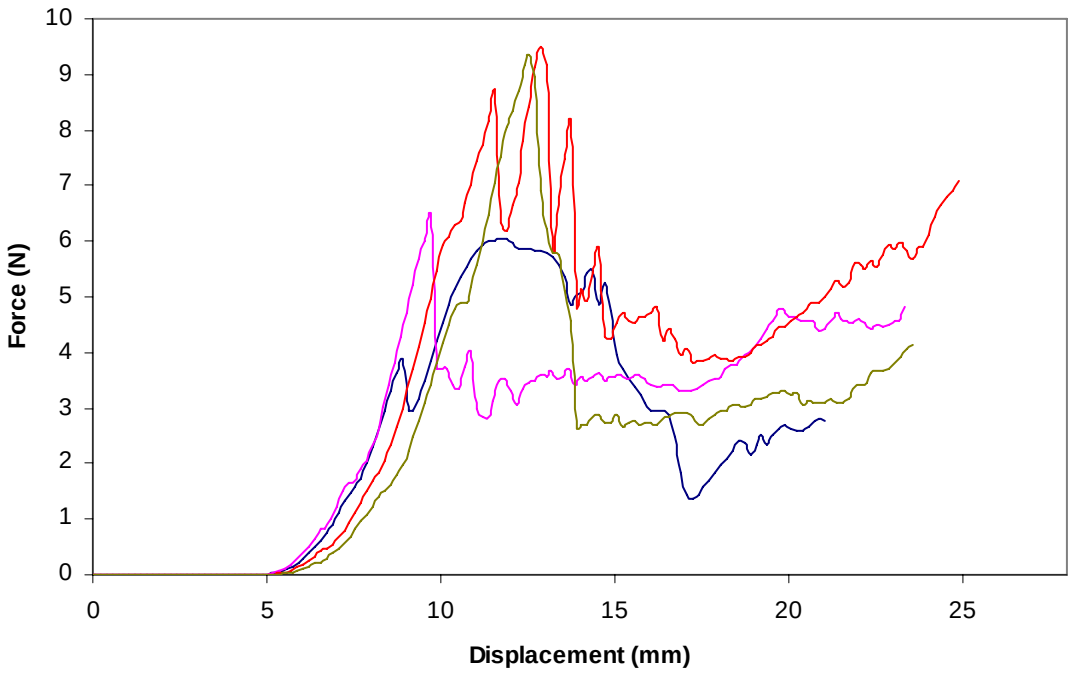

Figure 35 - Force vs. displacement graph for plastic needles in pig skin

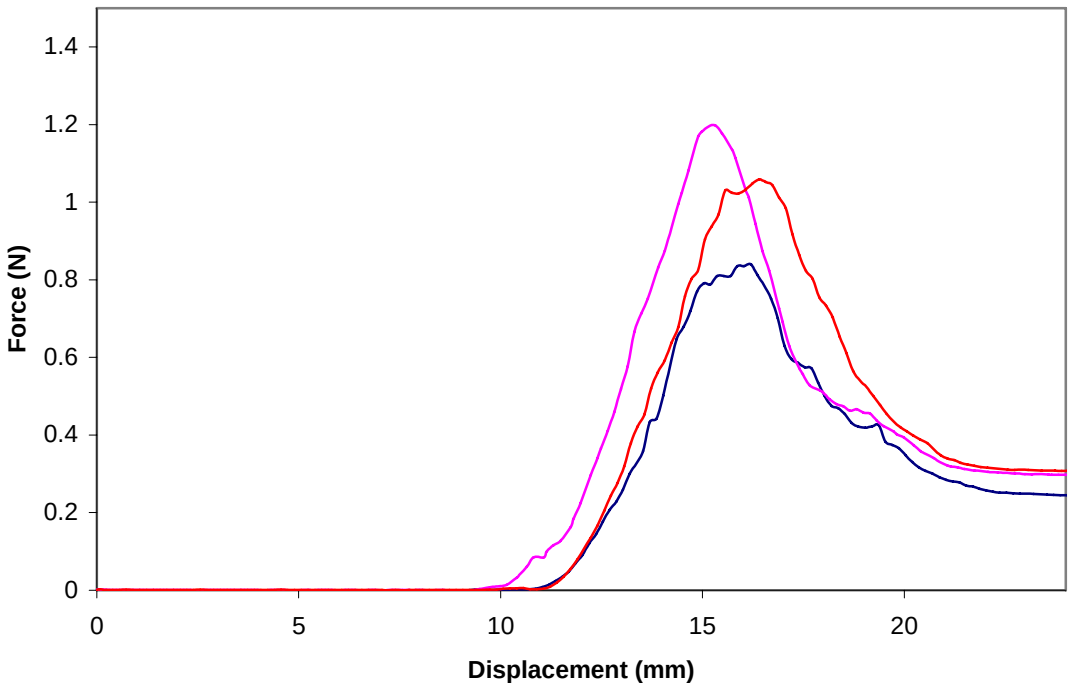

Figure 36 - Force vs. displacement graph for steel needles in pig skin

The penetration percentage for the 25.4 mm plastic needles with the pig skin was the same as with the polyurethane whereas the 38.1 mm length plastic needles all failed to penetrate the pig skin after achieving 30% penetration in the polyurethane. This indicates that 38.1 mm may be too long for 22 gage plastic needles to be effective in penetrating skin. These results are promising because pig skin is tougher to penetrate than human skin [45], so a high penetration percentage in pig skin should correspond to a higher percentage in human skin, with all other conditions being constant.

4.6 Butyl rubber stopper tests

Another penetration medium used to test the plastic needles was butyl rubber. The configuration replicated the needle insertion into a vial containing a drug being delivered to the patient. Each vial is capped with a rubber stopper, which is held in place by an aluminum seal. Upon using the vial, the seal is peeled back, and the needle penetrates the stopper to access the vial's contents. As this is a vital step in the delivery of drugs by hypodermic needles, it is necessary to test the plastic needles in this condition. For these tests, the butyl stoppers used were Kimble 20 mm gray butyl, art. # 73828A-21, the vials were Kimble serum vial, 20 ml, art. # 62121D-20, and the seals were Kimble 20 mm aluminum seal, tear-off, art. # 73821-20.

The penetration tests were conducted by affixing the stopper to the vial, securing the vial to the base of the Instron, and lowering the needle into the center of the stopper in the same manner as previous penetration tests. Each stopper was tested once. The seals were not used because they did not fit correctly. This was not a problem because they

also would not affect the penetration forces. Both the plastic and the steel (InviroMedical, 22 gage, 38.1 mm length) needles were lubricated for this test.

4.6.1 Standalone tests

The results for the rubber stopper penetration tests are summarized in Table 12 and detailed in Appendix G, Table 39. Penetration was achieved by six of the eight plastic needles with 25.4 mm length, and none of the 38.1 mm long needles. The 25.4 mm length needles had a consistent penetration force of 8.3 N. The buckling force for the two needles that failed was 8.1 N, which is consistent with failure forces in previous tests. The failure load of the 38.1 mm length needles, 5.4 N, suggests that 38.1 mm is too long for plastic needles to be able to penetrate the rubber stoppers because a force of over 8 N is required with the given tip geometry. By contrast, the two steel needles tested both penetrated the stopper. These results are encouraging because the butyl rubber is much harder than the polyurethane used for the skin mimic. This is evident in the steel needle penetration tests, as the penetration force was 4.0 N, much higher than the <1 N force seen with the polyurethane. The high penetration percentage of the shorter plastic needles in both this test and previous tests indicates that they can be effective as a replacement for steel needles.

Table 12 - Butyl rubber stopper penetration test results

Needle	Lubricated	Length (mm)	Penetration Rate	Avg. Penetration Force (N)	Avg. Buckling Force (N)
Plastic	Y	25.4	75%	8.3	8.1
Plastic	Y	38.1	0%	-	5.4
Steel	Y	25.4	100%	4.0	-

4.6.2 Tests with polyurethane

The six 25.4 mm length plastic needles that successfully penetrated the butyl rubber were then tested in penetration with polyurethane as the penetration medium, with the test conditions matching those from previous tests. This simulates the needles being pushed into skin following the insertion into a drug vial. All six needles failed to penetrate the polyurethane under these conditions. During the tests, the needles initially began to penetrate the polyurethane, but buckled before the tip could finish the penetration. Since the needles were strong enough to penetrate the butyl rubber, they should have also penetrated the polyurethane. There was no recognizable tip damage following the penetration into the butyl rubber.

This leads to the conclusion that the lubricant may have been wiped off by the first insertion and thus does not provide the necessary reduction in friction for complete penetration to occur. To test this conclusion, an additional ten 25.4 mm length needles that successfully penetrated the rubber stoppers then were relubricated for penetration into polyurethane. Six of these needles penetrated the polyurethane, which is comparable to the penetration rate of 25.4 mm length needles in polyurethane. These results are listed in Appendix G, Table 40. Since there was no recognizable tip damage following the first insertion, it is clear that the lubricant did not remain adhered to the needles following their first penetration. Therefore, the MDX4-4159, when applied to plastic needles, may only be a suitable lubricant for single insertions, but may not be effective when attempting to make multiple insertions with one needle. In light of these results, more research is necessary to better optimize the lubricant so that it can withstand multiple penetrations.

4.7 Steerability tests

Steerability tests were conducted to analyze the behavior of the needle after it passes through the rubber at an angle. These are necessary because injections are not always performed with the needle directly perpendicular to skin. Both the polyurethane and the silicone rubber were used for these tests because the needles have no trouble penetrating the silicone. The needles used for this test were lubricated with lengths of both 38.1 mm and 25.4 mm.

4.7.1 Steerability test setup

Each needle was tested three times under the same test conditions, but with a different portion of the tip making the initial contact with the rubber, as shown in Figure 35. The two factors analyzed in this test were the force and the location of the needle after penetration. The tests were performed with the rubber loaded at an angle, either 14° or 28°, from the horizontal plane, and the needle was lowered vertically into the rubber. These angles were chosen as representative angles for the test. The testing setup for this experiment is shown in Figure 7. For these tests, the conditions were fixed at a speed of 100 mm/min and an exposed area of 506.5 mm^2 (washer ID of 25.4 mm). With the rubber position unchanged (see Figure 7), the needle was lowered into the rubber with the tip initially to the left so that it impacted the rubber at the highest point of contact. For the second test run, the tip was initially to the right, impacting the rubber at the lowest point of contact. The final test for each sample involved the tip located at the center of the setup, ensuring that the contact with the rubber would occur in the middle of the height range (see Figure 37).

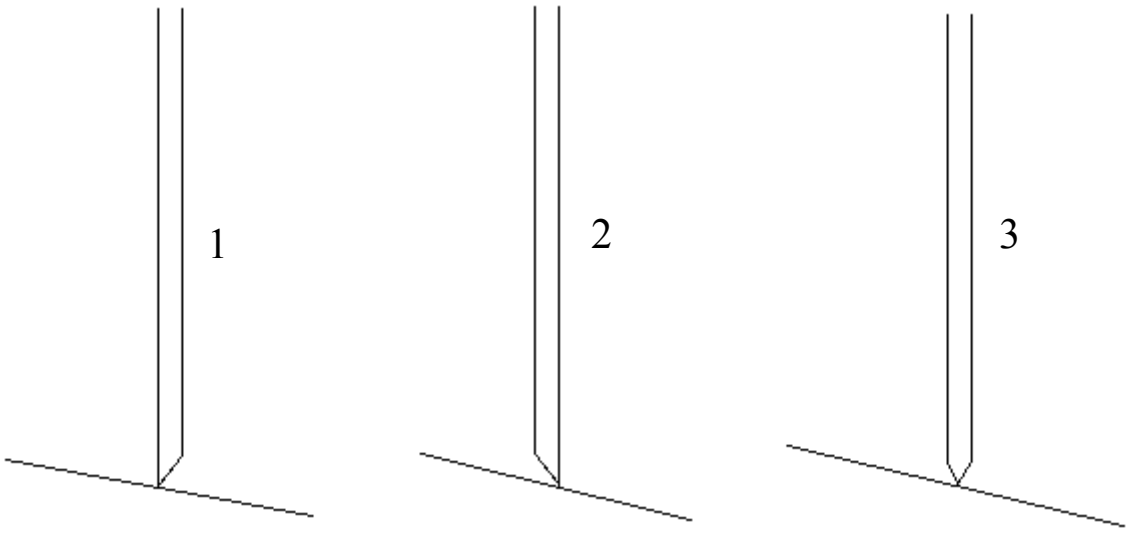

Figure 37 - Schematic of needle positioning during steerability tests

4.7.2 Steerability test results

The steerability tests showed that after penetration occurred with silicone rubber as the penetration medium, the needles were consistently bent in a direction normal to the surface, as shown in Figure 38. The black line in the figure represents the needle location if no bending occurred. The 38.1 mm needles were bent approximately 1-2° when the rubber was fixed at a 14° angle and 5° when the rubber was fixed at a 28° angle. This bend occurs because during penetration, the needles do not penetrate at the same angle at which they are being inserted, but they attempt to bend toward the rubber and penetrate normal to the rubber, or at least closer to 90° than they originally started. As a result, the needle tips are approximately 1-2 mm from their intended location when penetration is complete, so this would still pose a concern for an application requiring precise placement. The 25.4 mm needles experienced minimal bending after penetration, on the order of 1° for both angles of the silicone rubber. Forces on the needles were lower than

those achieved by the penetration tests, which is to be expected because of the relative ease of penetrating silicone rubber compared to polyurethane.

The results were consistent for all of the needle positions, and the resulting needle location was also relatively consistent. One area of concern was that the needles were consistently sliding along the rubber for about 3 mm before penetrating. The cause of this is most likely due to the relatively slippery nature of the silicone rubber. Skin has a higher coefficient of friction with the needle, and thus slippage will be minimal. The needles of both lengths were unable to penetrate the polyurethane during these tests, which indicates that the needles must be inserted perpendicular to the skin for penetration to occur. Steel needles were able to penetrate the skin at an angle with both rubber skin mimics. They did not bend following penetration, and they did not slip along the skin prior to penetration.

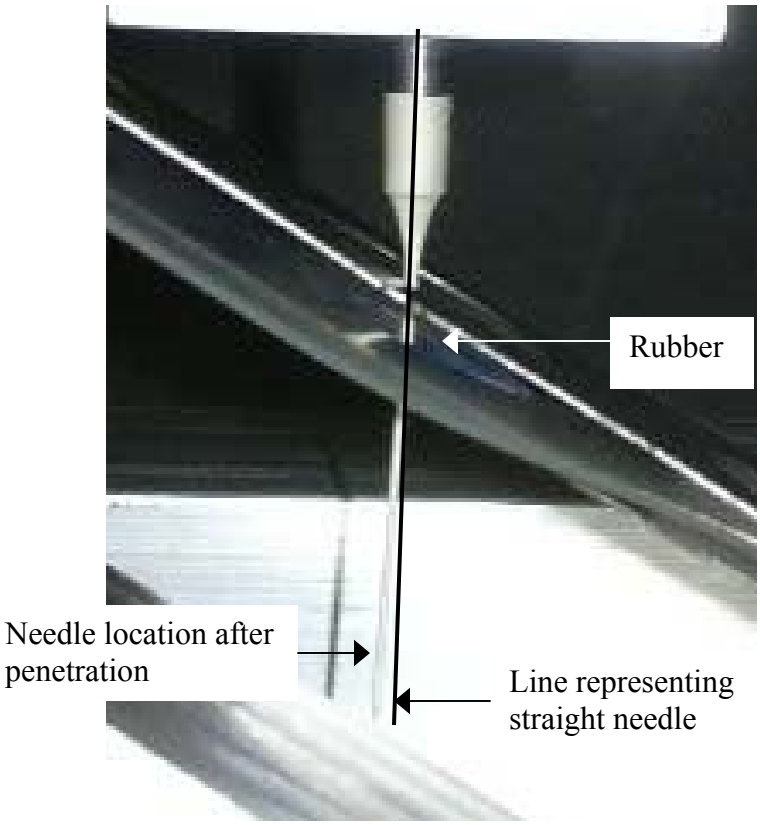

Figure 38 - Needle after penetration during steerability test (note the bend in the needle following penetration)

4.8 Subsequent needle designs

The previous tests all were performed with the first prototype design of the plastic needles. Upon obtaining the results, changes to the design were suggested to the needle manufacturer, and subsequent designs were created and tested. The first of these designs featured a slightly smaller (23 gage) solid needle, meaning that it did not contain a cavity for fluids to pass through the needle. This was done to expedite the manufacturing process. This needle featured a sharper tip, albeit a narrower one containing less material than the previous design. The reasoning behind this design is that the sharpness of the tip

will allow for easier penetration at a lower axial load than previously experienced. It also refined the previous design by incorporating a cylindrical cannula.

Upon testing this new design, it became apparent that there were multiple problems that prevented it from improving upon the previous design. For each penetration test attempted, the tip crumbled at a low load, and then the needles buckled, also at a much lower load than before. As a result, none penetrated the polyurethane. While the previous design experienced buckling along the cannula, this needle buckled closer to the tip, at a small indent where the exit of the inner bore would be present. The failure mode of these needles led to a number of conclusions. One is that the tip needs to contain more material, as thinning it out to provide sharpness makes it too weak to allow a penetration. As the failure occurred behind the indent, where the shape of the material creates a natural weak point, it was decided to create a ridge opposite that area. This ridge would be similar to the one that had existed on the previous design. By bulking up the weak area, buckling should be prevented. Combining the previous flaws with the fact that the needles had a smaller diameter (23 gage) created an overall weakness of the needles. Consequently, this design was removed from consideration.

Upon reaching these conclusions, two new mold cavities were designed, with one emulating the original design with some modifications, and the other featuring a stronger tip with more material. Also, different materials were considered, leading to six combinations of newer needles, which are described in Table 13.

Table 13 - Characteristics of new plastic hypodermic needles

Cavity	A950 (%)	B950 (%)	Semisolid	Quantity	Elastic modulus (GPa)
1	100	0	N	9	9.8
1	75	25	N	10	13.8
1	50	50	N	9	17.7
1	50	50	Y	11	17.7
2	80	20	N	11	13.0
2	80	20	Y	7	13.0

In the table, "semisolid" indicates a cannula without a bore for fluids. A950 and B950 are different grades of the Ticona LCP; A950 is similar to the 1300MT used for all the previous needles, except that it is not certified as medical grade, and B950 is a higher stiffness grade of polymer than the A950 (see Appendix D for material properties). All of these are unreinforced polymers. The percentages of each polymer used in the needles were altered to determine what effects would result from these changes, and the modulus given for each needle is calculated from the elastic modulus of each material and the rule of mixtures, shown in Equation 19.

$$E_c = v_A E_A + (1 - v_A) E_B , \tag{19}$$

where E_c is the elastic modulus of the mixture, v_A is the volume fraction of A950, and E_A and E_B are the elastic modulus of A950 and B950 respectively. Finally, cavity 1 is the one closer to the original design, and cavity 2 contains more material in the tip.

For the penetration testing involving these needles, all the needles were tested at 25.4 mm length because of the limited number of needles available. They were also lubricated with the MDX4-4159 and cured as per the "Lubrication Application Protocol" in Appendix B, and the penetration medium used was polyurethane. The results are shown below in Tables 14-19. The graphs of the tests and pictures of the needles' tips following the tests are shown in Figures 39-55.

Table 14 - Penetration test results for 100% A950, cavity 1

Sample	Penetrated	Buckling Load (N)	Penetration Load (N)	Failure Type
1	N	4.8	-	Tip
2	N	3.9	-	Tip
3	N	4.1	-	Tip
4	N	3.4	-	Tip
5	N	3.2	-	Tip
6	N	4.5	-	Tip
7	N	3.0	-	Tip
8	N	4.1	-	Tip
9	Y	-	1.8	N/A

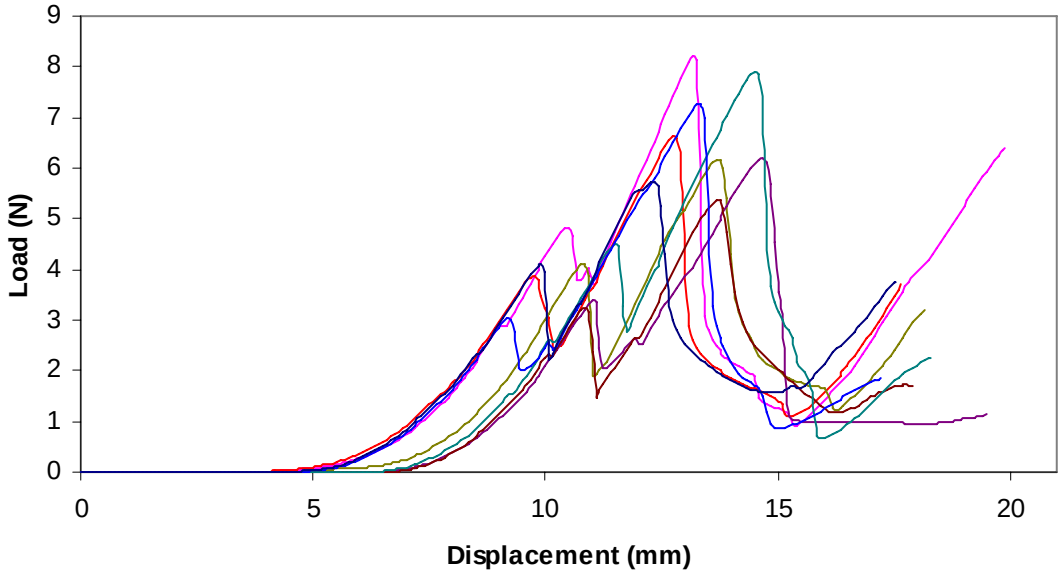

Figure 39 - Failed penetrations for 100% A950, cavity 1

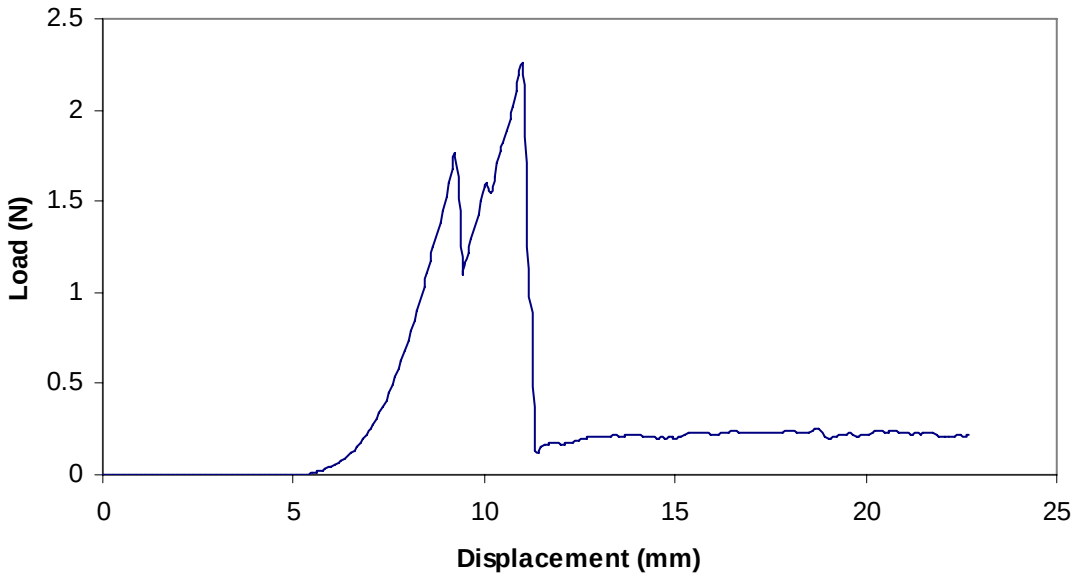

Figure 40 - Successful penetration for 100% A950, cavity 1

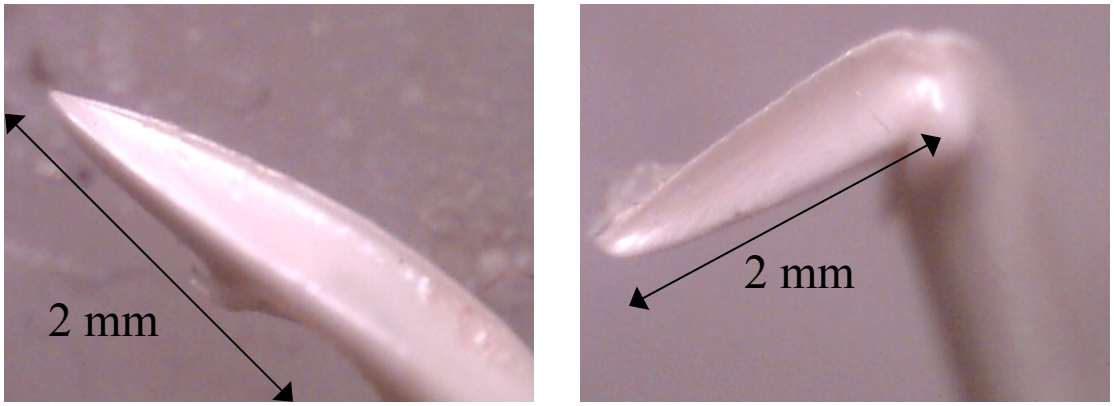

Figure 41 - Tips of 100% A950 needles after successful (left) and failed (right) penetrations

Table 15 - Penetration test results for 75% A950 / 25% B950, cavity 1

Sample	Penetrated	Buckling Load (N)	Penetration Load (N)	Failure Location
1	Y	-	3.0	N/A
2	N	4.0	-	Tip
3	N	3.6	-	Tip
4	N	3.7	-	Tip
5	N	4.9	-	Tip
6	N	4.5	-	Tip
7	N	3.7	-	Tip
8	Y	-	2.9	N/A
9	N	4.9	-	Tip
10	N	4.0	-	Tip

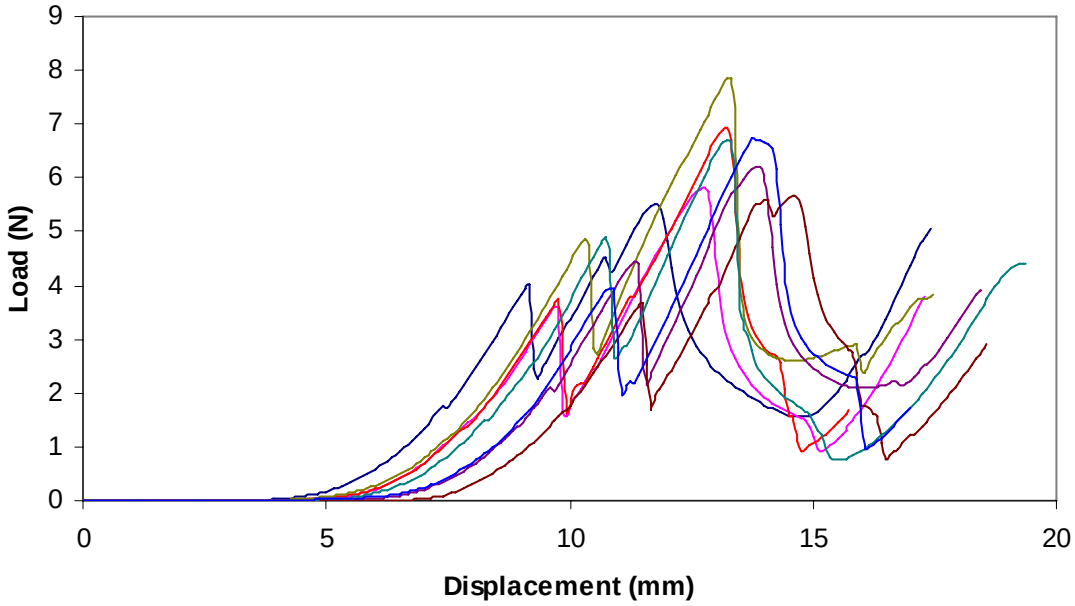

Figure 42 - Failed penetrations for 75% A950 / 25% B950, cavity 1

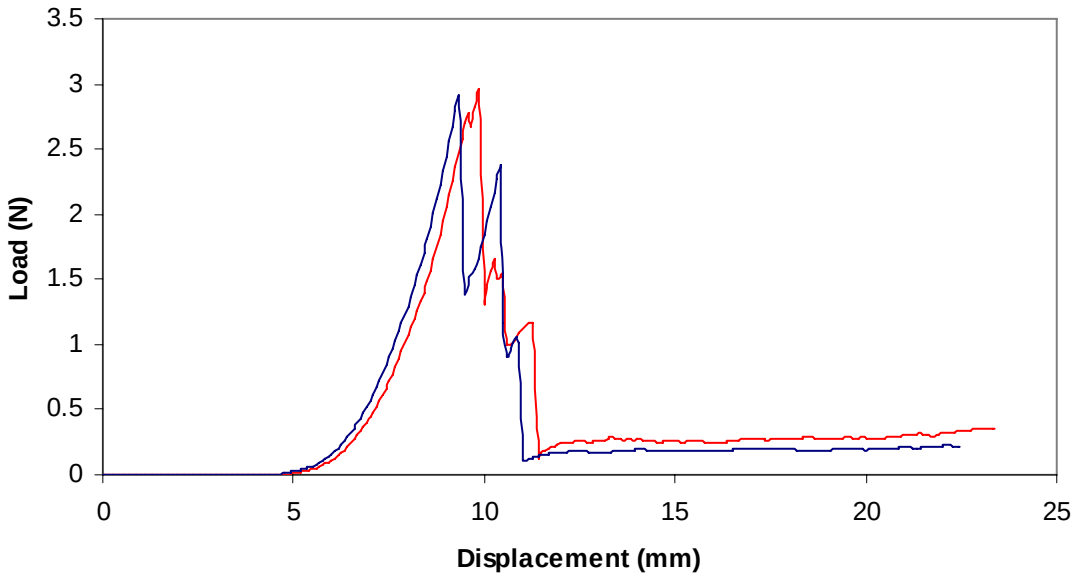

Figure 43 - Successful penetrations for 75% A950 / 25% B950, cavity 1

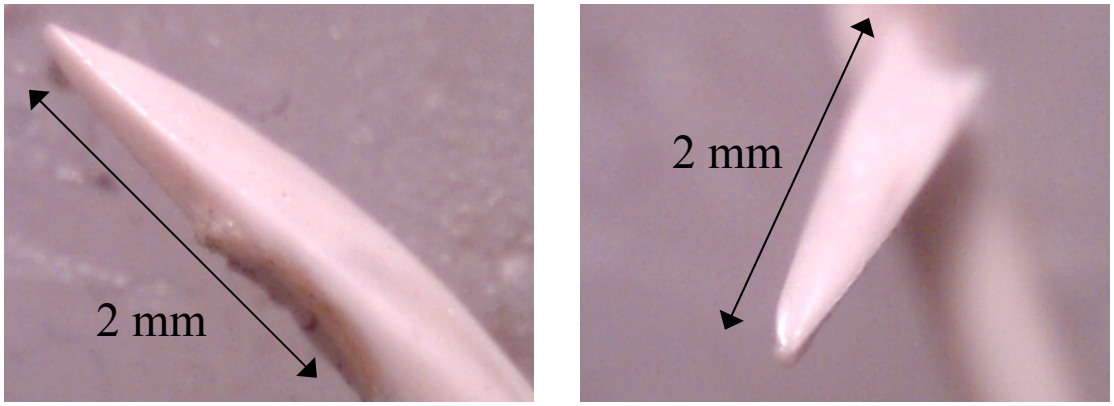

Figure 44 - Tips of 75% A950 / 25% B950 needles after successful (left) and failed (right) penetrations

Table 16 - Penetration test results for 50% A950 / 50% B950, cavity 1

Sample	Penetrated	Buckling Load (N)	Penetration Load (N)	Failure Location
1	N	6.9	-	Tip
2	N	3.7	-	Tip
3	N	4.5	-	Tip
4	Y	-	5.0	N/A
5	Y	-	2.4	N/A
6	N	4.7	-	Tip
7	N	4.0	-	Tip
8	Y	-	3.5	N/A
9	Y	-	2.9	N/A

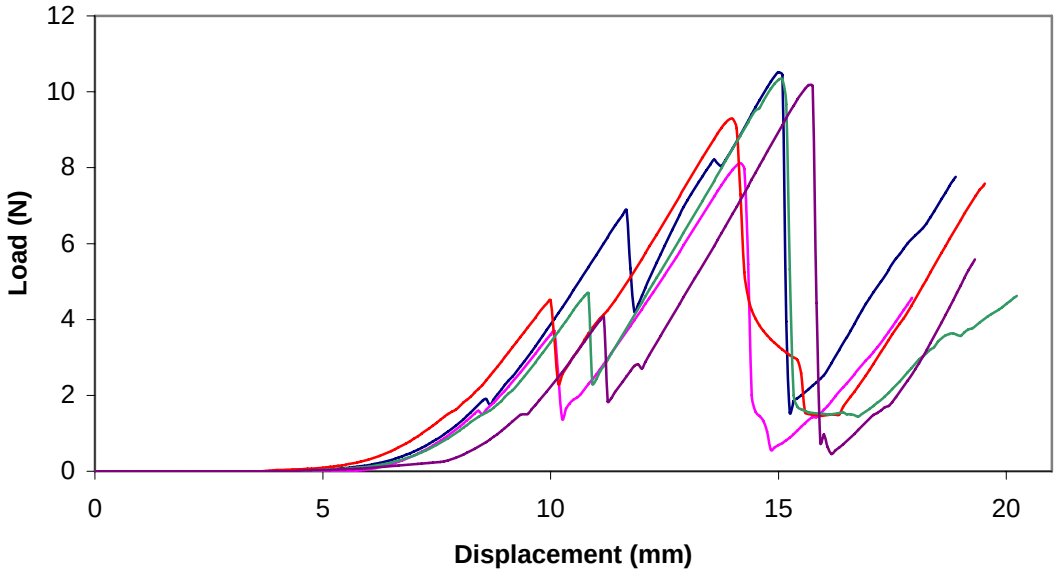

Figure 45 - Failed penetrations for 50% A950 / 50% B950, cavity 1

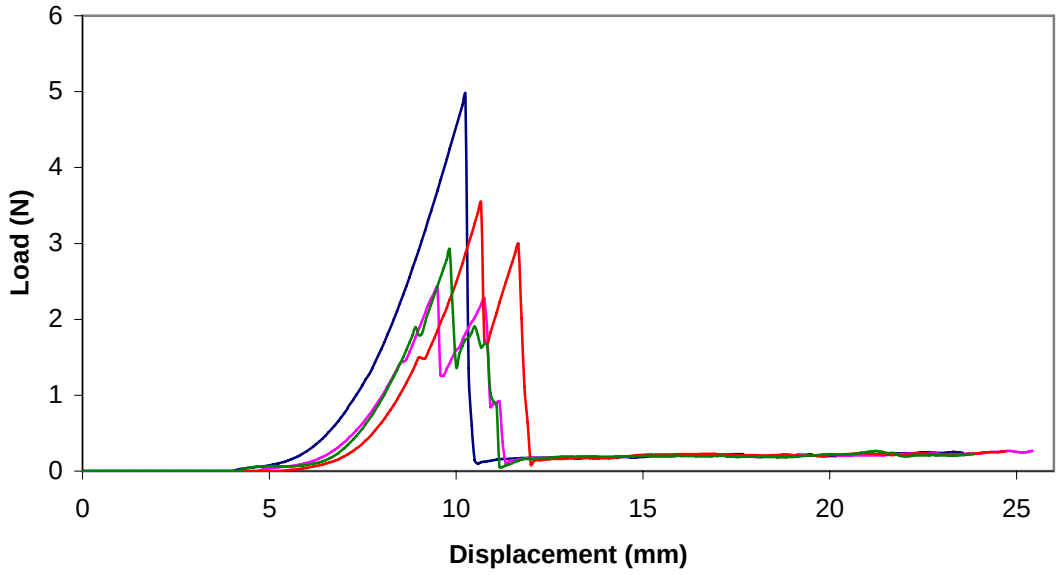

Figure 46 - Successful penetrations for 50% A950 / 50% B950, cavity 1

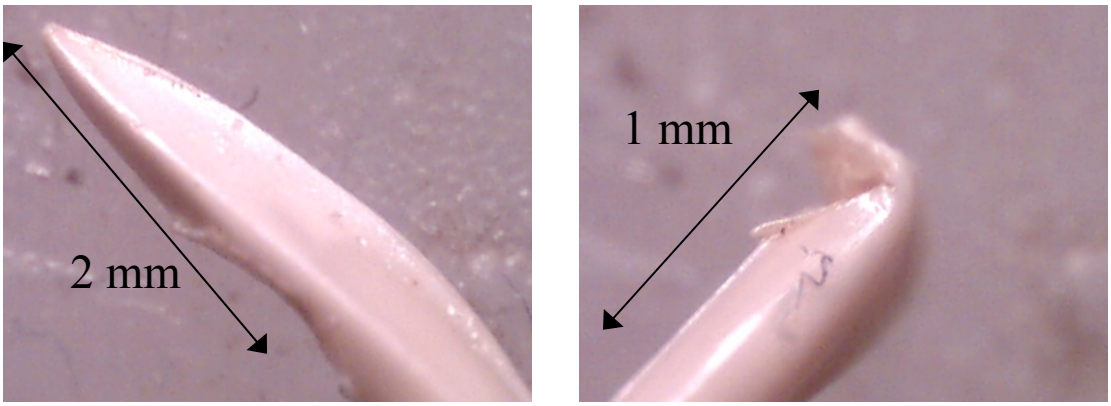

Figure 47 - Tips of 50% A950 / 50% B950 needles after successful (left) and failed (right) penetrations

Table 17 - Penetration test results for 50% A950 / 50% B950 semisolid, cavity 1

Sample	Penetrated	Penetration Load (N)	Failure Location
1	Y	4.5	N/A
2	Y	5.7	N/A
3	Y	3.2	N/A
4	Y	8.6	N/A
5	Y	8.7	N/A
6	Y	5.9	N/A
7	Y	5.5	N/A
8	Y	3.5	N/A
9	Y	4.1	N/A
10	Y	3.4	N/A
11	Y	3.6	N/A

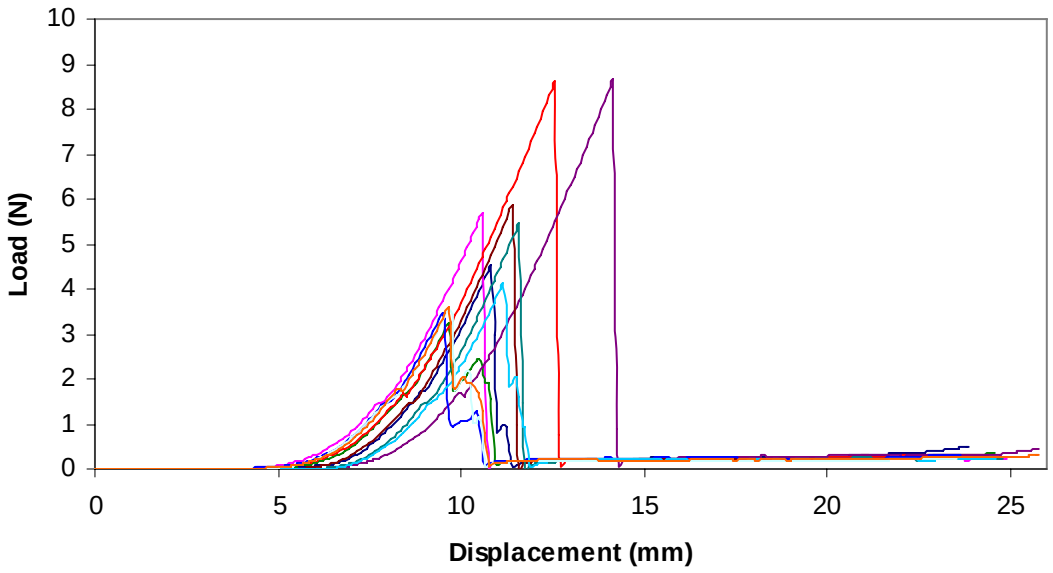

Figure 48 - Successful penetrations for 50% A950 / 50% B950 semisolid, cavity 1

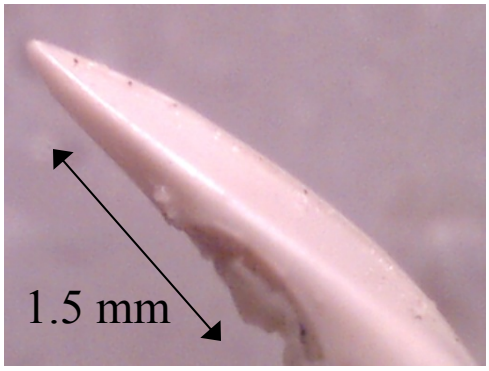

Figure 49 - Tip of 50% A950 / 50% B950 semisolid needle after successful penetration

Table 18 - Penetration test results for 80% A950 / 20% B950, cavity 2

Sample	Penetrated	Buckling Load (N)	Penetration Load (N)	Failure Location
1	Y	-	4.0	N/A
2	Y	-	4.6	N/A
3	Y	-	5.2	N/A
4	N	8.2	-	Tip
5	N	5.7	-	Tip
6	Y	-	3.7	N/A
7	Y	-	3.9	N/A
8	Y	-	5.5	N/A
9	N	4.7	-	Tip
10	Y	-	5.8	N/A
11	Y	-	6.5	N/A

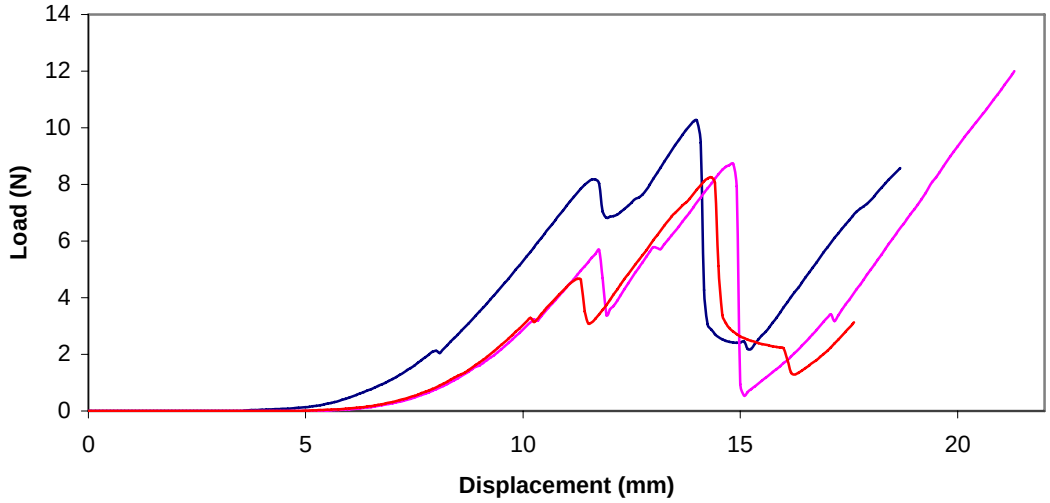

Figure 50 - Failed penetrations for 80% A950 / 20% B950, cavity 2

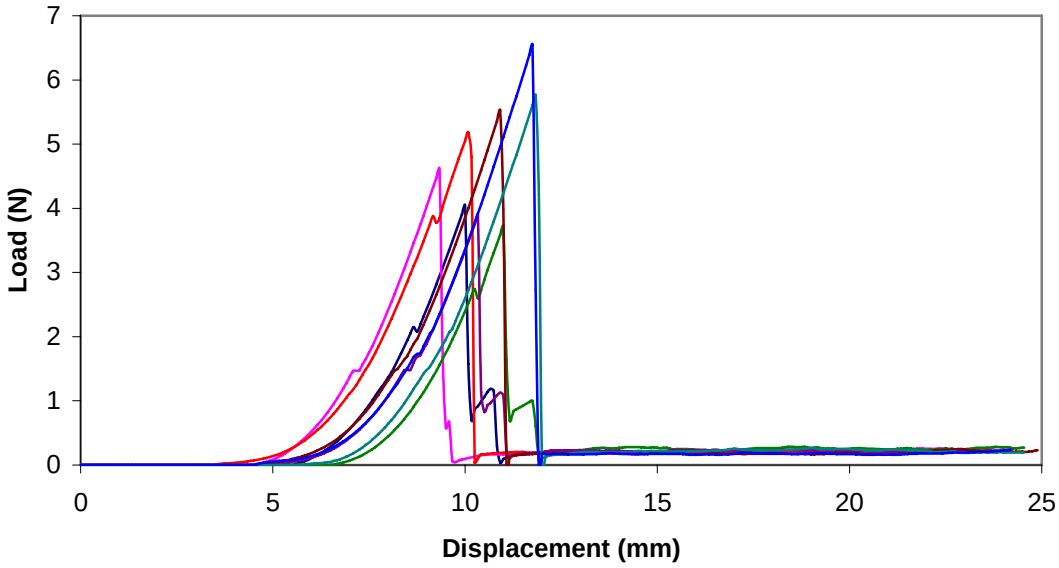

Figure 51 - Successful penetrations for 80% A950 / 20% B950, cavity 2

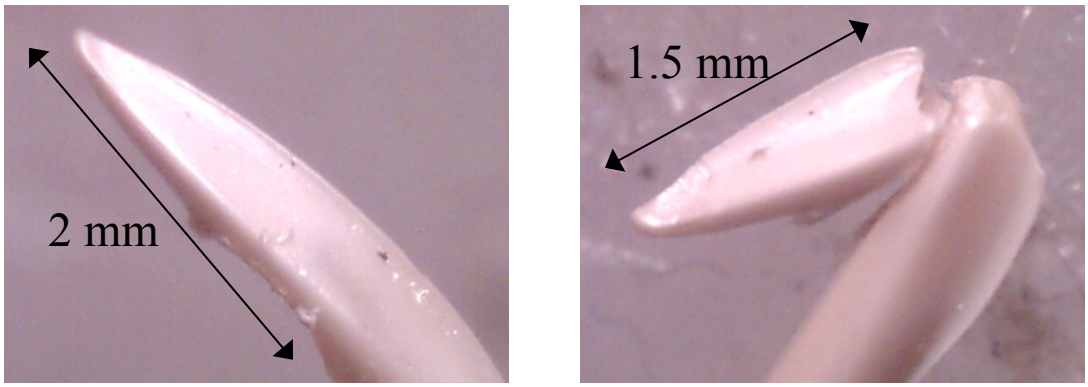

Figure 52 - Tips of 80% A950 / 20% B950 needles after successful (left) and failed (right) penetrations

Table 19 - Penetration test results for 80% A950 / 20% B950 semisolid, cavity 2

Sample	Penetrated	Buckling Load (N)	Penetration Load (N)	Failure Location
1	Y	-	6.8	N/A
2	N	6.2	-	Cannula
3	Y	-	5.0	N/A
4	Y	-	3.9	N/A
5	N	5.2	-	Cannula
6	N	5.8	-	Cannula
7	Y	-	4.2	N/A

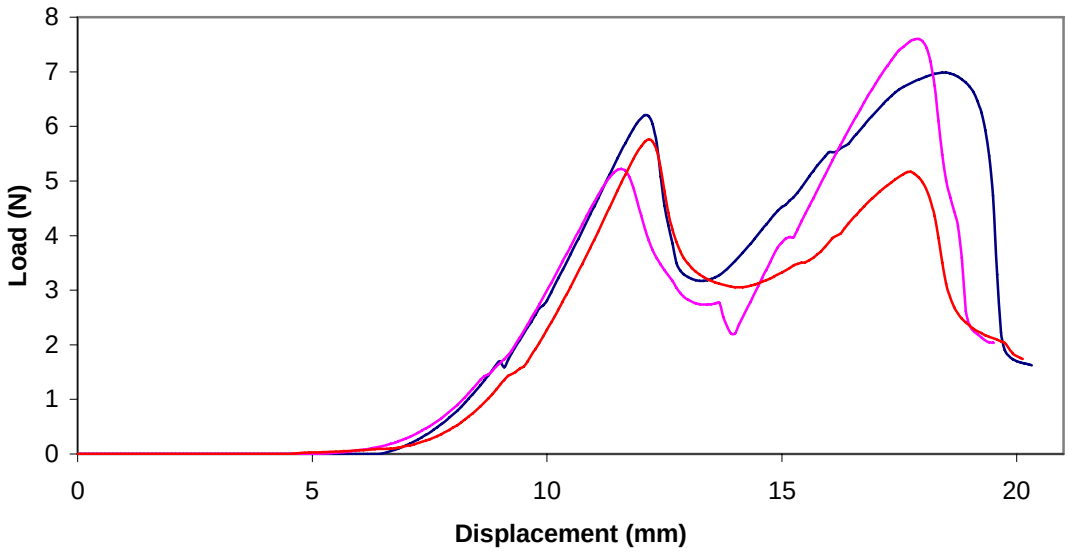

Figure 53 - Failed penetrations for 80% A950 / 20% B950 semisolid, cavity 2

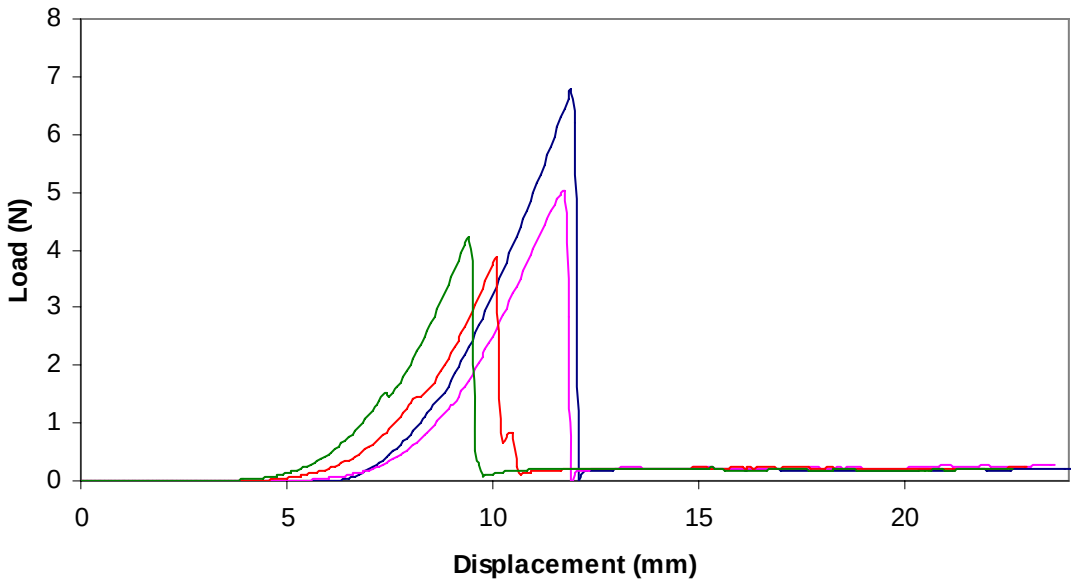

Figure 54 - Successful penetrations for 80% A950 / 20% B950 semisolid, cavity 2

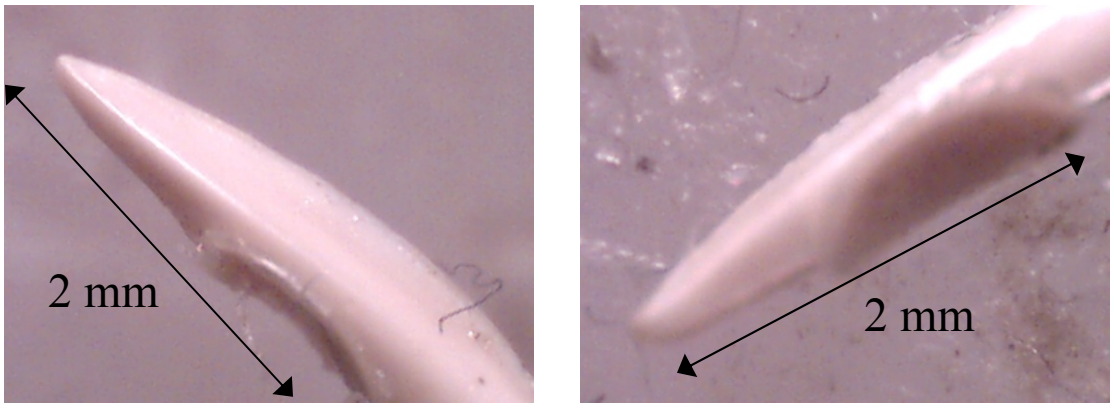

Figure 55 - Tips of 80% A950 / 20% B950 semisolid needles after successful (left) and failed (right) penetrations

From these results, it is evident that some of these combinations outperformed others. The needles with 100% A950 had the lowest percentage of penetration, with only 11% penetrating the polyurethane. These needles also had the lowest average buckling

load of 3.9 N. The failures all occurred at the tip, specifically at the indent where the bore exits the needle. This was also the location of failure for the needles comprising 75% A950 / 25% B950, 50% A950 / 50% B950, and 80% A950 / 20% B950 with the updated cavity, as seen in Figures 41, 44, and 47. However, the penetration percentage increased as the amount of B950 rose, with 20% penetration for needles with 25% B950 and 44% penetration for needles containing 50% B950. The average buckling loads also increased to 4.2 N with 25% B950 and 4.8 N with 50% B950. From this data, keeping the mold cavity the same and increasing the ratio of B950 to A950 in the needle creates a stronger needle that is less likely to buckle. This is as expected because of the higher stiffness of B950 relative to A950.

Also, it can also be inferred that the second mold cavity yields stronger needles because 73% penetration was achieved from this cavity with an average buckling load of 6.2 N, despite containing only 20% B950. The downside to the samples from this category is that the needles still broke at their tips. This is a much less preferable failure location because the tips have a tendency to break off from the needle, whereas a failure along the cannula does not lead to a broken part, only a bent part. The semisolid needles with 50% A950 / 50% B950 all penetrated the polyurethane, compared to a 57% rate from the 80/20 semisolid needles from the second cavity. However, as the failure location for the second set was along the cannula and not at the tip, it would appear that the second cavity provides a stronger tip design overall than the first cavity. Increasing the ratio of B950 to A950, and using the second cavity to provide more strength to the tip, should provide the best conditions for the needles so that failure does not occur before penetration.

One important factor to note when considering a change in the material is the price of the material. While the B950 is a stiffer material than the A950, it also has a considerably higher cost, and thus may not be cost-effective to use. The retail material cost for A950 is approximately $0.0485/g, which would equate to $0.0073/needle. The B950, on the other hand, costs $0.2225/g. The retail material cost of a needle made from 100% B950 would then cost $0.0334, which surpasses the cost of a needle made from either A950 or 1300MT ($0.0125/needle). Although the Ticona B950 has improved material properties for this application, its cost may be too high for use in developing countries.

4.9 Discussion

The early penetration tests yielded a number of interesting results. They demonstrated that polyurethane was the most effective rubber skin mimic and that lubrication was necessary for effective penetration. The lubricant tested was similar to that used on steel needles. Penetration testing showed that the lubricant with a 5% silicone content is more effective than with a 2.5% silicone content. The percent of successful penetrations increased from 21% to 30% as the silicone content increased for 38.1 mm length needles, and from 25% to 67% for 25.4 mm length needles. In addition, increasing the cure time from 3 to 7 days lowered the percentage of penetration from 26% to 20% for 38.1 mm length needles, and from 75% to 37% for 25.4 mm length needles. Similar testing with the silicone dispersion was performed on 38.1 mm length steel needles to compare the dispersion with the steel needles' as-received lubricant. The steel needles, even those not lubricated, all penetrated the polyurethane rubber. However,

the penetration forces increased from 0.52 N for as-received needles to 0.74 N for needles lubricated with the silicone dispersion to 1.12 N for unlubricated needles.

The load-displacement curves for the penetration tests showed some similarities between the plastic needles and the steel needles. The plastic needles primarily peaked at a maximum load before immediately dropping to the frictional load. The steel needles, however, catch at the location of their holes, creating what looks like a double penetration force. This is actually a drag of the hole on the polyurethane. It is also noted in some of the plastic needle tests, and could represent excess material gathered around the hole. As the hole is located on the side of the needle, as opposed to the tip, it will not catch on every penetration. Only when excess material is present will this catching be present. As a result, most of the plastic needles do not show this behavior.

For the successful penetration tests with the 38.1 mm length needles, penetration occurred after approximately 5 mm of vertical displacement following contact with the polyurethane. Given a constant speed of 100 mm/min, penetration therefore occurs after about 3 seconds of contact. With the 25.4 mm length needles, penetration occurs after 6-10 mm of vertical displacement, or about 3.6-6 seconds. The 19.0 mm needles penetrate the polyurethane after 6-8 mm, corresponding to penetration 3.6-4.8 seconds after initial contact with the polyurethane.

Penetration tests into other media also demonstrated the capabilities of the plastic needles. The 25.4 mm length needles exhibited a 75% penetration rate in the pig skin, compared to 0% of the 38.1 mm length needles penetrating. The penetration forces, averaging 8.4 N, were also similar to those from the polyurethane tests. The steel needles also achieved a 100% penetration rate on the pig skin, with a 1.0 N average penetration

force. Similar results and forces were found with the butyl rubber tests, except the steel needles experienced a 4.0 N average penetration force. The butyl rubber tests demonstrated an area of concern for the plastic needles, as they could not successfully penetrate the polyurethane following successful penetration into the butyl rubber. As relubricated needles penetrated the polyurethane at a comparable rate to needles that only made one penetration into the polyurethane, tip damage was not the cause for the failure to make the second penetration. As a result, the lubricant will need to be optimized to withstand two penetrations for each needle.

The steerability tests also demonstrated a need for greater development. The needles were unable to penetrate the polyurethane at an angle other than 90° to the needle. In addition, the 38.1 mm length needles were bent following penetration into silicone rubber, so the tips were located approximately 1-2 mm from their intended location. The 25.4 mm length needles did not bend following penetration, and their tips were in line with the intended needle location.

Subsequent needle designs showed increases in the penetration rates, indicating that changes in both the mold cavity and the needle material can be optimized to yield more favorable penetration rates. Applying combinations that were mentioned in section 4.8, but not tested, may yield the best results in penetration.

4.10 Summary

The penetration experiments indicated that the 25.4 mm plastic needles were more effective in penetration than the 38.1 mm length plastic needles with similar lubrication. Experiments were conducted to optimize the lubricant applied to the needles, and tests

were conducted to measure its effectiveness on both the plastic and steel needles. Once an adequate lubricant was chosen, the plastic needles were further tested with polyurethane and pig skin as mimics for human skin, and with butyl rubber stoppers to simulate insertion into a drug vial. With the 25.4 mm length plastic needles achieving a reasonable percentage of penetration for the first needle design, it is conceivable that further development of the tip design will yield even more favorable results in penetration. Given that the penetration tests indicated that the plastic needles have the capability to replace steel needles, more tests were needed to fully analyze the needles' strengths. These tests are described in Chapter 5.

CHAPTER 5

NEEDLE CHARACTERIZATION EXPERIMENTS

In addition to the penetration tests, other tests were performed to verify whether the needles complied with international standards that govern the performance of hypodermic needles. These included a perpendicular force test, a cannula stiffness test, and a fluid flow test. These tests are necessary to fully ensure the needles' viability as a substitute for steel needles.

5.1 Perpendicular force tests

The perpendicular force test, outlined in Appendix A, "Resistance to Breakage Testing Protocol" and ISO 9626 - Annex D [41], was used to test the plastic needle's ability to withstand breakage when a fluctuating load is applied at the tip perpendicular to the axis of the cannula. The needles used for this test were the original LCP needles with a 38.1 mm length. This test was performed on the Instron testing machine, with the needle supported from its hub, extending horizontally. An aluminum piece, consisting of two cylinders oriented perpendicular to the needle (see Figure 56), was attached to the crosshead which enabled the needle to bend vertically, both up and down, as the crosshead was moved in that direction. The test setup is shown in Figure 56. The needles were bent 25° from the horizontal in each direction, creating a 50° included angle, over 20 complete cycles. The objective of this test was for the needles to

withstand the applied bending without fracture occurring. Five repetitions of the test were performed. As the needles did not break during this test due to the flexibility of the LCP, they passed the test. This test was not performed on the steel needles, as it was assumed that they met the standard or would not be commercially available.

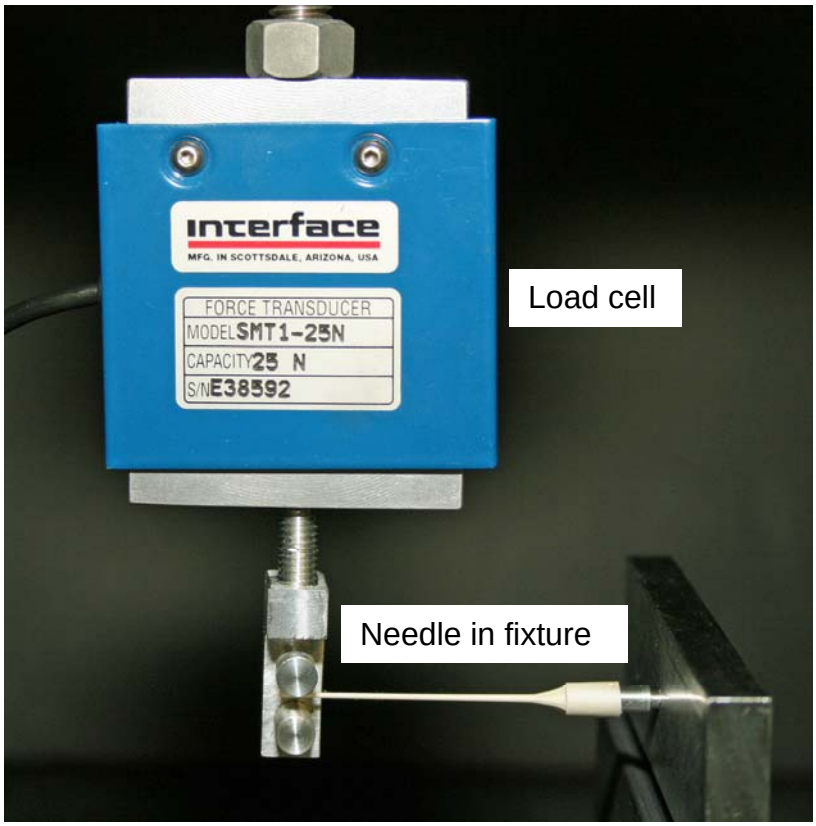

Figure 56 - Perpendicular force test setup

5.2 Cannula stiffness tests

Cannula stiffness tests were performed on the needles to determine their strength when subjected to an applied load normal to the cannula at its approximate midpoint. The conditions for the stiffness test are described in Appendix A, "Stiffness Testing

Protocol", and ISO 9626 - Annex C [41]. For the 22 gage plastic needles, the span between the two supports is 15 mm, and the required bending force is 10 N. This is the force that the needle is required to withstand over a maximum deflection of 0.45 mm. The tests were performed on the Instron machine; the setup was exactly as described in the ISO document and is shown in Figure 57. The needles were tested with a cannula length of 38.1 mm, and the hub was removed, leaving only the cannula. The needles were unable to withstand a 10 N force applied perpendicular to the length of the cannula at their midpoints. The maximum force applied was approximately 2.2-2.7 N, after which, the cannula continued deflecting without the load increasing. The test was stopped when the included angle formed by the bending cannula reached ~90°, and the needle had not broken by this point. By comparison, the steel needles were able to withstand the 10 N force, but not within the 0.45 mm maximum deflection that the standard requires. These results are summarized in Table 20.

Table 20 - Cannula stiffness testing results

Material	Maximum load (N)	Deflection at max. load (mm)	Load at 0.45 mm (N)
Plastic	2.7	2.6	0.44
Plastic	2.2	2.1	1.4
Plastic	2.6	1.5	1.6
Steel	10	0.75	4.5

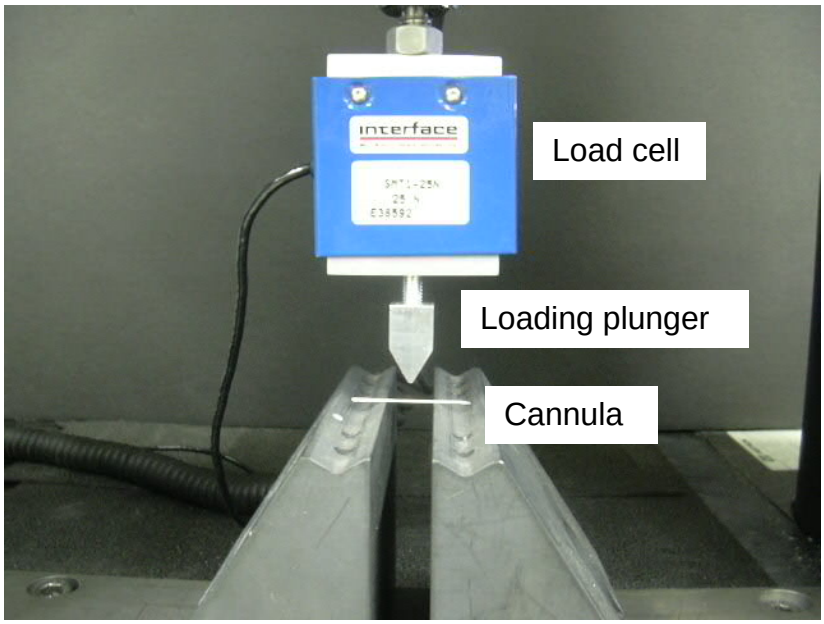

Figure 57 - Stiffness test setup

5.3 Fluid flow tests

Fluid flow tests also were performed on the needles. These are important because delivering fluid is the primary objective of a hypodermic needle insertion. The test was performed by affixing a syringe to the base of the Instron testing machine with the plunger extending upwards. The load cell was forced down onto the plunger, expelling the contents (water or air) while measuring the force required to push the plunger. Two different syringes are used, with volumes of 1 ml (Becton-Dickinson 1 ml Luer-Lok Syringe, #309628) and 3 ml (Becton-Dickinson 3 ml Syringe, Slip Top, #309586), and two speeds were tested, 20 mm/min and 200 mm/min. The full-length plastic needle (38.1 mm) was tested, as were the InviroMedical steel needles (38.1 mm length) and syringes without needles. The tests on the 1 ml syringe expelled approximately 0.8 ml of fluid, and the tests on the 3 ml syringe expelled approximately 2.5 ml of fluid. Both tests

were set to run for a 50 mm distance. Two tests were run for each needle/syringe/ liquid/speed combination.

The results are summarized in Tables 21-28. Each test shows an early spike in force to initiate plunger movement, labeled "initial" in the tables. The average force is the average of the highest and lowest values registered following the initial spike. The results show the forces required to depress the syringe at 20 mm/min are lower than those required for 200 mm/min for both the 1 ml syringe and the 3 ml syringe. In addition, the forces required to depress the 1 ml syringe are lower than those for the 3 ml syringe.

Table 21 - Fluid flow tests, 3 ml syringe, no needle (forces in N)

		20 mm/min	20 mm/min	200 mm/min	200 mm/min
air	initial	0.89	0.75	1.59	1.60
	average	0.67	0.73	1.29	1.22
water	initial	0.42	0.78	2.06	2.31
	average	0.44	0.78	1.28	1.55

Table 22 - Fluid flow tests, 3 ml syringe, plastic needle (forces in N)

		20 mm/min	20 mm/min	200 mm/min	200 mm/min
air	initial	1.60	0.86	1.53	1.35
	average	0.95	0.92	1.40	1.36
water	initial	0.86	0.94	1.70	2.50
	average	0.68	0.78	7.30	7.40

Table 23 - Fluid flow tests, 3 ml syringe, plastic needle (forces in N)

		20 mm/min	20 mm/min	200 mm/min	200 mm/min
air	initial	0.69	0.75	1.60	1.79
	average	0.63	0.80	1.24	1.42
water	initial	0.80	1.37	1.50	2.30
	average	0.81	0.78	3.30	3.80

Table 24 - Fluid flow tests, 3 ml syringe, steel needle (forces in N)

		20 mm/min	20 mm/min	200 mm/min	200 mm/min
air	initial	0.90	0.64	2.22	1.41
	average	0.59	0.57	1.08	1.06
water	initial	0.74	0.83	2.26	2.51
	average	0.68	0.63	1.91	2.19

Table 25 - Fluid flow tests, 1 ml syringe, no needle (forces in N)

		20 mm/min	20 mm/min	200 mm/min	200 mm/min
air	initial	0.22	0.40	0.81	0.65
	average	0.30	0.39	1.11	0.66
water	initial	0.44	0.24	1.04	1.04
	average	0.35	0.24	0.79	0.89

Table 26 - Fluid flow tests, 1 ml syringe, plastic needle (forces in N)

		20 mm/min	20 mm/min	200 mm/min	200 mm/min
air	initial	0.40	0.77	0.87	0.91
	average	0.29	0.55	1.10	0.98
water	initial	0.32	0.31	0.89	1.17
	average	0.33	0.28	1.09	0.93

Table 27 - Fluid flow tests, 1 ml syringe, plastic needle (forces in N)

		20 mm/min	20 mm/min	200 mm/min	200 mm/min
air	initial	0.36	0.48	0.79	0.86
	average	0.33	0.44	0.75	0.84
water	initial	0.23	0.28	1.04	1.34
	average	0.25	0.21	0.88	1.28

Table 28 - Fluid flow tests, 1 ml syringe, steel needle (forces in N)

		20 mm/min	20 mm/min	200 mm/min	200 mm/min
air	initial	0.27	0.14	0.73	0.71
	average	0.18	0.26	0.81	0.98
water	initial	0.33	0.36	1.15	1.11
	average	0.23	0.17	0.98	0.89

These results show that the plastic needles perform similarly to the steel needles for the delivery of air. With the 3 ml syringes, the plastic needles and steel needles show comparable forces, with the exception of one test with plastic needles and air. They are also comparable with air at both speeds with the 1 ml syringes. These forces are similar to the empty syringes with air. Using water, the plastic needles and steel needles have very similar forces to each other and to the empty syringes when tested with the 1 ml syringes. With the 3 ml syringes, the plastic needles and steel needles both have higher forces than the empty syringes at 20 mm/min. However, at 200 mm/min, the plastic needles have greatly increased forces, registering 3.3 N, 3.8 N, 7.3 N, and 7.4 N for their four tests, while the steel needles were again similar to the empty syringes. These forces are much higher than any other syringe/needle/speed combination. There are no required values for the force to empty a syringe-needle combination. The recommended values for filling the syringe-needle combination are 10 N to initiate plunger movement, and 5 N average value according to Annex G of ISO 7886-1 [46] and WHO standards [47]. So, the experimental values should be acceptable without modification of the needles, with the exception of the plastic needles at high speed with the 3 ml syringe. These values may be lowered by increasing the bore of the plastic needles, which when optimized will prevent high forces from occurring when emptying a syringe.

5.4 Summary

Additional tests performed on the plastic needles to determine their ability to replace steel needles indicated that they can be capable replacements. The plastic needles passed the perpendicular force test and showed positive results in the fluid flow tests.

They did not pass the cannula stiffness tests, but neither did the steel needles, so this may still be an acceptable result. The results from the tests described in Chapters 2-5 will be summarized in Chapter 6.

CHAPTER 6

DISCUSSION

The results show that these plastic needles have the potential to penetrate through a skin mimic without buckling, and thus may be a suitable replacement for steel hypodermic needles. Numerous tests were conducted throughout this thesis to both verify the plastic needle's ability to perform the tasks required of a hypodermic needle and to optimize its performance. These tests are summarized in Table 29, along with the section in which each test's particular methods and results can be found.

Table 29 - Summary of test results

Goal	Test(s) performed	Section	Results
Successful penetration	penetration (skin mimics, pig skin, butyl rubber)	4.4-4.9	pass (67-75%)
Model the needle penetration and buckling, determine penetration and buckling loads	penetration FEA, buckling FEA	2.2, 3.2	pass (calculations needed to determine penetration load), deformable needle result desired
Determine maximum loads on needle	buckling	2.3	pass
Optimize lubricant	lubricant optimization	4.5	pass
No breakage after perpendicular load applied at tip	perpendicular force	5.1	pass
Adequate cannula stiffness	cannula stiffness	5.2	fail (use steerability results)
No bending after insertion at non-orthogonal angle	steerability	4.8	fail
Pass fluid through needle	fluid flow	5.3	pass

Theory was developed to characterize the penetration action and predict the needles' behavior during penetration. These equations described the strain exhibited by the skin mimic prior to penetration as well as the load required for penetration. They show that the elastic strain achieved by the solid is 0.9; beyond this point, the strain will be plastic. The load required for penetration into polyurethane to occur is estimated from these equations to be 1.6 to 3.5 N, which is comparable to some of the penetration loads achieved during the polyurethane tests. In addition, Euler buckling equations were used to analyze the buckling loads on the needles. These approximated the needles' buckling loads to be 6.1 N for the 38.1 mm length needles and 9.7 N for the 25.4 mm length needles.

From the buckling tests, it is evident that shorter needles are more robust than longer needles of the same construction and diameter. This is noted in column buckling theory and supported by the simulated and experimental data (see section 2.4). This observation correlates to the penetration behavior of these needles as well. The 25.4 mm length plastic needles can achieve a higher percentage of penetration because they can withstand higher axial loads. Whereas a 38.1 mm length plastic needle requires a penetration load less than 6 N (see Figures 30-31 and 59-64), the 25.4 mm length plastic needles can sustain loads up to 11 N before buckling (see Figures 65-72). Thus, any penetration that would occur between 6 and 11 N may take place with the 25.4 mm length needles, but will not with the 38.1 mm length needles. This is the primary reason that, as long as the tip is designed so that, when correctly lubricated, penetration forces greater than 6 N may be present, 25.4 mm length needles will be superior in penetration than 38.1 mm length needles.

While the 25.4 mm length needles can sustain higher penetration forces, they also have lower friction forces. These can be seen in the graphs in Appendix E. The friction forces increase as the needle is inserted further into the skin because the taper creates an increase in the needle's diameter. This causes two things to occur. First, the size of the needle/skin interface increases because of the larger circumference, and thus surface area, of the cannula as it is inserted. Assuming that the friction forces resisting the needle's movement do not change for a constant area, as seen in the graphs of the steel needle penetrations, they will increase as the area increases. Second, stretching will occur in the skin as the needle continues penetrating because the initial hole created is smaller than the diameter of the needle at its tip (see Equation 17, where a/R is found to be less than 1). This is also evident by the fact that frictional forces are present. Expanding this hole, which is necessary for the increased diameter to continue insertion, creates stretching in the skin. This results in the friction forces increasing during insertion. As the 25.4 mm length needles do not experience as great a taper as the 38.1 mm length needles, the friction forces are lower. This is a significant benefit for the 25.4 mm length needles.

The penetration tests compared reasonably well to the finite element penetration simulations. The simulations, which were performed with a model of a 38.1 mm length needle, indicated that the needle tip would fail prior to penetration. A prediction of failure is reasonable because the 38.1 mm length needles penetrated at a 30% success rate. The rigid body penetration simulations also compare favorably to the tests, as they showed penetration at approximately 2.7 seconds after initial contact. The successful penetration tests with the 38.1 mm length lubricated needles penetrated the polyurethane 3 seconds after initial contact, indicating that the simulation is accurate. Of course,

differences exist between the simulation and the actual testing, such as the frictionless condition considered in the simulation, so the results will not perfectly match. The simulation does provide a benchmark for the results in the actual tests.

These results are in contrast to the other results obtained by the simulation. Contact forces between the needle model and the rubber were modeled in the finite element simulation, and the output was significantly greater than the actual forces seen in the penetration testing. Whereas both the theory and the penetration tests showed penetration forces of 4-6 N for 38.1 mm length needles, the FEA estimated the penetration force to be around 10^8 N. This value is clearly not consistent with the actual test data. Thus, it can be determined that the penetration force output from ABAQUS is incorrect, and it will not be considered when using the model to predict needle penetration behavior. Overall, the FEA is a good predictor of needle penetration behavior and stresses, but does not compute the force values well.

The penetration tests into other useful media also generated positive results for the plastic needles. Initially, penetration tests were conducted using photoelastic sheets and silicone rubber as skin mimics. These, however, were ineffective mimics, and other materials were considered. Pig skin and butyl rubber were more useful penetration media. The needles' ability to penetrate the pig skin is important because of pig skin's greater toughness as compared to human skin. Pig skin is also tougher than the polyurethane, resulting in a lower percentage of penetration than the polyurethane, which is to be expected. On the other hand, the butyl rubber is not as tough as the pig skin, and the percentage of penetration was higher. This is important because needles often will need to be inserted into butyl rubber prior to penetration in skin. The shortcomings of the

needle and lubrication were noted when the needles failed to penetrate the polyurethane following insertion into the butyl rubber. The needle must remain lubricated after its first insertion in order to reduce the penetration forces and therefore the pain felt by a person receiving the injection.

Overall, lubrication proved to be beneficial for aiding penetration. Early lubrication testing with the silicone oil demonstrated that the silicone oil was an inefficient lubricant, as it did not adhere to the needle. As a result, it could not be effective because the lubricant would need to be applied well in advance of the needle's usage. In addition, it did not assist penetration. The Dow Corning MDX4-4150 silicone dispersion, a commercial lubricant used on steel needles, increased the percentage of penetration for plastic needles of both 38.1 mm length and 25.4 mm length. In addition, the friction forces decreased compared to unlubricated needles.

These results were similar to those for steel needle penetrations. The needles cleaned and then relubricated with MDX4-4159 showed a decrease in the penetration force from an average of 1.12 N to an average of 0.74 N compared to steel needles that had their original lubricant removed. The average friction force also decreased overall and was more consistent than unlubricated steel needles. Work was performed to optimize the lubricant in terms of both silicone content and cure time. Although these factors were chosen to be 5% and three days respectively, more work may be necessary for complete optimization of these factors. This was evident with the steel needles as well, as both the average penetration force and friction force were slightly higher for the relubricated needles than for the needles containing their original lubrication. Although

other factors may have influenced these results, it is still reasonable to infer that potential exists for improving the lubrication on the needles.

The needles' tips held up relatively well for successful penetrations. Comparing them from pre-test to post-test using the polyurethane, the pig skin, and the butyl rubber indicated that the tips did not deform during the test. Failed penetrations, on the other hand, occasionally led to tip damage. The two types of tip damage that resulted were tip breakage at the hole and a blunting at the immediate tip. The breakage only occurred for the newer needle designs, and the damage is evident in Figures 41, 44, and 47. Figure 11 shows tip blunting, which is most common during failed penetrations using the original set of needles. These observations held for needles of both 38.1 mm length and 25.4 mm length.

The other tests conducted on the plastic needles also verified their strength, which is necessary for worldwide certification. The perpendicular force test, in particular, was significant because it demonstrated that the needle can be repeatedly bent laterally without breaking. Although this motion is similar to buckling in that it would render the needle useless, it is still important that the needle does not break under these circumstances. The cannula stiffness tests were unable to be successfully completed, which is to be expected as the steel needles also did not pass this test. The plastic needle's strength can be determined from the steerability test, which measure the bend after penetration. The steerability test shows that some bending occurs, specifically for the longer needles. The knowledge of the needle's strength is pertinent for generating its next design. The penetration tests on the new designs, found in section 4.9, showed a frequent flaw in that the tips broke off during failure, compared to the needle buckling

seen in the first design. In fact, only one of the five new designs that did not achieve a 100% percentage of penetration experienced cannula buckling as opposed to tip breakage as its failure mechanism. Knowing that the material is robust, the tip must be strong enough to prevent breakage in the event of failure.

When compared to steel needles, the plastic needles are somewhat inferior. Even when lubricated with the silicone dispersion, the plastic needles show higher penetration forces and friction forces when inserted into the same material. One factor to consider is that the steel needles have benefited from years of design and research, while these plastic needles are still in the prototype phase. The plastic needles will ultimately need to achieve a 100% penetration rate to be considered for mass use as an alternative to the steel needles, and recommendations to attain this target are discussed in Chapter 7.

CHAPTER 7

CONCLUSIONS AND RECOMMENDATIONS FOR FUTURE WORK

7.1 Conclusions

The plastic needles studied for this research have the capabilities to replace steel hypodermic needles, but more work is necessary to refine them so that the needles are sufficient for each penetration. The penetration tests indicate that the plastic needles are capable of penetrating a rubber skin mimic, with penetration loads lower than their buckling loads. The buckling simulations and tests demonstrate that shorter needles can withstand greater buckling loads than longer needles of the same diameter. However, the needles performed differently in the penetration tests, with the 25.4 mm length needles achieving a higher percentage of penetration in multiple skin mimics than both 38.1 mm length needles and 19.0 mm length needles. This result, coupled with the constraint that 19.0 mm length needles may be too short to be used effectively in practice, indicates that 25.4 mm may be the optimal length for manufacturing 22 gage plastic hypodermic needles. Further research should continue with 25.4 mm length needles because of their overall effectiveness compared to the 38.1 mm length needles.

The finite element simulations effectively modeled the penetration with a 38.1 mm length needle. The time required for penetration to occur was comparable to the time recorded during actual penetration tests, and the resulting von Mises stress field in the rubber was similar to what would be expected from the given loading scenario.

However, the contact forces between the needle and the rubber given by the simulation were many orders of magnitude larger than those measured from the penetration tests, so these numbers fail to provide an accurate representation of the forces present during the penetration. In addition, the needle experienced a failure at the tip with the deformable needle model. While tip deformation may occur during a penetration test, the test is allowed to run until either penetration occurs or failure in the cannula takes place. Thus, the simulation ended prematurely, and it is unknown whether the needle would be predicted to penetrate the rubber following the tip deformation.

The skin mimics used for the plastic needle testing, specifically the polyurethane rubber and the pig skin, are effective for predicting needle and skin behavior during penetration. This is noted by the similar results achieved between the two materials. The plastic needles of 25.4 mm length attained 67% penetration into the polyurethane and 75% penetration into the pig skin, with comparable penetration forces as well. The steel needles successfully penetrated both materials without failure, and the penetration forces were also consistent. One area in which the plastic needles failed, and thus will need to be developed, was in the test of multiple penetrations without relubrication, with butyl rubber and polyurethane acting as the materials into which the needle would be injected. This test demonstrates a needle's ability to be inserted first into a vial and then into skin. While all the plastic needles penetrated the butyl rubber, none then pierced the polyurethane, which is an issue that must be addressed by optimizing the lubricant applied to the needles.

The silicone dispersion lubricant is beneficial for improving the needles' performance during penetration into the rubber skin mimic. The lubricated needles not

only showed a higher penetration percentage, but they also had reduced penetration and friction forces compared to unlubricated needles under similar conditions. This would result in decreased pain for the subject receiving the injection. However, the plastic needles do not meet the performance characteristics of the steel needles currently used for injections, as the forces are greatly increased for needles of the same length. This is due to many factors, such as the tip design, which is still in the prototype phase for the needles tested in this thesis, the taper in the needles, which causes increased friction forces, inconsistent lubrication, and an inherently weaker material than steel. Testing on the lubricant's silicone content and cure time, using the manufacturer's recommended ranges as guidelines, has helped to optimize these variables, thus improving the lubricant's ability to aid penetration.

Additional testing on the plastic needles, apart from penetration testing, generated mostly positive results, as the needles are structurally capable. The needles passed a perpendicular force test, but failed a cannula strength test, both of which are required by ISO 9626 to meet international certification. However, the steel needles also did not pass the cannula stiffness test. Although the plastic needles withstood a lower force than the steel needles, they are in the same position as the steel needles with regards to this test. Fluid flow testing on the plastic needles demonstrated that they are mostly equal to the steel needles in terms of the force required to expel fluid from an attached syringe. Although the design is dissimilar, with the hole exiting on the side of the needle as opposed to through the tip, the difference in measured force to cause fluid flow is minimal for most of the tests. While one particular syringe/speed combination did

generate high forces for the plastic needles, the forces were still well below those specified by ISO 7886 and WHO standards.

The theory governing needle penetration accurately predicts the forces required for penetration to occur. The pre-penetration equations show that a combination of bending and stretching occurs in the rubber prior to penetration, and the maximum force achieved before penetration is governed by the rubber's mechanical properties and the needle's tip radius. The results show that as the needle's tip radius increases, which represents a tip with lower sharpness, the force generated prior to penetration similarly increases. The penetration equations indicate that lower penetration forces can be achieved with optimal tip sharpness. In addition, the work necessary for crack formation in the rubber remains constant over varying possible fracture toughness values, as the size of the crack formed decreases for increasing values of fracture toughness. Thus, the work required to open the crack increases because a larger area must be created for the crack to attain the needle's size. Therefore, the dominant force in penetration is primarily the crack growth phase, especially for increasing fracture toughness values.

As the plastic needles often did not either completely penetrate or fail to penetrate the penetration medium used in the tests, there were clearly differences among the needles that caused them to perform differently during these tests. One particular issue was the lubricant. As the lubrication process was not automated and new samples of the lubricant were created for each test, there was no guarantee of perfect replication of application each time. The lubricant may have had slight differences in the composition or coverage area on the needle, which could contribute to their variation in performance. Another primary difference in the needles included the tip radius. With the tip radius

covering a range of values, a variation in the penetration force would be expected. This was actually predicted to occur using the pre-penetration equations, which were dependent upon tip radius. More uniformity can be expected in the experimental tests if the plastic needles have the same lubricant and tip consistency.

7.2 Recommendations for future work

This thesis has shown that plastic hypodermic needles are capable of penetration into rubber skin mimics. However, it has also indicated that penetration is not guaranteed, and more work is required to fully ensure that the needles achieve a higher penetration rate. Table 30 summarizes the tests that did not pass their objectives and lists suggestions for attaining the goals in these tests.

Table 30 - Methods to improve upon failed tests

Test	Challenges	Changes
Cannula Stiffness	Increase stiffness in cannula	Steel needles also failed this test. Use steerability test to measure cannula strength, as it measures the bend in the cannula following penetration.
Steerability	Increase stiffness to eliminate bend	Focus on the material choice and the cannula design, specifically wall thickness.
Penetration	Achive a higher penetration rate	Focus on improving tip design, starting with the new cavity. Use stiffer materials, such as PEEK, ABS, polycarbonate and metal or glass reinforced polymers. Increase the consistency in the lubricant, including trying hydrocarbons, esters, or ethers.
Penetration force	Lower the penetration force	Focus on tip sharpness, material, and lubricant. Compensating a weak tip with more material should increase the penetration rate, but will not decrease the force.
FEA	Improve the deformable needle result	Distribute the load better, moving it off the stressed element. This could include flattening the tip or applying the load in sections down the cannula.

The alterations in the tip design that have begun should continue. The tip needs to contain the optimal amount of material relative to its sharpness. It must be sharp enough to cause penetration, but sufficiently bulky to prevent breakage. It should also contain the ridge behind the outlet hole (see the tip in Figure 9). This provides extra reinforcement in a weaker area of the needle, as evidenced by the frequent tip failures in the newer models, which would provide an opportunity for a higher percentage of penetration, thus reducing the number of needles that would be wasted due to failure. Multiple shapes of the tip should also be considered. Some of these may include the current tip, slight alterations of that design, tips utilized by steel needles (see ISO 7864, Figure 2 [40] for examples), and modifications of those designs. Optimization of the tip is crucial for producing the best design of a plastic hypodermic needle.

Also, the lubrication technique needs to be refined using the MDX4-4159. A process similar to the way that steel needles are lubricated would need to be developed and introduced for use on the plastic needles. The lubricant itself must also be refined and tested to determine the most appropriate silicone content in the dispersion. In addition, the needles can be tested with different lubricants, including hydrocarbons, ethers, and esters. The tests will include successful penetrations into both the butyl rubber and either the polyurethane or pig skin consecutively. This is necessary to ensure that the needles can extract fluid from a vial before safely depositing it into the subject.

The material comprising the needles should also be optimized. While the Ticona 1300MT, which has comparable properties to A950, is a reasonable choice as a medical grade polymer, the experiments show that increasing the proportion of B950 creates a stronger product, with fewer failures given the same mold cavity. Tests should be

performed to determine the appropriate amount of B950 (or a medical grade of B950) to be used in the needle. The needles also should be tested comprised of different plastics or composites. PEEK (polyetheretherketone) is one example of a plastic that has been used in medical applications, and its cost ($0.0633/g , $0.0095/needle) is comparable to the Ticona 1300MT used for the current needle. Other potential plastics include ABS (acrylonitrile butadiene styrene) or a polycarbonate, such as Lexan, both of which are significantly less expensive than the materials mentioned previously, at approximately $0.0028/g ($0.0004/needle) and $0.0066/g ($0.0010/needle) respectively.

Other factors that should be included in the material selection are the attainable sharpness level of the tip, overall material stiffness, and the ease of manufacture, given the material used. The stiffness should be high enough so that the needles do not bend following insertion at non-orthogonal angles. To ensure that the next iteration of the needles can sufficiently replace steel needles, more penetration testing should be performed, using the guidelines presented in this thesis. A greater number of tests should also be conducted using the pig skin, as its toughness provides a safety factor that will increase the likelihood of penetration into human skin, given that the penetrations into the pig skin are successful.

In order to simulate whether these modifications will prove beneficial, FEA simulations should continue, with solid models created from the new needle designs. The general parameters can be maintained, but updates to the models and the material definitions, including the coefficient of friction between the needle and the rubber, will be necessary. Another approach is to break up the needle FEA into multiple sections, including the cannula, hole, and tip, to relieve pressure off the lone excessively stressed

element in the deformable needle solution. The tip can also be flattened somewhat to create more elements through which the load can be better distributed.

Modification to the methods in which the simulation calculates the contact forces will also be required. Once corrected, the forces and stresses present in the analysis should be compared to those found in this thesis, and a positive result would include a reduction in the forces with penetration still occurring. Future research should include the FEA performed with a full skin model to predict the needles' behavior when penetrating human skin. These guidelines should provide direction for future research to improve the current plastic hypodermic needles and ultimately lead them to become used as an enhancement over the steel needles that are currently creating many health and environmental hazards throughout the world.

APPENDIX A

NEEDLE TESTING PROTOCOL

"Single Needle Testing Protocol"

1) Attach the 25 N load cell to the crosshead of Instron Model 33R4466.
2) Attach the needle so it is vertically suspended from the load cell.
3) Secure the polyurethane skin mimic between two 1 inch ID steel washers using C-clamps, and clamp it to the base of the Instron.
4) Position the polyurethane directly beneath and perpendicular to the needle, making sure that the center of the 1 inch diameter hole aligns with the needle.
5) Run the Instron penetration program, in a three-point bending flexural setup, at a speed of 100 mm/min.
6) Analyze the results, specifically the penetration and friction forces acting on the needle.
7) For buckling tests, align the needle with an aluminum plate in place of the skin mimic.

"Resistance to Breakage Testing Protocol"

1) Load the needle horizontally into the fixture shown in Figure 47.
2) Attach a fixture to the load cell that will allow for movement at the needle's tip in both vertical directions.

3) Raise the load cell so the needle is bent up at a 25° angle from horizontal.
4) Immediately lower the load cell so the needle is bent down at a 25° angle from horizontal.
5) Repeat for a total of 20 cycles.
6) Analyze the needle, noting any breakage along the cannula.

"Stiffness Testing Protocol"

1) Load the needle horizontally onto the raised base of the Instron in a 3 point bend test setup so that the center of the cannula is directly beneath the load cell, as shown in Figure 39.
2) Attach a piece to the load cell that will contact the needle, as specified by ISO 9626 – Annex C [39].
3) Apply the proper spacing of the two sides of the base according to ISO 9626 – Annex C [39].
4) Lower the load cell onto the cannula at a constant speed.
5) Measure the force recorded as well as the deflection and force as the needle breaks.

APPENDIX B

LUBRICATION APPLICATION PROTOCOL

"Lubrication Application Protocol"

1) If necessary, cut the needles to the proper length and glue into hubs.
2) Dip the needles in acetone for 3 minutes and then allow them to dry.
3) Dip the needles in isopropyl alcohol for 3 minutes and then allow them to dry.
4) Rinse the needles with deionized water.
5) Dilute the Dow Corning MDX4-4159 dispersion solution to the desired concentration using a solution of 70% mineral spirits and 30% isopropyl alcohol.
6) Dip the needles in the dispersion solution for 30 seconds.
7) Hang the needles to cure in an oven at 70 ˚C and 40%-70% humidity for three days.

APPENDIX C

ABAQUS CODE

Penetration1 – Deformable Needle

```
*Heading
** Job name: penetration1 Model name: Model-1
*Preprint, echo=NO, model=NO, history=NO, contact=NO
**
** PARTS
**
*Part, name=Part-10
*Node

node listing excluded

*Element, type=C3D8R

element listing excluded

*Nset, nset=_PickedSet6, internal, generate
    1,  1432,     1
*Elset, elset=_PickedSet6, internal, generate
   1,  690,    1
*Elset, elset=_Surf-1_S2, internal, generate
 301,  690,    1
*Surface, type=ELEMENT, name=Surf-1
_Surf-1_S2, S2
** Region: (Section-1:Picked), (Controls:EC-1)
*Elset, elset=_PickedSet6, internal, generate
   1,  690,    1
** Section: Section-1
*Solid Section, elset=_PickedSet6, controls=EC-1, material=Material-1
1.,
*End Part
**
*Part, name=taper3-2
*Node

node listing excluded

*Element, type=C3D4

element listing excluded

*Nset, nset=_PickedSet7, internal, generate
    1,  1679,     1
*Elset, elset=_PickedSet7, internal, generate
    1,  4924,     1
```

```
*Elset, elset=_Surf-1_S2, internal

elset listing excluded

*Surface, type=ELEMENT, name=Surf-1
_Surf-1_S2, S2
_Surf-1_S3, S3
_Surf-1_S4, S4
_Surf-1_S1, S1
** Region: (Section-2:Picked), (Controls:EC-2)
*Elset, elset=_PickedSet7, internal, generate
    1,  4924,     1
** Section: Section-2
*Solid Section, elset=_PickedSet7, controls=EC-2, material=Material-2
1.,
*End Part
**
**
** ASSEMBLY
**
*Assembly, name=Assembly
**
*Instance, name=Part-10-1, part=Part-10
*End Instance
**
*Instance, name=taper3-2-1, part=taper3-2
   14.849344,   -14.001413,    51.654755
   14.849344,   -14.001413,    51.654755,    14.849344,   -13.001413,
51.654755, 89.9999990194245
*End Instance
**
*Nset, nset=_PickedSet120, internal, instance=Part-10-1
   2,   3,   5,   6,   7,   8,   9,  10,  11,  12,  13,  14,  15,  16,
17,  18
  19,  20,  21,  22,  23,  24,  25,  26,  27,  28,  29,  30,  31,  32,
33,  34
  35,  36,  37,  38,  39,  40,  41,  42,  43,  44,  45,  46,  47,  48,
49,  50
  51,  52,  53, 103, 104, 105, 106, 107, 108, 109, 110, 111, 112, 113,
114, 115
 116, 117, 118, 119, 120, 121, 122, 123, 124, 125, 126, 127, 128, 129,
130, 131
 132, 133, 134, 135, 136, 137, 138, 139, 140, 141, 142, 143, 144, 145,
146, 147
 148, 149, 150, 151
*Elset, elset=_PickedSet120, internal, instance=Part-10-1
   6,  12,  18,  24,  30,  36,  42,  48,  49,  55,  61,  67,  73,  79,
85,  91
  97, 103, 109, 115, 121, 127, 133, 139, 145, 151, 157, 168, 174, 180,
186, 192
 198, 204, 210, 216, 222, 228, 229, 235, 241, 247, 253, 259, 265, 276,
282, 288
 294, 300
*Nset, nset=_PickedSet127, internal, instance=taper3-2-1
   1,   2,  20,  21,  22,  23,  24,  25,  26,  27,  28,  29,  30,  31,
32,  33
```

```
  34,  50,  51,  52,  53,  54,  55,  56,  57,  58,  59,  60,  61,  62,
63,  64
 137, 138, 139, 140, 141, 142, 143, 144, 145, 146, 147, 148, 149, 150,
151, 152
 153, 154, 155, 156, 157, 158, 159, 160, 161, 162, 163, 164, 165, 166,
167, 168
*Elset, elset=_PickedSet127, internal, instance=taper3-2-1
  281,  284,  286,  325,  329,  350,  364,  461,  462,  469,  470,
472,  485,  614,  639, 1046
 1111, 1180, 1312, 1566, 1700, 1773, 1984, 1985, 2024, 2026, 2027,
2187, 2188, 2244, 2245, 2609
 2611, 2891, 3013, 3015, 3197, 3199, 3203, 3265, 3352, 3362, 3365,
3377, 3419, 3561, 3626, 3913
 4153, 4181, 4183, 4216, 4327, 4388, 4411, 4414, 4481, 4482, 4532,
4536, 4621, 4626, 4779, 4921
*End Assembly
**
** ELEMENT CONTROLS
**
*Section Controls, name=EC-1, DISTORTION CONTROL=YES, length ratio=1.,
ELEMENT DELETION=YES
1., 1., 1.
*Section Controls, name=EC-2, DISTORTION CONTROL=YES, length ratio=1.,
ELEMENT DELETION=NO
1., 1., 1.
**
** MATERIALS
**
*Material, name=Material-1
*Density
1000.,
*Elastic
 5e+06, 0.5
*Plastic
 4.48e+06,0.
  4.7e+06,1.
 4.96e+06,2.
 5.24e+06,3.
*Shear Failure
1.0,
*Material, name=Material-2
*Density
1400.,
*Elastic
 1.06e+10, 0.3
**
** INTERACTION PROPERTIES
**
*Surface Interaction, name=IntProp-1
**
** BOUNDARY CONDITIONS
**
** Name: BC-6 Type: Displacement/Rotation
*Boundary
_PickedSet120, 1, 1
_PickedSet120, 2, 2
_PickedSet120, 3, 3
```

```
_PickedSet120, 4, 4
_PickedSet120, 5, 5
_PickedSet120, 6, 6
**
** INTERACTIONS
**
** Interaction: Int-1
*Contact, op=NEW
*Contact Inclusions
Part-10-1.Surf-1 , taper3-2-1.Surf-1
*Contact property assignment
 ,  , IntProp-1
** ----------------------------------------------------------------
**
** STEP: Step-1
**
*Step, name=Step-1
*Dynamic, Explicit
, 3.
*Bulk Viscosity
0.06, 1.2
*Diagnostics, Cutoff Ratio=10.0, Warning Ratio=5.0
**
** BOUNDARY CONDITIONS
**
** Name: BC-8 Type: Velocity/Angular velocity
*Boundary, type=VELOCITY
_PickedSet127, 3, 3, -1.667
**
** OUTPUT REQUESTS
**
*Restart, write, number interval=1, time marks=NO
**
** FIELD OUTPUT: F-Output-1
**
*Output, field
*Node Output
A, RF, RT, U, V, VT
*Element Output, directions=YES
DMICRT, E, LE, MISESMAX, PE, PEEQ, S, SF
*Contact Output
CFORCE, CSTRESS
**
** HISTORY OUTPUT: H-Output-1
**
*Output, history, variable=PRESELECT
*End Step
```

Penetration2 – Rigid Needle

```
*Heading
** Job name: penetration2 Model name: Model-1
*Preprint, echo=NO, model=NO, history=NO, contact=NO
**
```

```
** PARTS
**
*Part, name=Part-10
*Node

node listing excluded

*Element, type=C3D8R

element listing excluded

*Nset, nset=_PickedSet6, internal, generate
    1,  1432,     1
*Elset, elset=_PickedSet6, internal, generate
   1,  690,    1
*Elset, elset=_Surf-1_S2, internal, generate
 301,  690,    1
*Surface, type=ELEMENT, name=Surf-1
_Surf-1_S2, S2
** Region: (Section-1:Picked), (Controls:EC-1)
*Elset, elset=_PickedSet6, internal, generate
   1,  690,    1
** Section: Section-1
*Solid Section, elset=_PickedSet6, controls=EC-1, material=Material-1
1.,
*End Part
**
*Part, name=taper3-2
*Node

node listing excluded

*Element, type=C3D4

element listing excluded

*Node
   1515,  0.200000003,          14.,       -15.21
*Nset, nset=taper3-2-RefPt_, internal
1515,
*Nset, nset=_PickedSet7, internal, generate
    1,  1514,     1
*Elset, elset=_PickedSet7, internal, generate
    1,  4333,     1
*Elset, elset=_Surf-1_S1, internal

elset listing excluded

*Surface, type=ELEMENT, name=Surf-1
_Surf-1_S1, S1
_Surf-1_S3, S3
_Surf-1_S4, S4
_Surf-1_S2, S2
** Region: (Section-2:Picked), (Controls:EC-2)
*Elset, elset=_PickedSet7, internal, generate
    1,  4333,     1
** Section: Section-2
```

```
*Solid Section, elset=_PickedSet7, controls=EC-2, material=Material-2
1.,
*End Part
**
**
** ASSEMBLY
**
*Assembly, name=Assembly
**
*Instance, name=Part-10-1, part=Part-10
*End Instance
**
*Instance, name=taper3-2-1, part=taper3-2
   14.849344,   -14.001413,    51.654755
   14.849344,   -14.001413,    51.654755,    14.849344,   -13.001413,
51.654755, 89.9999990194245
*End Instance
**
*Nset, nset=_PickedSet120, internal, instance=Part-10-1
   2,   3,   5,   6,   7,   8,   9,  10,  11,  12,  13,  14,  15,  16,
17,  18
  19,  20,  21,  22,  23,  24,  25,  26,  27,  28,  29,  30,  31,  32,
33,  34
  35,  36,  37,  38,  39,  40,  41,  42,  43,  44,  45,  46,  47,  48,
49,  50
  51,  52,  53, 103, 104, 105, 106, 107, 108, 109, 110, 111, 112, 113,
114, 115
 116, 117, 118, 119, 120, 121, 122, 123, 124, 125, 126, 127, 128, 129,
130, 131
 132, 133, 134, 135, 136, 137, 138, 139, 140, 141, 142, 143, 144, 145,
146, 147
 148, 149, 150, 151
*Elset, elset=_PickedSet120, internal, instance=Part-10-1
   6,  12,  18,  24,  30,  36,  42,  48,  49,  55,  61,  67,  73,  79,
85,  91
  97, 103, 109, 115, 121, 127, 133, 139, 145, 151, 157, 168, 174, 180,
186, 192
 198, 204, 210, 216, 222, 228, 229, 235, 241, 247, 253, 259, 265, 276,
282, 288
 294, 300
*Nset, nset=_PickedSet142, internal, instance=taper3-2-1, generate
    1,  1514,     1
*Elset, elset=_PickedSet142, internal, instance=taper3-2-1, generate
    1,  4333,     1
*Nset, nset=_PickedSet143, internal, instance=taper3-2-1
 1515,
*Nset, nset=_PickedSet144, internal, instance=taper3-2-1
 1515,
** Constraint: Constraint-1
*Rigid Body, ref node=_PickedSet144, elset=_PickedSet142
*End Assembly
**
** ELEMENT CONTROLS
**
*Section Controls, name=EC-1, DISTORTION CONTROL=YES, length ratio=1.,
ELEMENT DELETION=YES
1., 1., 1.
```

```
*Section Controls, name=EC-2, DISTORTION CONTROL=YES, length ratio=1.,
ELEMENT DELETION=NO
1., 1., 1.
**
** MATERIALS
**
*Material, name=Material-1
*Density
1185.,
*Elastic
 5e+06, 0.5
*Plastic
 4.48e+06,0.
  4.7e+06,1.
 4.96e+06,2.
 5.24e+06,3.
*Shear Failure
1.0,
*Material, name=Material-2
*Density
1400.,
*Elastic
 1.06e+10, 0.3
**
** INTERACTION PROPERTIES
**
*Surface Interaction, name=IntProp-1
**
** BOUNDARY CONDITIONS
**
** Name: BC-6 Type: Displacement/Rotation
*Boundary
_PickedSet120, 1, 1
_PickedSet120, 2, 2
_PickedSet120, 3, 3
_PickedSet120, 4, 4
_PickedSet120, 5, 5
_PickedSet120, 6, 6
**
** INTERACTIONS
**
** Interaction: Int-1
*Contact, op=NEW
*Contact Inclusions
Part-10-1.Surf-1 , taper3-2-1.Surf-1
*Contact property assignment
 ,  , IntProp-1
** ----------------------------------------------------------------
**
** STEP: Step-1
**
*Step, name=Step-1
*Dynamic, Explicit
, 2.75
*Bulk Viscosity
0.06, 1.2
**
```

```
** BOUNDARY CONDITIONS
**
** Name: BC-8 Type: Velocity/Angular velocity
*Boundary, type=VELOCITY
_PickedSet143, 3, 3, -1.667
**
** OUTPUT REQUESTS
**
*Restart, write, number interval=1, time marks=NO
**
** FIELD OUTPUT: F-Output-1
**
*Output, field
*Node Output
A, RF, RT, U, V, VT
*Element Output, directions=YES
DMICRT, E, LE, MISESMAX, PE, PEEQ, S, SF
*Contact Output
CFORCE, CSTRESS
**
** HISTORY OUTPUT: H-Output-1
**
*Output, history, variable=PRESELECT
*End Step
```

APPENDIX D

MATERIAL DATA

Table 31 - Material properties for plastic needles (Ticona 1300MT) [23]

Elastic modulus	10.6 GPa
Yield strength	60 MPa
Moment of inertia (38.1 mm)	4.17×10^{-14} m^4
Moment of inertia (25.4 mm)	2.94×10^{-14} m^4
Cross sectional area (38.1 mm)	7.24×10^{-7} m^2
Cross sectional area (25.4 mm)	6.08×10^{-7} m^2
Radius of gyration (38.1 mm)	0.00024
Radius of gyration (25.4 mm)	0.00022
K (buckling)	0.7
Poisson's ratio	0.3
Density	1400 kg/m^3
Cost	$0.0836/g

Table 32 - Material properties for polyurethane rubber [34]

Elastic modulus	5.0 MPa
Yield strength	4.48 MPa
Poisson's ratio	0.5
Density	1185 kg/m^3
Thickness	0.37 mm

Table 33 - Material properties of Ticona A950

Tensile Strength	205 MPa
Tensile Modulus	9.8 GPa
Compressive Strength	142 MPa
Compressive Modulus	11.7 GPa
Poisson's Ratio	0.47
Density	1400 kg/m^3
Cost	$0.0485/g

Table 34 - Material properties of Ticona B950 [48]

Elastic Modulus (E_{11})	25.6 GPa
Poisson's Ratio	0.48
Cost	$0.2225/g

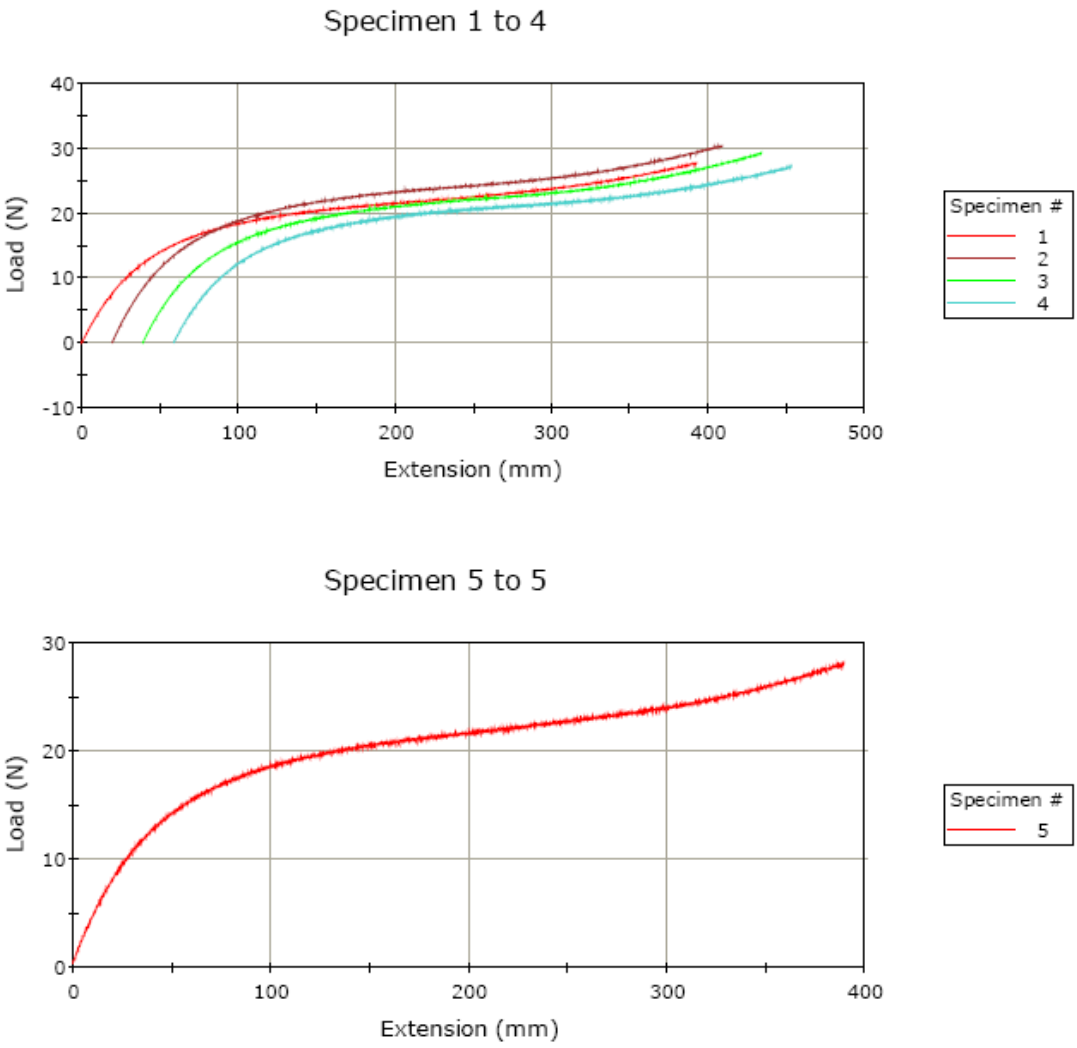

Figure 58 - Polyurethane tensile test data

APPENDIX E

SUPPLEMENTAL GRAPHS

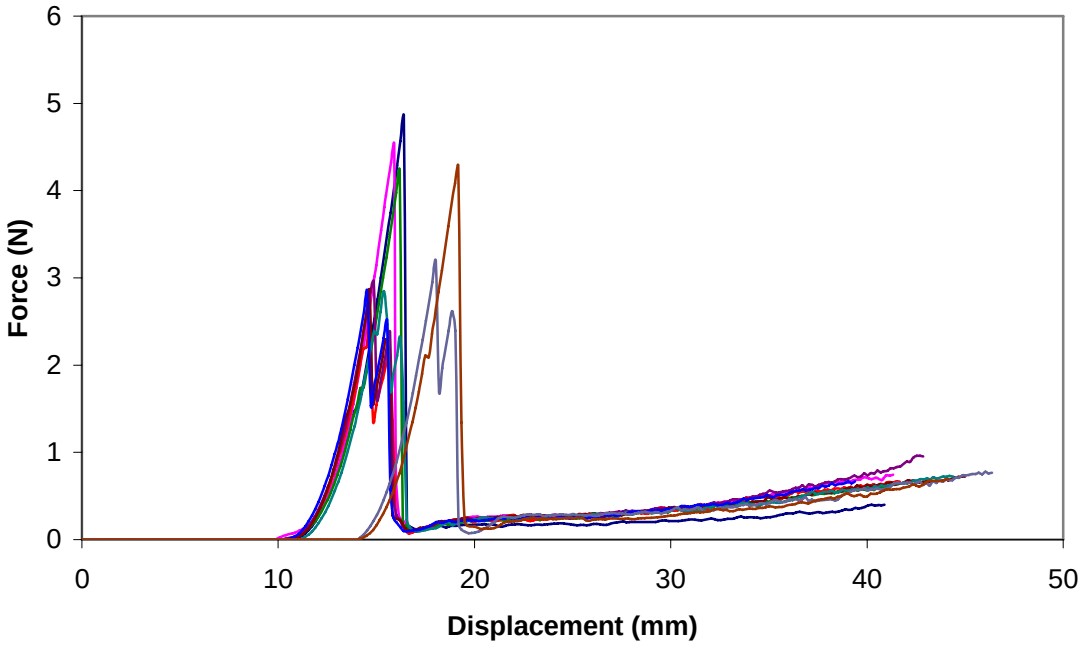

Figure 59 - Successful penetrations for 38.1 mm, 5% silicone content, cleaned plastic needles

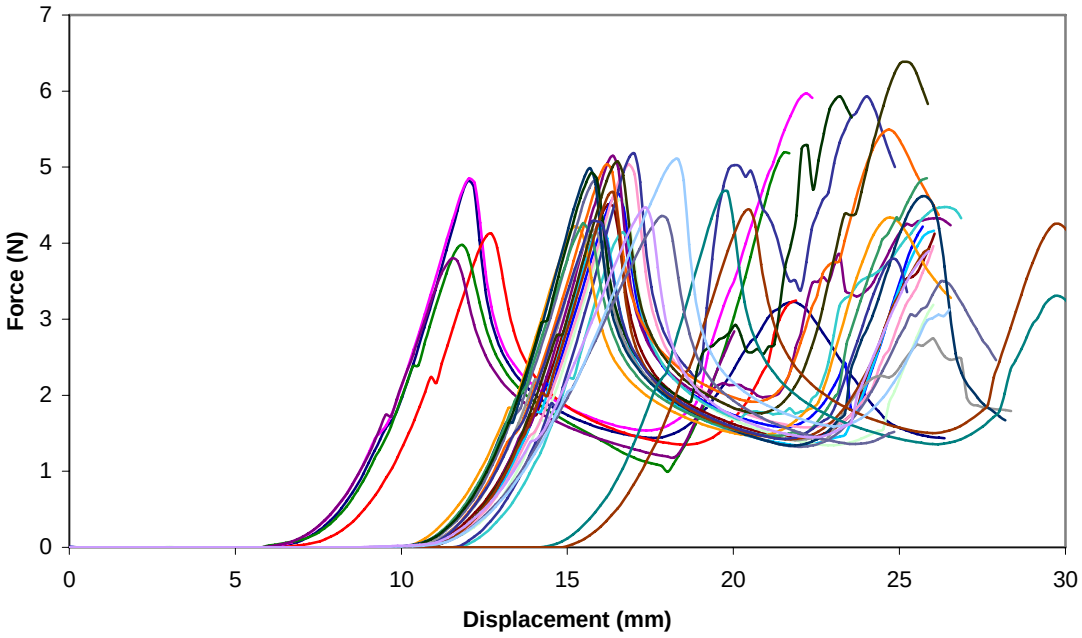

Figure 60 - Failed penetrations for 38.1 mm, 5% silicone content, cleaned plastic needles

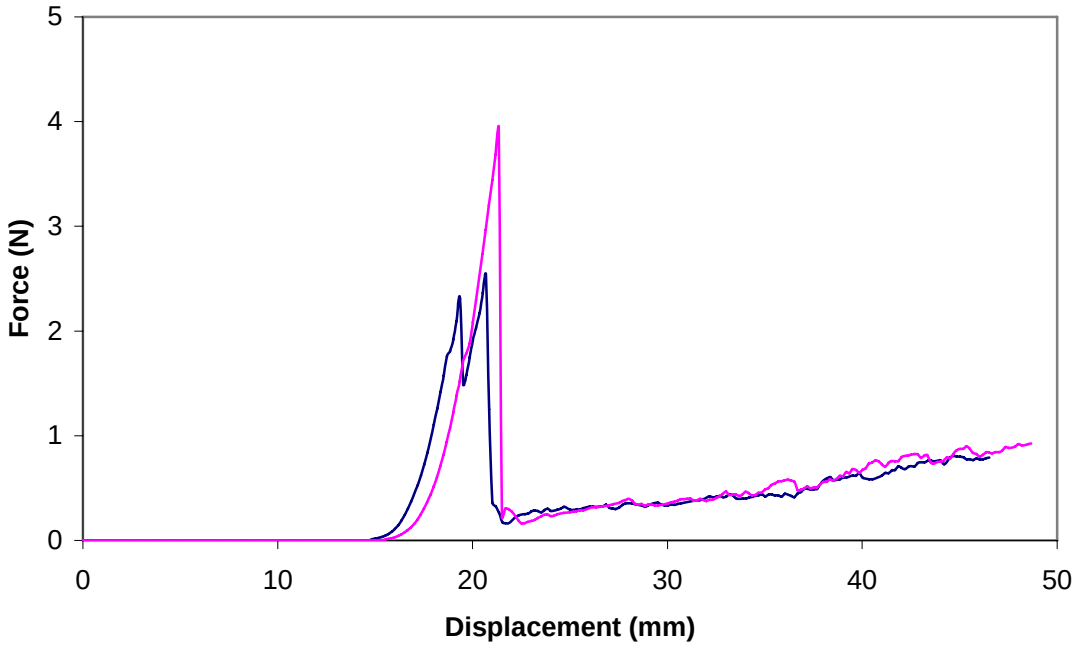

Figure 61 - Successful penetrations for 38.1 mm, 2.5% silicone content, uncleaned plastic needles

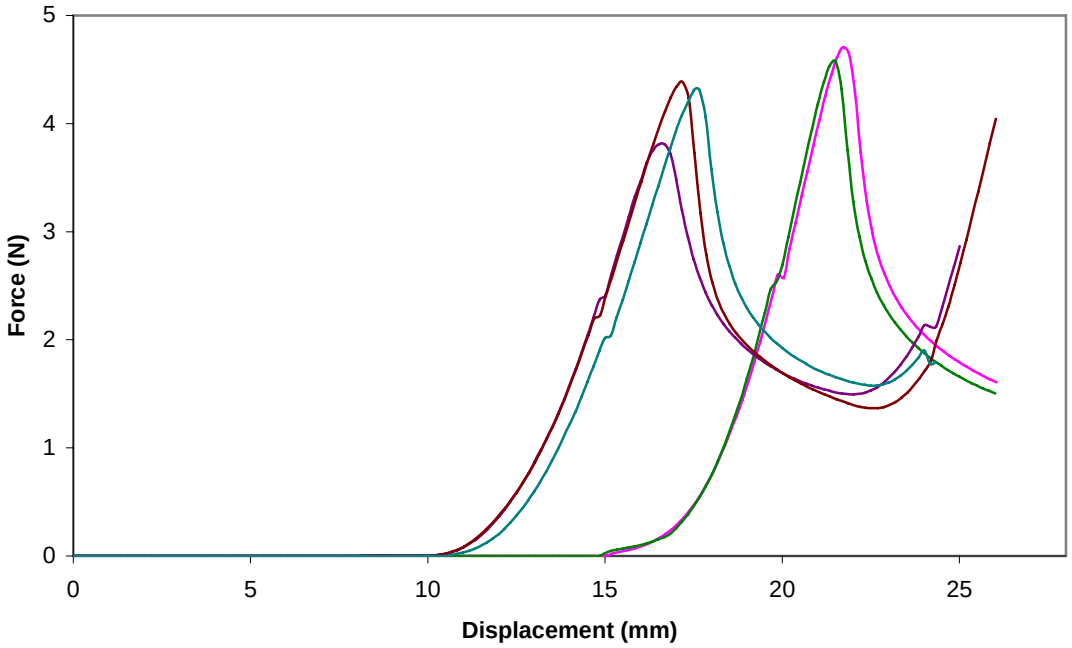

Figure 62 - Failed penetrations for 38.1 mm, 2.5% silicone content, uncleaned plastic needles

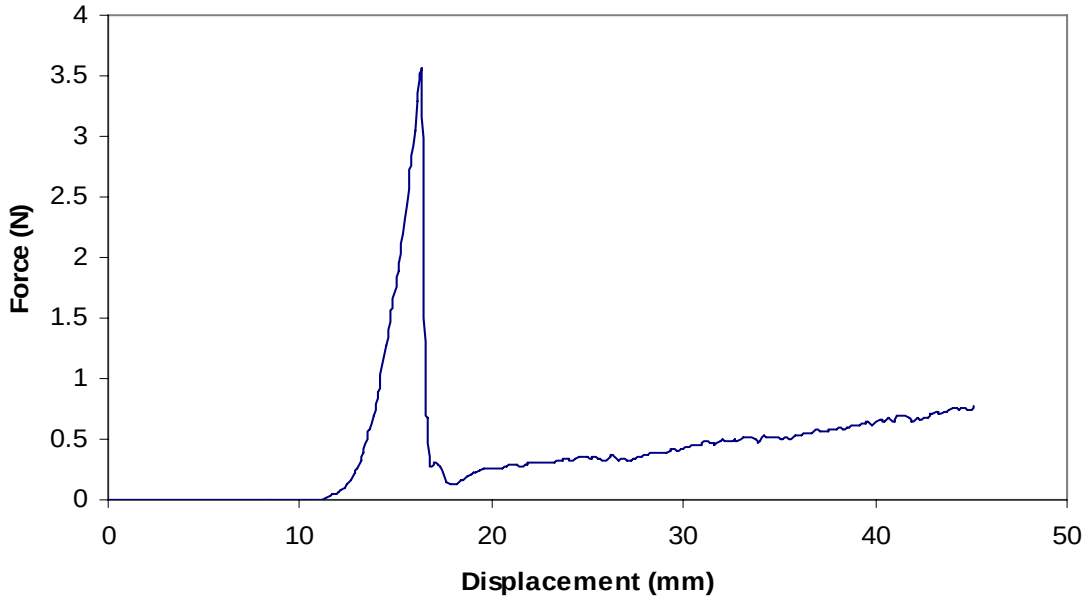

Figure 63 - Successful penetration for 38.1 mm, 2.5% silicone content, cleaned plastic needle

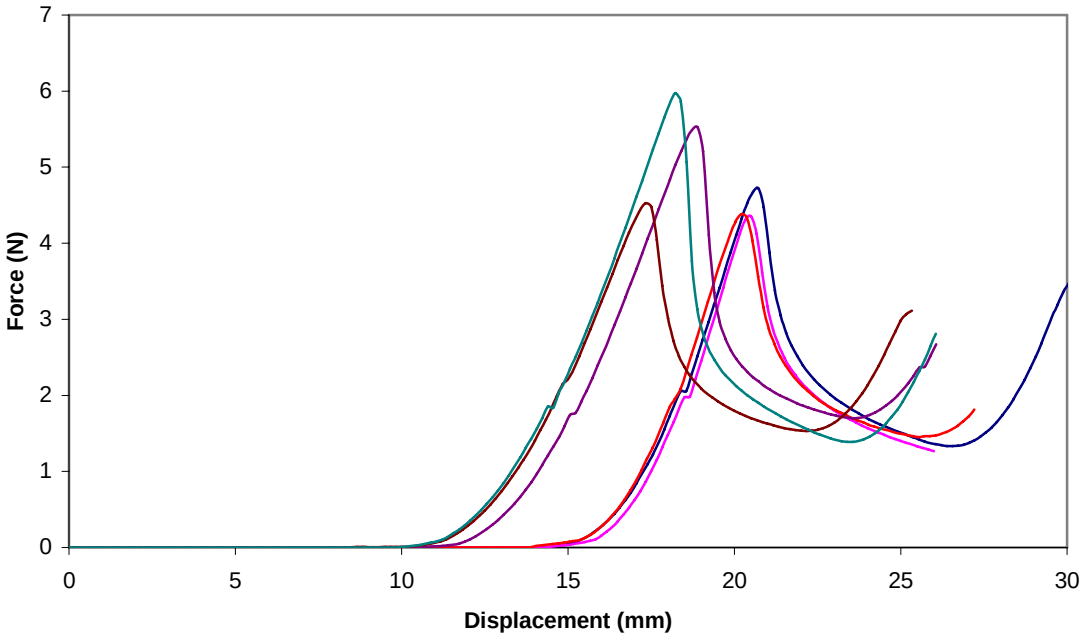

Figure 64 - Failed penetrations for 38.1 mm, 2.5% silicone content, cleaned plastic needles

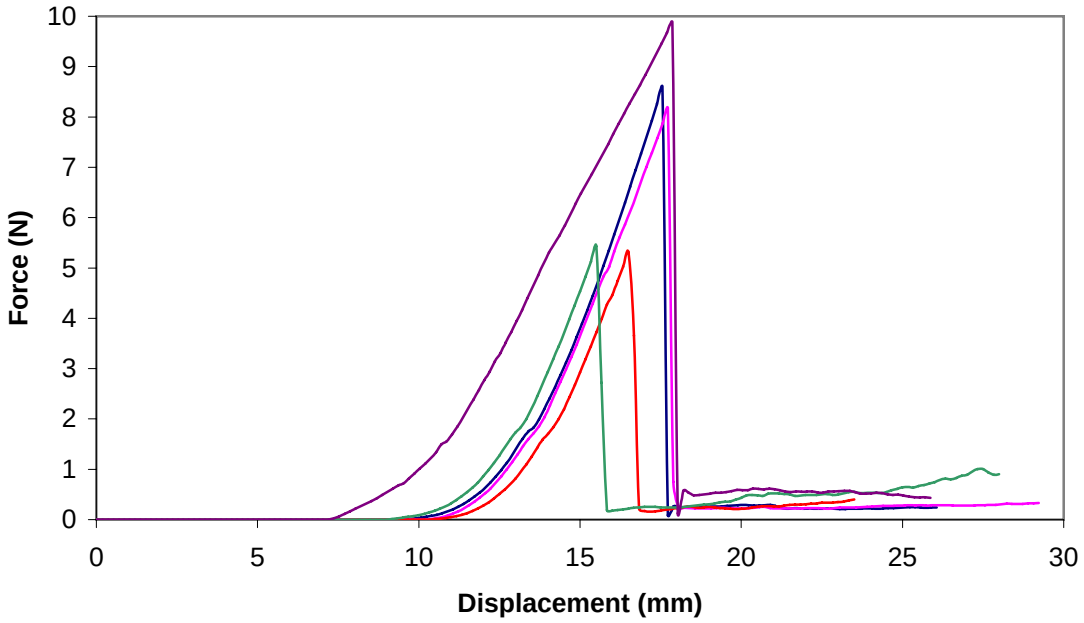

Figure 65 - Successful penetrations for 25.4 mm, 5% silicone content, uncleaned plastic needles

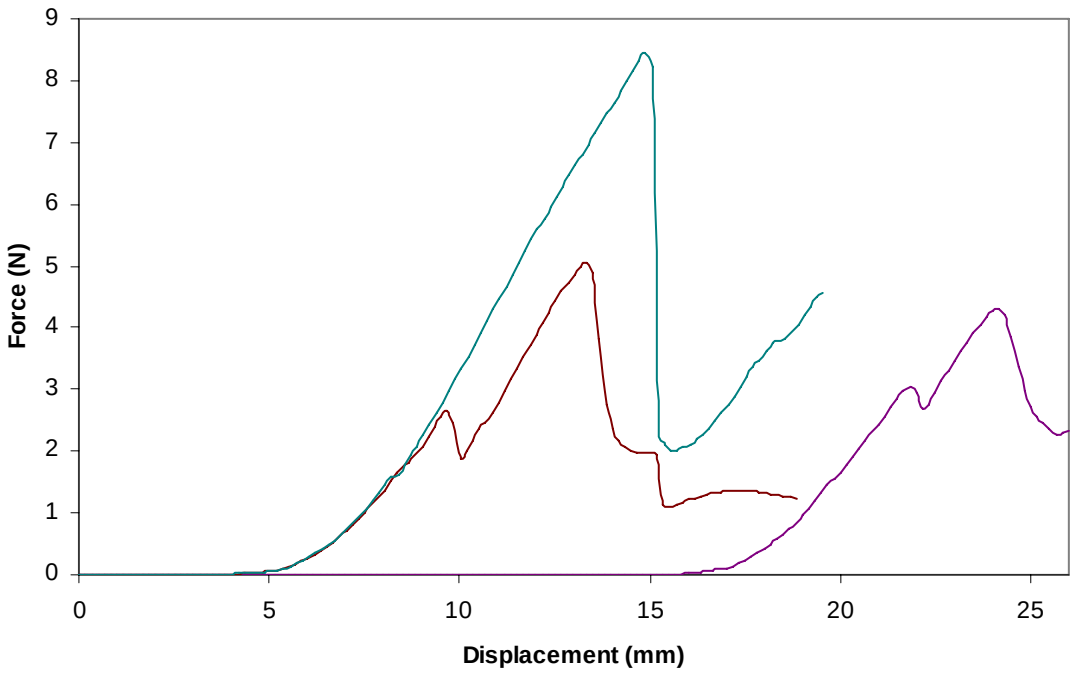

Figure 66 - Failed penetrations for 25.4 mm, 5% silicone content, uncleaned plastic needles

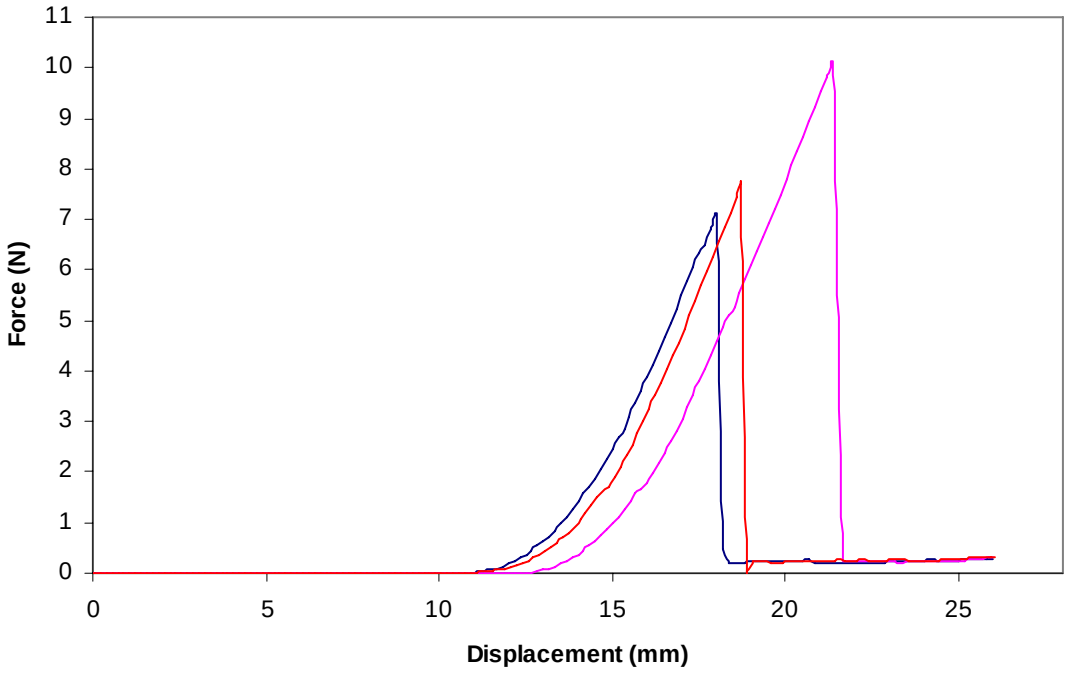

Figure 67 - Successful penetrations for 25.4 mm, 5% silicone content, cleaned plastic needles

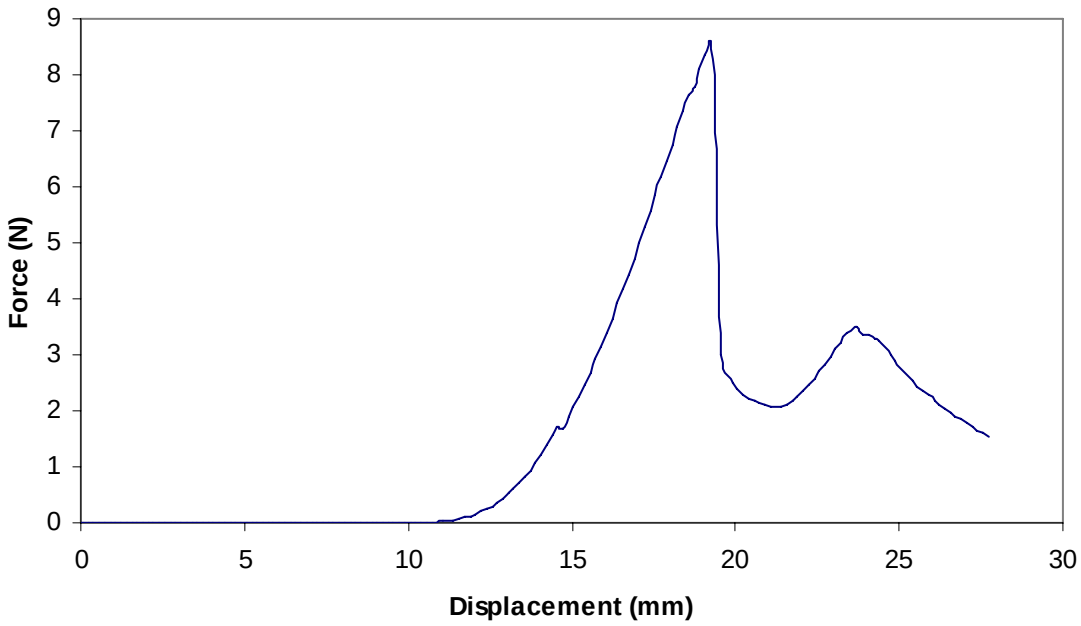

Figure 68 - Failed penetration for 25.4 mm, 5% silicone content, cleaned plastic needle

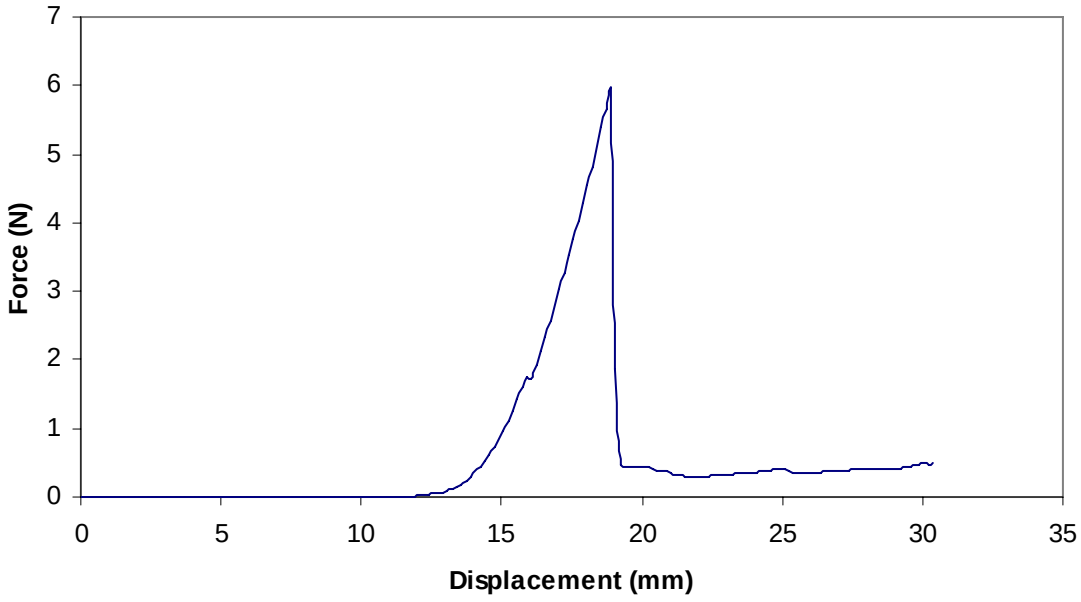

Figure 69 - Successful penetration for 25.4 mm, 2.5% silicone content, uncleaned plastic needle

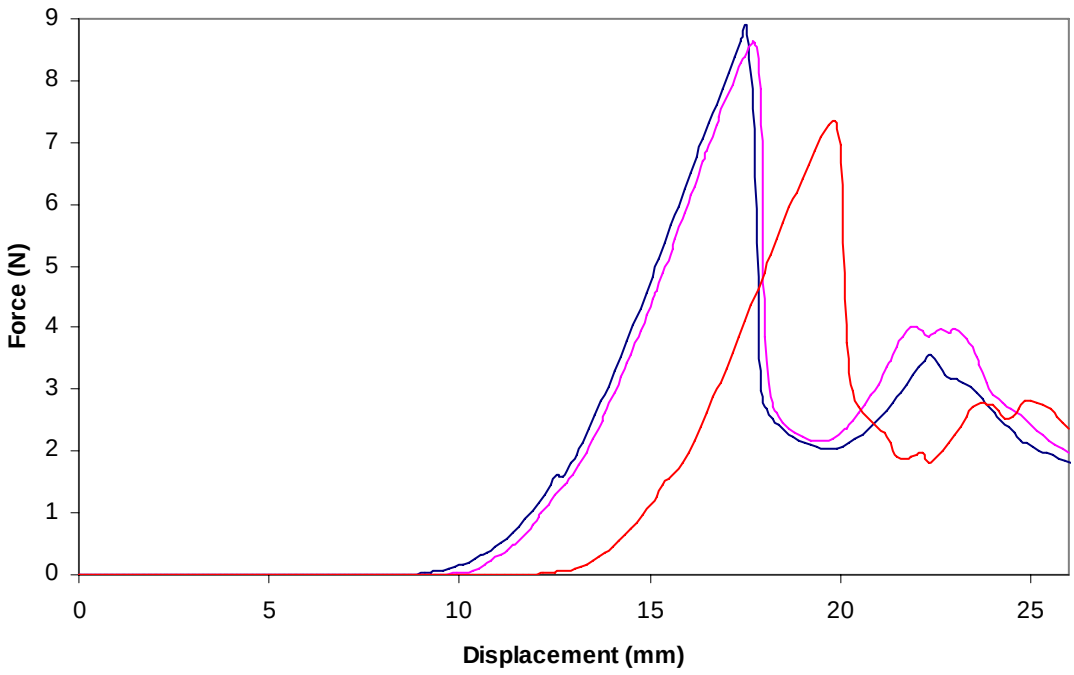

Figure 70 - Failed penetrations for 25.4 mm, 2.5% silicone content, uncleaned plastic needles

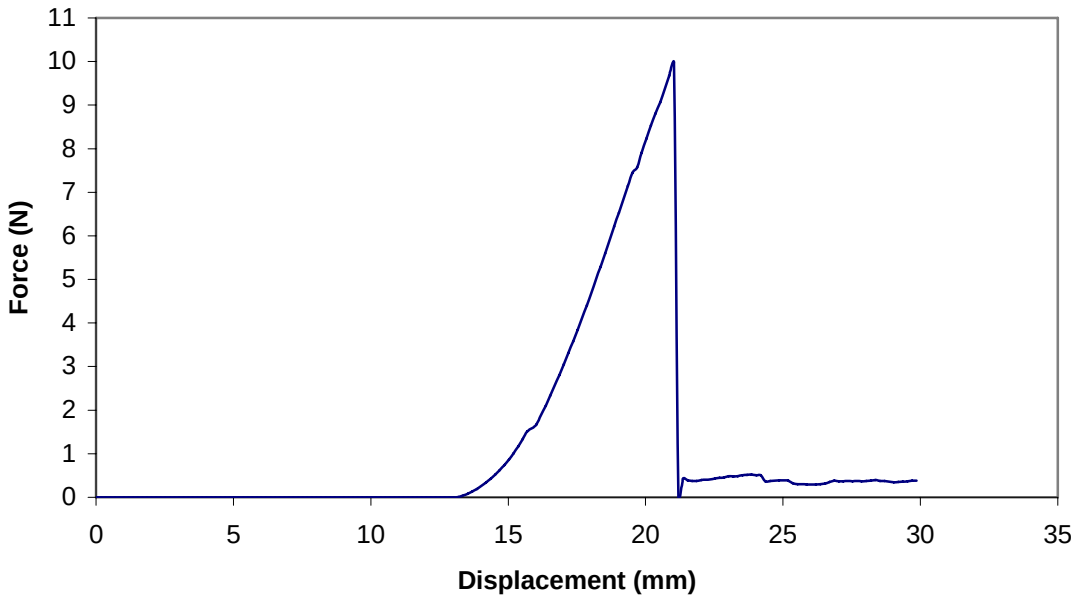

Figure 71 - Successful penetration for 25.4 mm, 2.5% silicone content, cleaned plastic needle

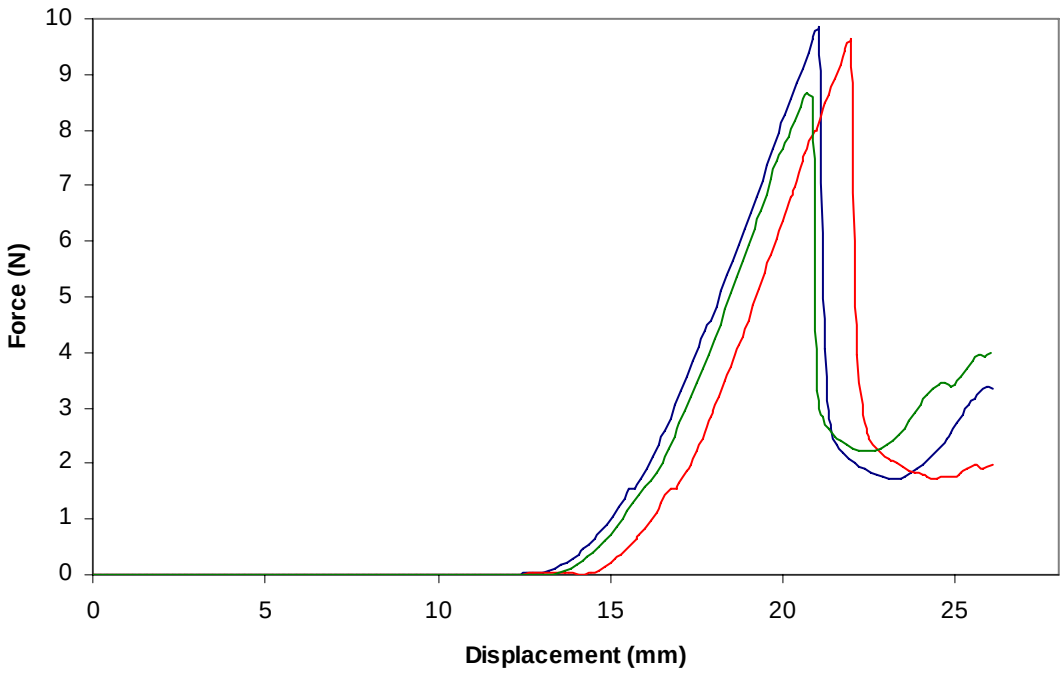

Figure 72 - Failed penetrations for 25.4 mm, 2.5% silicone content, cleaned plastic needles

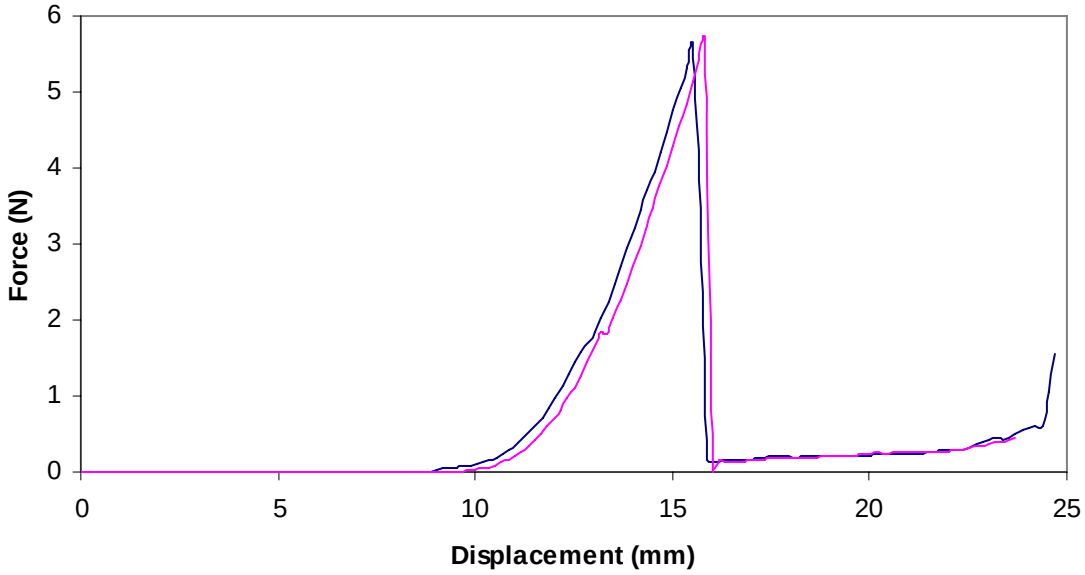

Figure 73 - Successful penetrations for 19.0 mm, 5% silicone content, uncleaned plastic needles

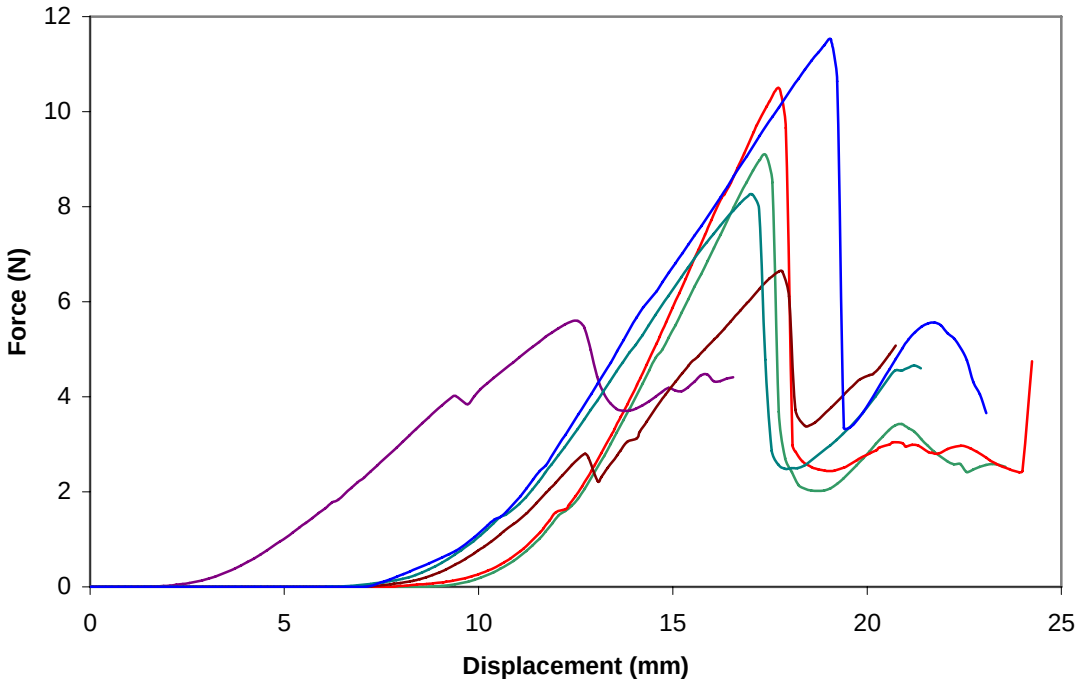

Figure 74 - Failed penetrations for 19.0 mm, 5% silicone content, uncleaned plastic needles

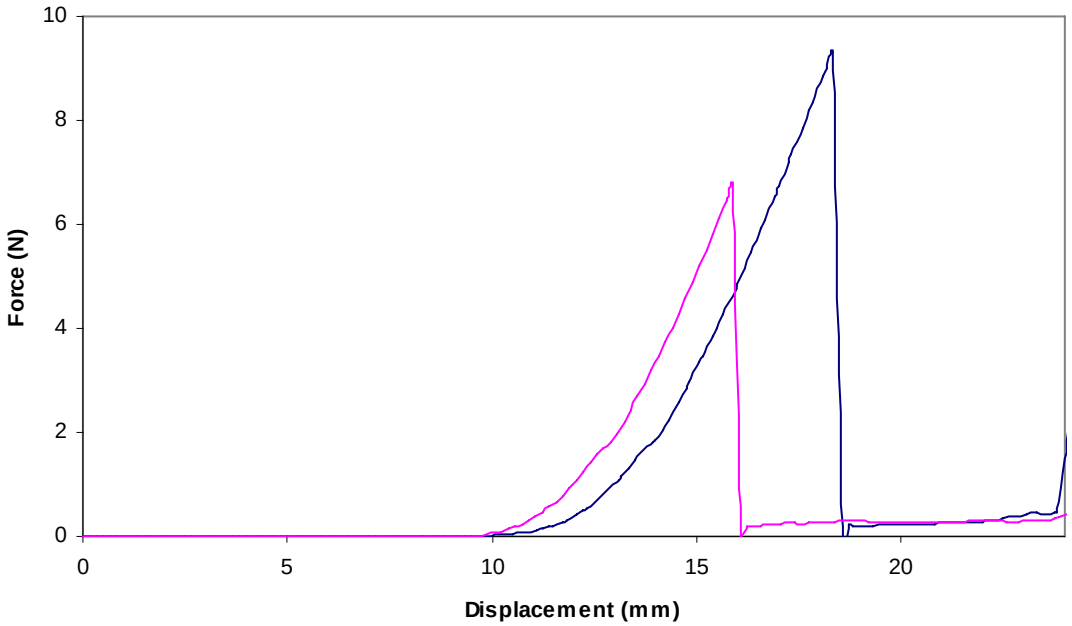

Figure 75 - Successful penetrations for 19.0 mm, 5% silicone content, cleaned plastic needles

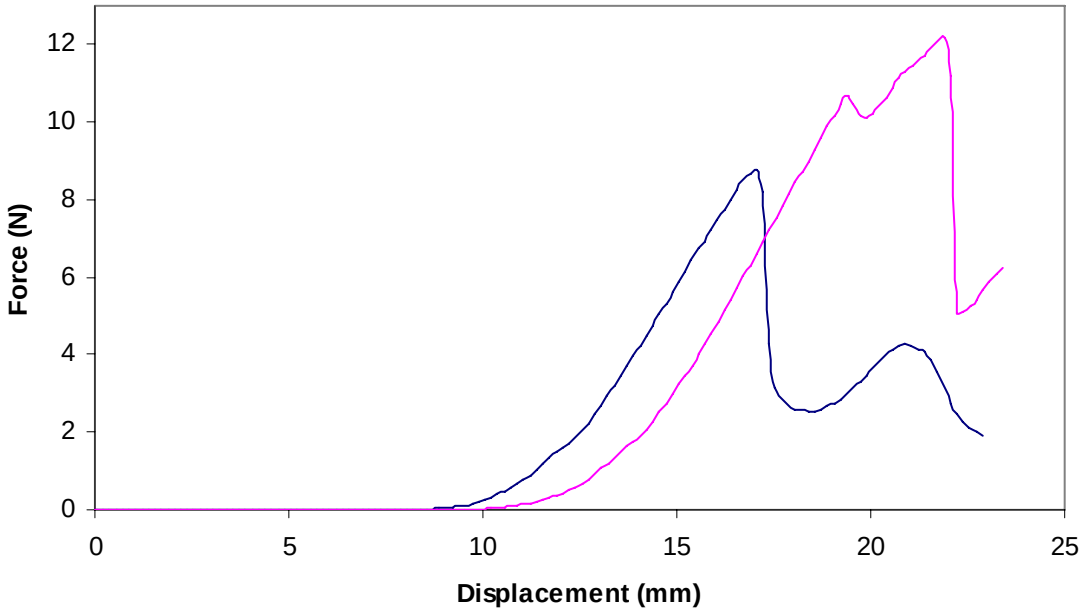

Figure 76 - Failed penetrations for 19.0 mm, 5% silicone content, cleaned plastic needles

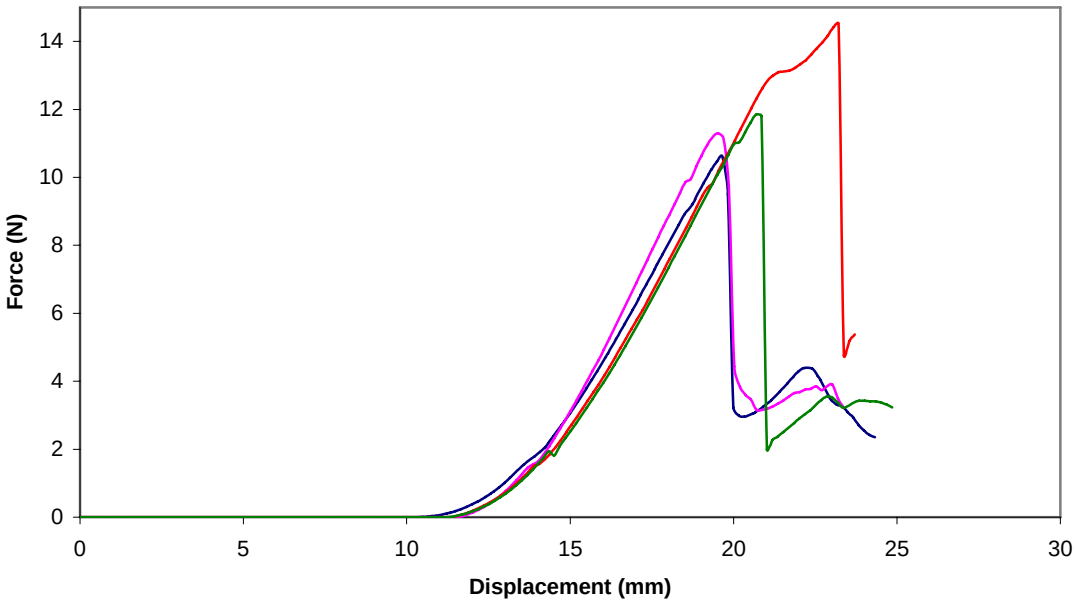

Figure 77 - Failed penetrations for 19.0 mm, 2.5% silicone content, uncleaned plastic needles

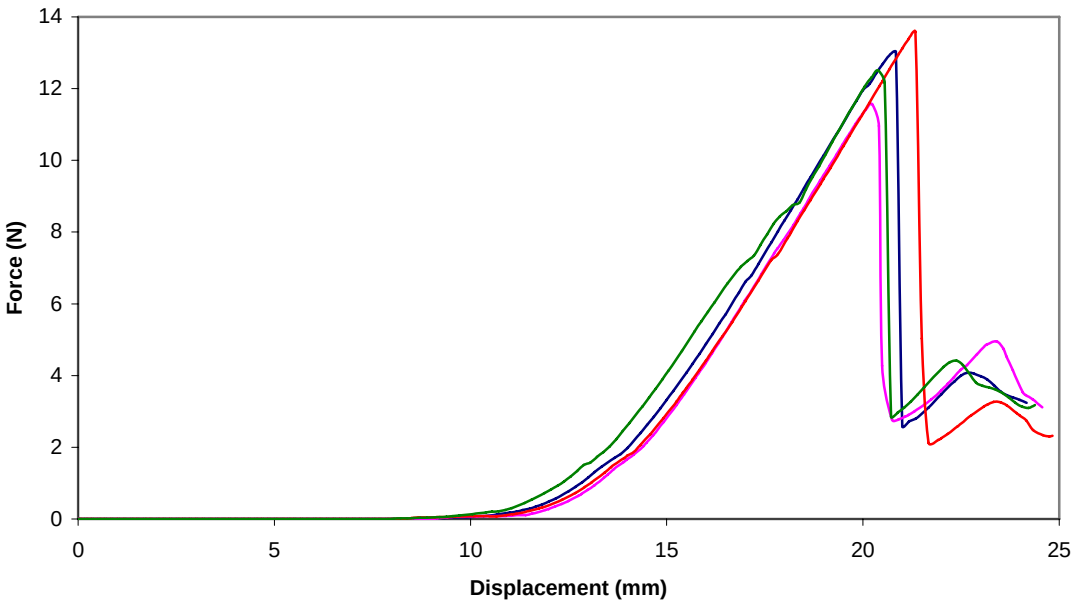

Figure 78 - Failed penetrations for 19.0 mm, 2.5% silicone content, cleaned plastic needles

APPENDIX F

NEEDLE BUCKLING FEA RESULTS

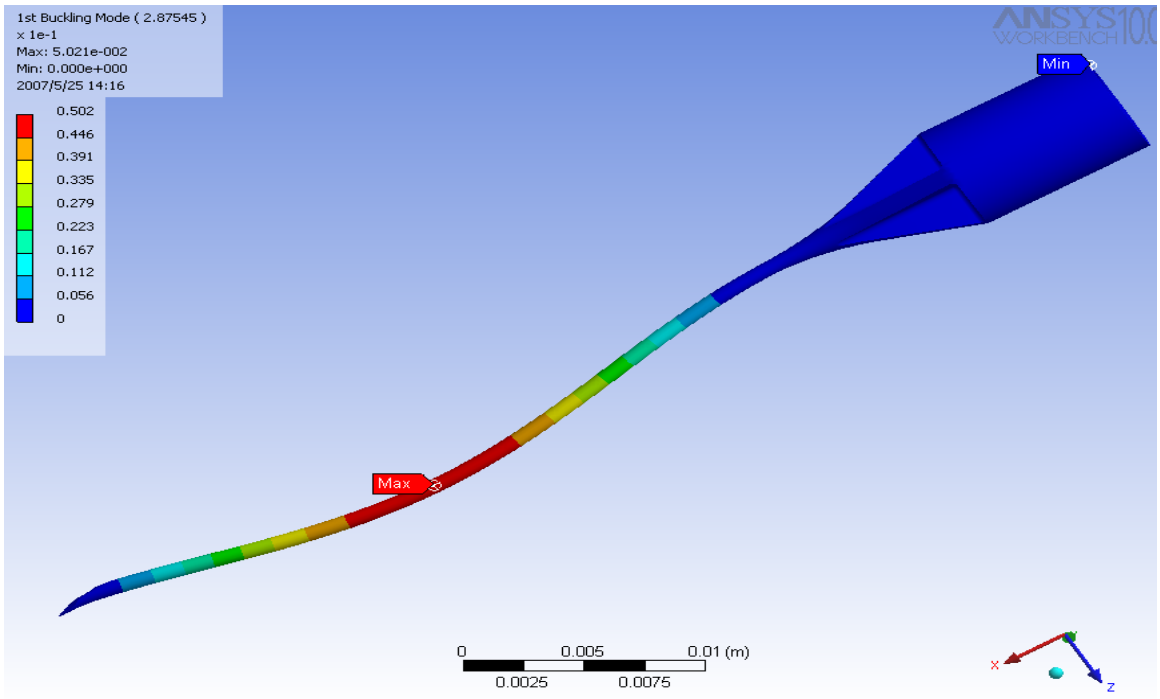

Figure 79 - Needle deformation in ANSYS buckling simulation (38.1 mm length, straight cannula, circular cross section)

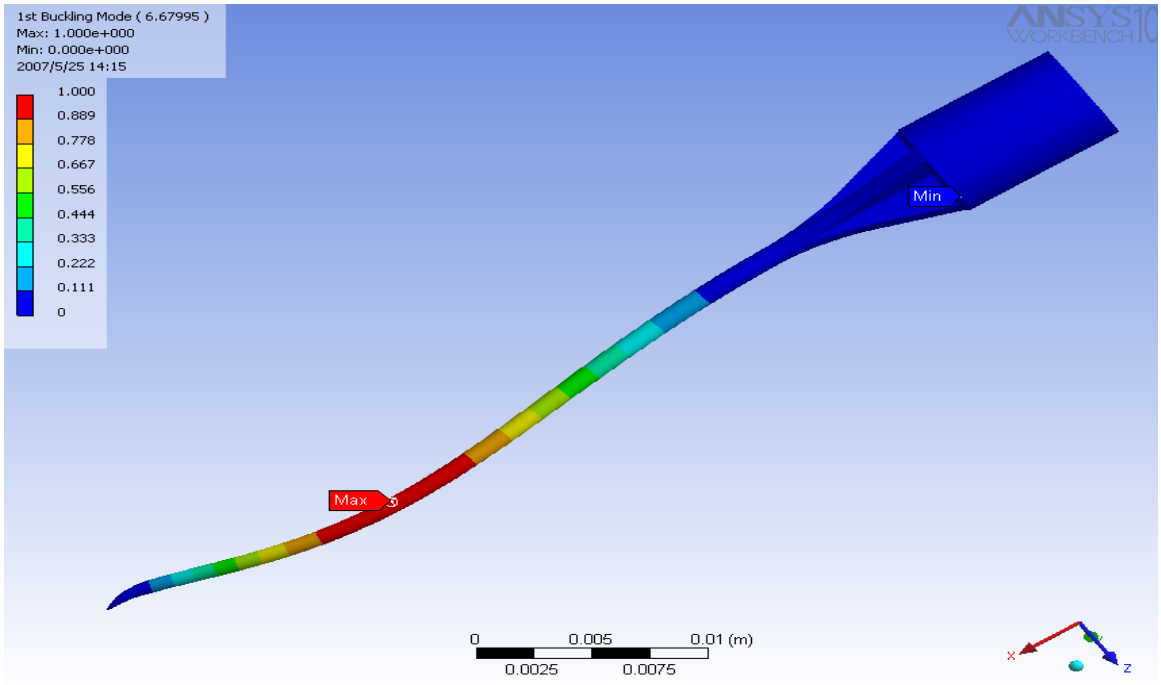

Figure 80 - Needle deformation in ANSYS buckling simulation (38.1 mm length, tapered cannula, elliptical cross section)

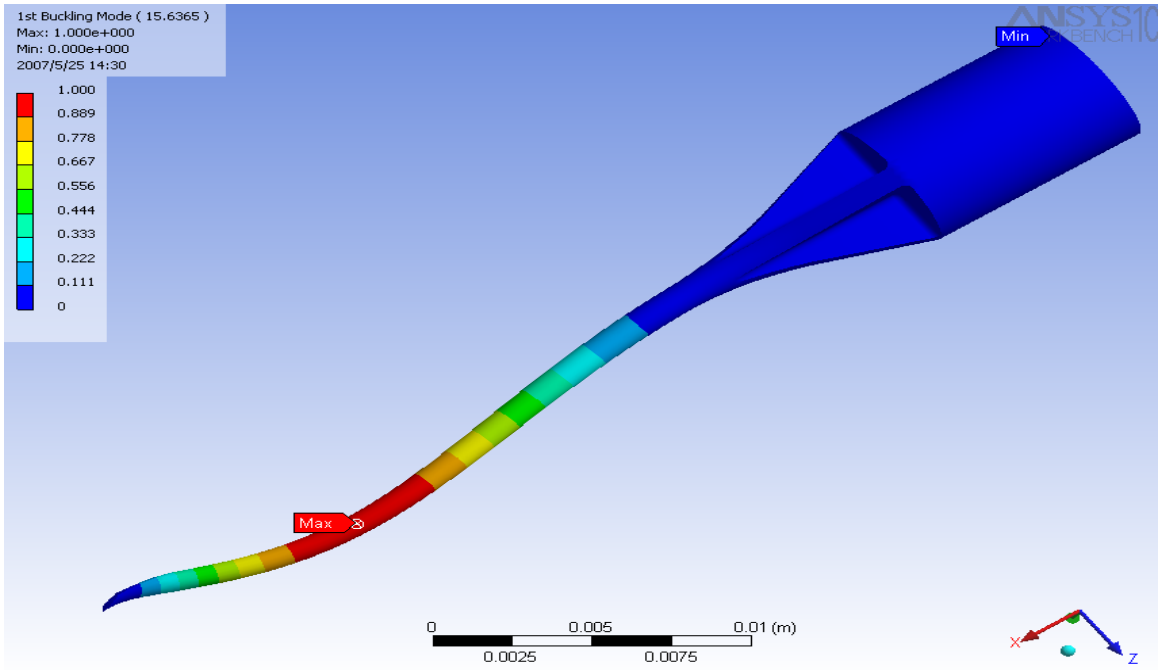

Figure 81 - Needle deformation in ANSYS buckling simulation (25.4 mm length, tapered cannula, circular cross section)

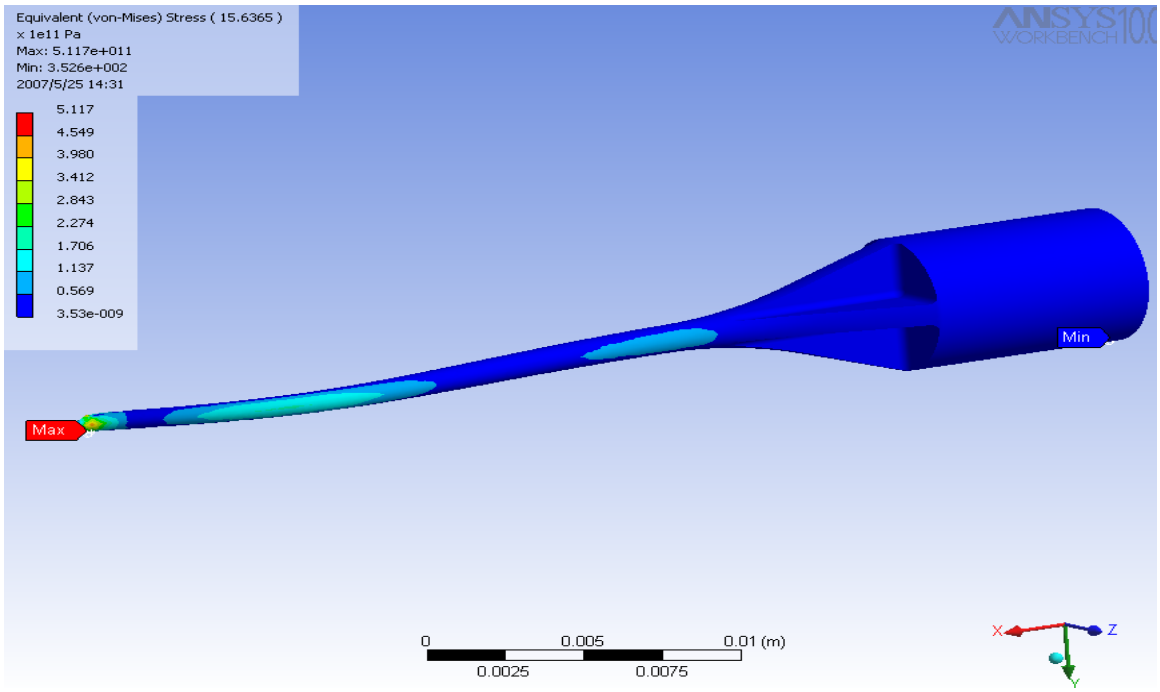

Figure 82 - von Mises stress distribution in ANSYS buckling simulation (25.4 mm length, tapered cannula, circular cross section)

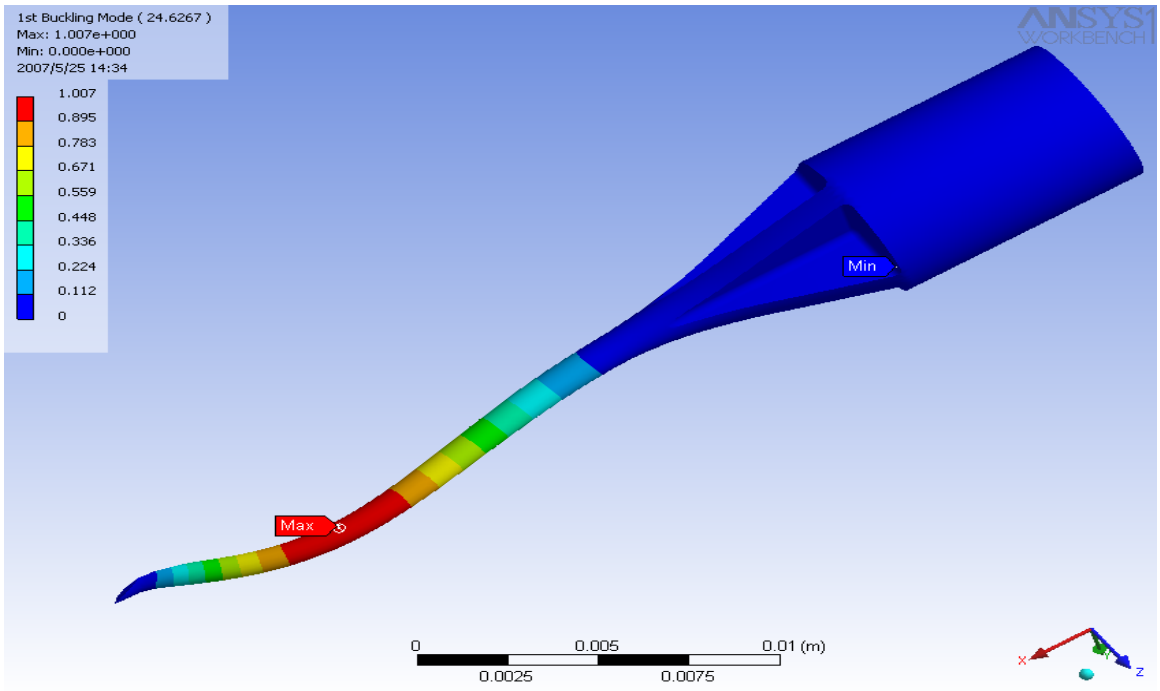

Figure 83 - Needle deformation in ANSYS buckling simulation (19.0 mm length, tapered cannula, circular cross section)

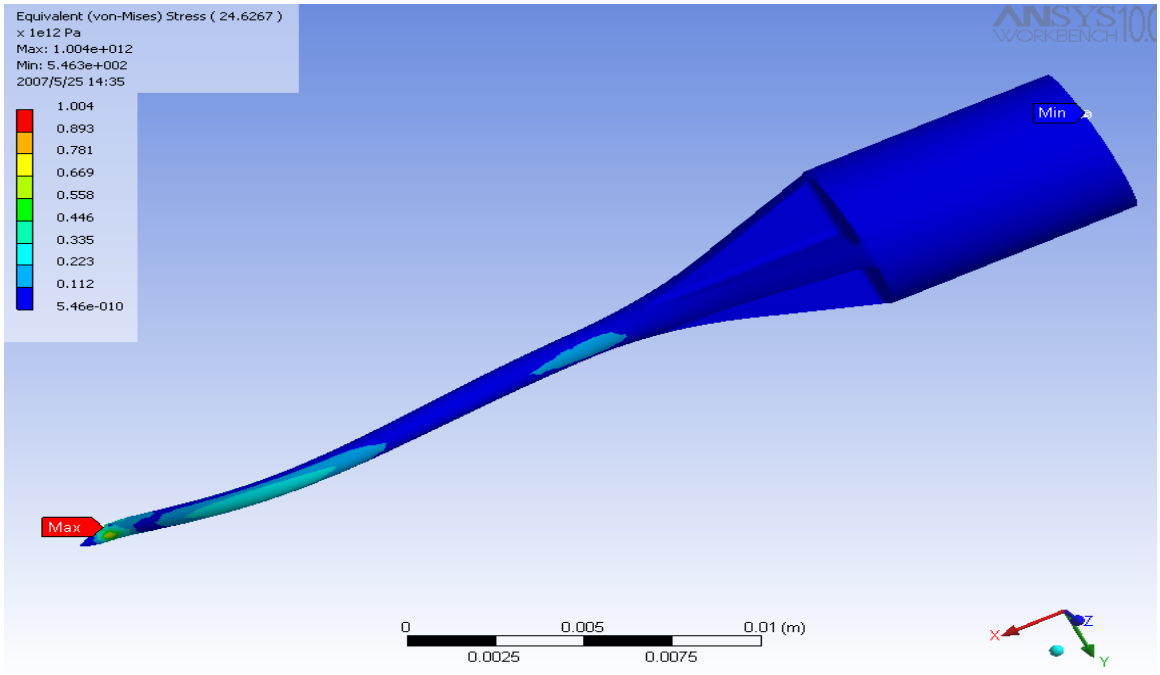

Figure 84 - von Mises stress distribution in ANSYS buckling simulation (19.0 mm length, tapered cannula, circular cross section)

APPENDIX G

TEST DATA

Table 35 - Plastic needle penetration test data

Solution	Cleaned before coating	Length (mm)	Penetration Force (N)	Buckling Force (N)
5%	N	38.1		4.9
5%	N	38.1	2.5	
5%	N	38.1	3.1	
5%	N	38.1		3.9
5%	N	38.1		4.3
5%	N	38.1		4.2
5%	N	38.1		3.7
5%	N	38.1		4
5%	N	38.1		4.2
5%	N	38.1	2.2	
5%	N	38.1	2.1	
5%	N	38.1		4.2
5%	N	38.1		7.2
5%	N	38.1	2.2	
5%	N	38.1	1.7	
5%	Y	38.1	2.6	
5%	Y	38.1		4.7
5%	Y	38.1	4.3	
5%	Y	38.1		4.4
5%	Y	38.1		4.4
5%	Y	38.1		5.1
5%	Y	38.1		4.5
5%	Y	38.1		4.8
5%	Y	38.1		4.8
5%	Y	38.1		4.1

Table 36 (cont.) - Plastic needle penetration test data

Solution	Cleaned before coating	Length (mm)	Penetration Force (N)	Buckling Force (N)
5%	Y	38.1		3.8
5%	Y	38.1		4.5
5%	Y	38.1	4.8	
5%	Y	38.1		4
5%	Y	38.1		4.2
5%	Y	38.1	4.5	
5%	Y	38.1		4.6
5%	Y	38.1	4.2	
5%	Y	38.1	2.5	
5%	Y	38.1		5
5%	Y	38.1		4.7
5%	Y	38.1	3	
5%	Y	38.1		5.2
5%	Y	38.1	2.8	
5%	Y	38.1		4.1
5%	Y	38.1		5.2
5%	Y	38.1	2.8	
5%	Y	38.1		4.2
5%	Y	38.1		5
5%	Y	38.1		4.8
5%	Y	38.1		4.2
5%	Y	38.1		5
5%	Y	38.1		4.3
5%	Y	38.1		4.9
5%	Y	38.1		5.1
5%	Y	38.1		4.7
5%	Y	38.1	2.8	
5%	Y	38.1		4.3
2.5%	N	38.1	2.5	
2.5%	N	38.1		4.7
2.5%	N	38.1		4.6
2.5%	N	38.1	3.9	
2.5%	N	38.1		3.8
2.5%	N	38.1		4.4
2.5%	N	38.1		4.3
2.5%	Y	38.1		4.7
2.5%	Y	38.1		4.4
2.5%	Y	38.1		4.4

Table 37 (cont.) - Plastic needle penetration test data

Solution	Cleaned before coating	Length (mm)	Penetration Force (N)	Buckling Force (N)
2.5%	Y	38.1		5.5
2.5%	Y	38.1		4.5
2.5%	Y	38.1		6
2.5%	Y	38.1	3.5	
5%	N	25.4	8.2	
5%	N	25.4	5.3	
5%	N	25.4	5.4	
5%	N	25.4		4.3
5%	N	25.4		5
5%	N	25.4		8.4
5%	N	25.4	8.6	
5%	N	25.4	9.9	
5%	Y	25.4	7.1	
5%	Y	25.4	10.1	
5%	Y	25.4		8.6
5%	Y	25.4	7.7	
2.5%	N	25.4		8.9
2.5%	N	25.4		8.6
2.5%	N	25.4		7.4
2.5%	N	25.4	6	
2.5%	Y	25.4		9.8
2.5%	Y	25.4	10	
2.5%	Y	25.4		9.6
2.5%	Y	25.4		8.7
5%	N	19.0	5.6	
5%	N	19.0	5.7	
5%	N	19.0		9.1
5%	N	19.0		10.5
5%	N	19.0		5.6
5%	N	19.0		6.6
5%	N	19.0		8.3
5%	N	19.0		11.5
5%	Y	19.0	9.3	
5%	Y	19.0	6.8	
5%	Y	19.0		8.2
5%	Y	19.0		11.2
2.5%	N	19.0		10.6
2.5%	N	19.0		11.3

Table 38 (cont.) - Plastic needle penetration test data

Solution	Cleaned before coating	Length (mm)	Penetration Force (N)	Buckling Force (N)
2.5%	N	19.0		14.5
2.5%	N	19.0		11.8
2.5%	Y	19.0		13
2.5%	Y	19.0		11.6
2.5%	Y	19.0		13.6
2.5%	Y	19.0		12.5

Table 39 - Plastic needle cure time test data

Solution	Cure Time (days)	Length (mm)	Penetration Force (N)	Buckling Force (N)
5%	7	38.1		5.1
5%	7	38.1	3.9	
5%	7	38.1		5.7
5%	7	38.1		6
5%	7	38.1		4
5%	7	38.1	3.5	
5%	7	38.1		4.5
5%	7	38.1		5.1
5%	7	38.1		4.4
5%	7	38.1		4.5
5%	7	38.1		5.4
5%	7	38.1		3.9
5%	7	38.1		5.1
5%	7	38.1		4.8
5%	7	38.1		4.6
5%	7	38.1		4.2
5%	7	38.1	2.7	
5%	7	38.1		3.9
5%	7	38.1		5.3
5%	7	38.1	4.4	
5%	7	38.1		4.3
5%	7	38.1	3.3	
5%	7	38.1		4.8
5%	7	38.1		4.6

Table 40 (cont.) - Plastic needle cure time test data

Solution	Cure Time (days)	Length (mm)	Penetration Force (N)	Buckling Force (N)
5%	7	38.1		4.8
5%	7	38.1		4
5%	7	38.1		5
5%	7	38.1		5.2
5%	7	38.1		4.9
5%	7	38.1	4.2	
5%	7	25.4		8.1
5%	7	25.4		8.3
5%	7	25.4		7.9
5%	7	25.4		8.2
5%	7	25.4	6.7	
5%	7	25.4		10.2
5%	7	25.4	5.8	
5%	7	25.4		10.4
5%	7	25.4		8
5%	7	25.4		7.3
5%	7	25.4	8.1	
5%	7	25.4		8.8
5%	7	25.4	7.7	
5%	7	25.4	11.8	
5%	7	25.4		8.1
5%	7	25.4		9
5%	7	25.4		9.5
5%	7	25.4		9.4
5%	7	25.4		9.9
5%	7	25.4	6.5	
5%	7	25.4		8.5
5%	7	25.4	9.2	
5%	7	25.4	8.7	
5%	7	25.4	6.5	
5%	7	25.4	8.5	
5%	7	25.4		9.3
5%	7	25.4		9.1
5%	7	25.4	4.7	
5%	7	25.4		11.2

Table 41 - Steel needle test data

Condition	Penetration Force (N)
As-received	0.55
As-received	0.51
As-received	0.50
Stripped	1.07
Stripped	0.93
Stripped	0.89
Stripped	1.18
Stripped	1.38
Stripped	1.25
Relubricated	0.66
Relubricated	0.77
Relubricated	0.69

Table 42 - Pig skin test data

Needle	Length (mm)	Penetration Force (N)	Buckling Force (N)
Plastic	38.1		4.5
Plastic	38.1		4.5
Plastic	38.1		4.4
Plastic	38.1		3.8
Plastic	38.1		5.2
Plastic	25.4		6.0
Plastic	25.4	6.5	
Plastic	25.4	9.5	
Plastic	25.4	9.4	
Steel	25.4	0.8	
Steel	25.4	1.2	
Steel	25.4	1.1	

Table 43 - Butyl rubber stopper test data

Needle	Length (mm)	Penetration Force (N)	Buckling Force (N)
Plastic	38.1		5.4
Plastic	38.1		5.5
Plastic	25.4		7.7
Plastic	25.4		8.4
Plastic	25.4	8.3	
Plastic	25.4	8.3	
Plastic	25.4	8.2	
Plastic	25.4	8.3	
Plastic	25.4	8.4	
Steel	25.4	3.6	
Steel	25.4	4.5	

Table 44 - Butyl rubber stopper test data - relubricated 25.4 mm length plastic needles

Penetration force in butyl rubber (N)	Penetration force in polyurethane (N)	Buckling load in polyurethane (N)
8.7	3.3	
6.5	6.0	
7.8		8.0
7.2		7.5
8.1	7.3	
7.9	7.3	
7.4		7.2
8.9	5.0	
8.0	5.1	
7.3		8.0

Table 45 - Plastic needle punch radius measurements

Tip radius (mm)
0.056
0.065
0.05
0.062
0.057
0.056
0.065
0.043
0.064
0.053

REFERENCES

[1] Miller, M.A. and E. Pisani, The cost of unsafe injections, *Bulletin of the World Health Organization*, 1999, 77(10), pg. 808.

[2] Tamplin, S.A. et al, Issues and options for the safe destruction and disposal of used injection materials, *Waste Management*, 2005, 25, pp. 655-665.

[3] Mujeeb, Syed Abdul et al, Recycling of Injection Equipment in Pakistan. *Infection Control and Hospital Epidemiology*, 2003, 24:2, pp. 145-146.

[4] Kou, U.K. The costs of waste management of sharps from immunization activities: a case study from South Africa, Department of Vaccines and Biologicals, Unpublished WHO report; 2001.

[5] Haltmeier, Mark et al, Putting injection waste out of harm's way, *GAVI Immunization Focus*, March 2002, pp. 6-8.

[6] Ekwueme, Donatus U. et al, Model-based estimates of risks of disease transmission and economic costs of seven injection devices in sub-Saharan Africa, *Bulletin of the World Health Organization*, 2002, 80(11), pp. 859-870.

[7] Hauri, Anja M. et al, The global burden of disease attributable to contaminated injections given in health care settings, *International Journal of STD & AIDS*, 2004, 15, pp. 7-16.

[8] Dziekan, Gerald et al, The cost-effectiveness of policies for the safe and appropriate use of injection in healthcare settings, *Bulletin of the World Health Organization*, 2003, 81(4), pp. 277-285.

[9] Simonsen, L. et al, Unsafe injections in the developing world and transmission of bloodborne pathogens: a review, *Bulletin of the World Health Organization*, 1999, 77(10), pp. 789-800.

[10] Kane, A. et al, Transmission of hepatitis B, hepatitis C and human immunodeficiency viruses through unsafe injections in the developing world: model-based regional estimates, *Bulletin of the World Health Organization*, 1999, 77(10), pp. 801-807.

[11] Lloyd, J.S. and J.B. Milstien, Auto-disable syringes for immunization: issues in technology transfer, *Bulletin of the World Health Organization*. 1999, 77(12), pp. 1001-1007.

[12] Nelson, C.M. et al, Use of SoloShot autodestruct syringes compared with disposable syringes, in a national immunization campaign in Indonesia, *Bulletin of the World Health Organization*, 1999, 77(1), pp. 29-33.

[13] Hutin, Y.J.F. and R.T. Chen, Injection safety: a global challenge, *Bulletin of the orld Health Organization*, 1999, 77(10), pp.787-788.

[14] Battersby, A. et al, Sterilizable syringes: excessive risk or cost-effective option?, *Bulletin of the World Health Organization*, 1999, 77(10), pp. 812-819.

[15] Steinglass, R. et al, Safety, effectiveness and ease of use of a non-reusable syringe in a developing country immunization programme, *Bulletin of the World Health Organization*, 1995, 73(1), pp. 57-63.

[16] McAllister, Devin V. et al, Microfabricated needles for transdermal delivery of macromolecules and nanoparticles: Fabrication methods and transport studies, *PNAS*, 2003, 100(24), pp. 13755-13760.

[17] Haider, Ishaq et al, Biomedical and Fluid Flow Characterization of Microneedle Based Drug Delivery Devices, American Society of Biomechanics, 25th Annual Meeting, August 2001.

[18] Chandrasekaran, Shankar et al, Characterization of Surface Micromachined Metallic Microneedles, *Journal of Microelectromechanical Systems*, 2003, 12(3), pp. 289-295.

[19] Park, Jung-Hwan, et al, Biodegradable polymer microneedles: Fabrication, mechanics and transdermal drug delivery, *Journal of Controlled Release*, 2005, 104, pp. 51-66.

[20] Kim, H. and J.S. Colton, Fabrication and Analysis of Plastic Hypodermic Needles, *SPE-ANTEC Tech. Papers,* 2004, 3727.

[21] Kim, H. and J.S. Colton, Fabrication and Analysis of Plastic Hypodermic Needles, *J. Medical Eng. and Tech.*, 2005, 29(4), pp. 181-186.

[22] Love, Jo and Allen Green, A Novel Polymer Needle For Insulin Delivery, *Medical Device Technology*, October 2003, pp. 22-23.

[23] Ticona GmbH, *Vectra liquid crystal polymer (LCP)*, VC-7, September, 2001.

[24] Acierno, D. and A.A. Collyer, *Rheology and Processing of Liquid Crystal Polymers*, London: Chapman & Hall, 1996, pg. 226.

[25] Acierno, D. and A.A. Collyer, *Rheology and Processing of Liquid Crystal Polymers*, London: Chapman & Hall, 1996, pg. 2.

[26] Stevens, John F., Smith, Trevor G., and Bartlett, Jack H. US Patent 5620639. 1997.

[27] Hibbeler, R.C., *Mechanics of Materials 5th edition*, Pearson Education, Inc., Upper Saddle River, NJ, 2003, pp. 649-659.

[28] Kim, Hoyeon, Fabrication and Analysis of Plastic Hypodermic Needles by Micro Injection Molding, Master of Science Thesis, Georgia Institute of Technology, May 2004, pg. 93.

[29] Hendriks, F.M. et al, Mechanical Properties of Different Layers of Human Skin, Department of Materials Technology, Eindhoven University of Technology, http://www.bmt.tue.nl/pdf/postersonderzoekdag2001/fhendriks.pdf.

[30] Oomens, C.W.J. et al, Deformation Analysis of a Supported Buttock Contact, BED – Vol. 50, 2001 Bioengineering Conference, ASME, 2001.

[31] Shergold, Oliver A. and Fleck, Norman A., Mechanisms of deep penetration of soft solids, with application to the injection and wounding of skin, *Proc. R. Soc. Lond.* A, 2004, 460, pp. 3042, 3048–3050.

[32] Shergold, Oliver A., Fleck, Norman A., and Radford, Darren, The uniaxial stress versus strain response of pig skin and silicone rubber at low and high strain rates, *International Journal of Impact Engineering*, 2006, 32(9), pg. 1395.

[33] Acierno, D. and A.A. Collyer, *Rheology and Processing of Liquid Crystal Polymers*, London: Chapman & Hall, 1996, pg. 30.

[34] McMaster-Carr specifications for polyurethane film, #1446T31, Catalog 10/09/07, pg. 3460.

[35] ASTM D882-02, Standard Test Method for Tensile Properties of Thin Plastic Sheeting.

[36] DIN 13097 (09/2002) Medical Needles – Point Designs and Testing.

[37] Simone, Christina, Modeling of Needle Insertion Forces for Percutaneous Therapies, Master of Science Thesis, Johns Hopkins University, May 2002, pg. 18.

[38] Henkel, Jonathan W. and Eric J. Wall, Needle penetration forces of ultra fine hypodermic needles, *Journal of Biomechanics*, Manuscript BM-D-06-00735, pg. 10.

[39] Test Protocol – Insulin Needle Penetration, Sherwood Medical, St. Louis, MO.

[40] ISO 7864:1993(E) Sterile Hypodermic Needles for Single Use.

[41] ISO 9626: 1991(E) Stainless Steel Tubing for Manufacture of Medical Devices.

[42] Dow Corning, MDX4-4159 Fluid 50% Medical Grade Dispersion, Product Information, Healthcare, 51-0599F-01, 2002-05-11.

[43] Dow Corning, Dow Corning MDX4-4159, 50% Medical Grade Dispersion, Frequently Asked Questions, 52-1039-01, 2002.

[44] Cartus, Kimberly R., Testing of Penetration and Friction Forces of Metal Hypodermic Needles to Further Development of Plastic Hypodermic Needles, Research report, Georgia Institute of Technology, 2004.

[45] Shergold, Oliver A. and Fleck, Norman A., Experimental Investigation Into the Deep Penetration of Soft Solids by Sharp and Blunt Punches, With Application to the Piercing of Skin, *Journal of Biomechanical Engineering*, 2005, 127(5), pg. 839.

[46] ISO 7886-1:1993/Correction 1:1995 Sterile Hypodermic Syringes for Single Use - Part 1: Syringes for Manual Use.

[47] WHO/EPI/LHIS/97.11 Equipment performance specifications and test procedures - E8: Injection devices, World Health Organization, Geneva, 1997- Updated 1 January 1998.

[48] Price, C.D. et al, Modelling the elastic and thermoelastic properties of short fibre composites with anisotropic phases, *Composites Science and Technology*, 2006, 66(1), pg. 72.